



INTRODUCTION TO METAL FATIGUE

Mechanical Engineering
Technical Report ME-TR-11



AARHUS
UNIVERSITY
DEPARTMENT OF ENGINEERING

DATA SHEET

Title: Introduction to Metal Fatigue

Subtitle: Concepts and Engineering Approaches

Series title and no.: Technical report ME-TR-11

Author: Mikkel Melters Pedersen, mmp@eng.au.dk
Department of Engineering – Mechanical Engineering,
Aarhus University

Internet version: The report is available in electronic format (pdf) at the Department of Engineering website <http://www.eng.au.dk>.

Publisher: Aarhus University©

URL: <http://www.eng.au.dk>

Year of publication: 2018 Pages: 91

Editing completed: November 2018

Abstract: This report contains a compendium written for a fatigue course at Aarhus University during 2016-2018. It introduces the basic concepts governing fatigue strength of metals and presents associated engineering approaches needed for practical application. Both machined components and welded (steel) structures are covered and similarities and differences are discussed.

Keywords: Fatigue, Machine Design, Manufacturing, Mechanics of Materials, Structural mechanics.

Financial support: No external financial support

Please cite as: M. M. Pedersen, 2018. Introduction to Metal Fatigue. Department of Engineering, Aarhus University. Denmark. 91 pp. - Technical report ME-TR-11

ISSN: 2245-4594

Reproduction permitted provided the source is explicitly acknowledged

INTRODUCTION TO METAL FATIGUE

Mikkel Melters Pedersen, Aarhus University

Abstract

This report contains a compendium written for a fatigue course at Aarhus University during 2016-2018. It introduces the basic concepts governing fatigue strength of metals and presents associated engineering approaches needed for practical application. Both machined components and welded (steel) structures are covered and similarities and differences are discussed.

Preface

This document is written as a compendium for the Advanced Metal Fatigue course at Aarhus University given by the author. The present version have accompanied 4 classes of students in draft form without causing significant harm to any them and have thus been deemed ready for publication as a first edition. It is implied that more editions will follow. Future editions will be made freely available through the AU Mechanical Engineering section journal and at the author's website www.fatiguetoobox.org. Feedback, proposals and corrections are highly appreciated.

Disclaimer: The content herein is presented in a manner intended for learning rather than practical application. For example, rules and methodologies from different codes are mixed which is generally considered bad practice in engineering. Likewise, no safety factors or partial coefficients are applied. Therefore, in an actual engineering context, it is recommended to follow relevant codes/textbooks in full.

To-do

The following topics will hopefully be included in a future version of the document:

- Low-cycle fatigue; using the strain-life ($\varepsilon - N$) approach
- Bolt fatigue after VDI 2230 and EC3
- Better explanation of the statistical treatment of SN data, scatter index T_σ
- Spectrum factor describing VA loading, such that $\sigma_{a,eq} = K_{spec} \cdot \sigma_{a,max}$
- Probabilistic fatigue assessment
- Nonlinear damage accumulation, sequence effects, effect of overloads
- Example fatigue calculations (benchmark studies, e.g. from SAE)
- Relative fatigue analysis, reserve factors
- Tubular welded joints
- More on residual stresses in welded joints
- Chapter on cast iron and cast aluminum
- Fatigue of additively manufactured (3D printed) metal
- Prediction of fatigue strength from CT scan or similar advanced NDT

Contents

Contents	2
1 Introduction	1
1.1 Fatigue phenomenon	1
1.2 Fatigue loading	2
1.3 Fatigue stress	3
1.4 Fatigue strength	4
1.5 Summary	8
I Machined components and general concepts	9
2 Fatigue strength modifications	11
2.1 Material strength effect	12
2.2 Mean stress effect	13
2.3 Surface roughness effect	15
2.4 Size/thickness effect	15
2.5 Environmental effects	17
2.6 Variable amplitude loading	17
3 Effect of notches	19
3.1 Stress concentrations	19
3.2 Notch support effect	21
4 Synthetic SN curves	25
4.1 Nominal stress SN curve	26
4.2 Comparison of synthesis frameworks	29
4.3 Local stress SN curve	30
5 Variable amplitude loading	34
5.1 Stress-time series generation	34
5.2 Cycle counting	36
5.3 Damage accumulation	40
5.4 Damage equivalent stress range	41
6 Multiaxial fatigue	43
6.1 Multiaxial loading	43
6.2 Simple approaches	44
6.3 The critical plane approach	44
6.4 Multiaxial fatigue criteria	47

II Welded joints and steel structures	51
7 Fatigue of welded joints	53
7.1 General	53
7.2 Toe vs. root failure	54
7.3 SN-curves for welded joints	55
7.4 Assessment approaches	56
8 Factors affecting the fatigue strength of welded joints	58
8.1 General	58
8.2 Misalignment	59
8.3 Thickness	60
8.4 Environmental effects	61
8.5 Post weld treatment (PWT)	62
8.6 Weld quality	65
8.7 Residual stress	66
9 Hot-spot approach	68
9.1 Introduction	68
9.2 Definition of the hotspot stress	68
9.3 Determination of the hotspot stress	70
9.4 SN curve	71
9.5 Weld root assessment	72
10 Notch approach	74
10.1 Introduction	74
10.2 Background	75
10.3 SN curves	76
10.4 Mild notch joint issues	77
10.5 Comparative studies	79
10.6 Limitations and variants	80
11 Fracture mechanics approach	81
11.1 Introduction to fracture mechanics	81
11.2 Application to welded joints	84
Bibliography	88

Notation

N, N_f	Fatigue life (total)	D	Damage (fraction of life consumed)
N_i	Crack initiation life	UR	Utilization ratio
N_p	Crack propagation life	$\Delta\sigma_{eq}$	Damage equivalent stress range
N_D	Knee point (no. cycles)	L	Load (force F or moment M)
N_C	Life at characteristic fatigue strength	δ	Shift between two concurrent loads
N_L	Transition to infinite life	τ_a	Shear stress amplitude
σ_a	Stress amplitude	τ_R	Shear stress fatigue strength
$\Delta\sigma$	Stress range	\mathbf{S}_n	Stress vector (one plane)
σ_m	Mean stress, membrane stress	σ_n	Normal stress (on plane)
$\boldsymbol{\sigma}$	Stress tensor	$\boldsymbol{\tau}$	Shear stress vector (in plane)
$\sigma_1, \sigma_2, \sigma_3$	Principal stresses	τ_m	Mean shear stress
σ_{vm}	von Mises equivalent stresses	\mathbf{n}	Normal vector to search plane
σ_{max}	Maximum stress in cycle	θ, ϕ	Search plane direction
σ_{min}	Minimum stress in cycle	σ_H	Hydrostatic stress
R	Stress ratio	$\Delta\sigma_{uni}$	Equivalent uniaxial stress range
C	Fatigue capacity	$\Delta\sigma_{R,C}$	Characteristic fatigue strength
m	Negative, inverse of SN curve slope	$\Delta\sigma_{R,C}^*$	Un-corrected $\Delta\sigma_{R,C}$
m_1, m_2	Pre-/post-knee slopes	σ_k	Local notch stress
P_S	Probability of survival	σ_s	Structural stress
P_F	Probability of failure	σ_{hs}	Hot spot stress
t	Thickness, time	K_{hs}	Hot spot stress concentration factor
T	Temperature	K_w	Notch relative to hotspot stress
R_z	Surface roughness	k_{qual}	Weld quality correction factor
R_m	Ultimate tensile strength	k_{rs}	Residual stress correction factor
σ_R	Fatigue strength (amplitude)	k_{mis}	Misalignment correction factor
$\sigma_{R,-1}$	Fatigue strength at $R = -1$	k_{PWT}	Post weld treatment factor
$\sigma_{R,0}$	Fatigue strength at $R = 0$	e	Misalignment offset
$\sigma_{R,n}$	Nominal fatigue strength (often implicit)	γ_{Mf}	Material safety factor
$\sigma_{R,k}$	Local fatigue strength (always explicit)	σ_b	Bending stress
$\sigma_{R,D}$	Fatigue strength at knee point	σ_{nl}	Nonlinear part of stress
$\sigma_{R,D}^*$	Material fatigue strength at knee point	r_{ref}	Reference notch radius
K_t	Stress concentration factor	r_{real}	Real notch radius
K_f	Fatigue notch factor	r_f	Fictitious notch radius
n	Notch support factor	$\bar{\sigma}_k$	Local stress averaged over ρ^*
q	Notch sensitivity	a	Crack length
χ^*	Normalized stress gradient	K	Stress intensity factor (SIF)
V_{90}	Highly stressed volume	$f(a)$	Geometry factor
α, β	Fitting parameters	da/dN	Crack growth rate
M	Mean stress sensitivity	A, n	Fitting parameters for Paris' eq.
k_{mean}	Mean stress correction factor	da	Crack increment
k_{surf}	Surface roughness correction factor	dN	Cycle increment
k_{size}	Size effect correction factor	ΔK_{th}	Threshold SIF
k_{reliab}	Reliability factor	K_C	Fracture toughness
k_{env}	Environmental effects correction factor		
k_{load}	Loading correction factor		
k_{tech}	Technological size effect correction factor		
k_{temp}	Temperature correction factor		
k_{treat}	(Surface) treatment correction factor		

1 Introduction

The nature of the fatigue phenomenon is discussed and the basic notation and terminology is presented. The prevailing method of fatigue assessment called the stress-life approach, i.e. using SN curves, is introduced. Initially, we consider uniaxial high-cycle fatigue only and limit the material and deformation behavior to the linear region.

1.1 Fatigue phenomenon

Fatigue can be defined as “The process of progressive localized permanent structural change occurring in a material subjected to conditions that produce fluctuating stresses and strains at some point or points and that may culminate in cracks or complete fracture after a sufficient number of fluctuations” [80].

Schijve [70] explains the crack initiation process as follows; at stress amplitudes below the yield limit, so-called cyclic slip can occur, Fig. 1, at the microscopic level, involving only few grains in the material. It happens on the surface, because here the material is less constrained, compared to the inside. As seen in Fig. 1 slip tends to occur in the plane of maximum shear stress (45°) in ductile materials. The slip is not reversible, because the exposed fresh material surface is covered by an oxide layer and also because of strain hardening. Following slips will therefore not close the initial slip, but instead accumulate close to it. A microcrack is then formed which may continue to grow under further cyclic loading.

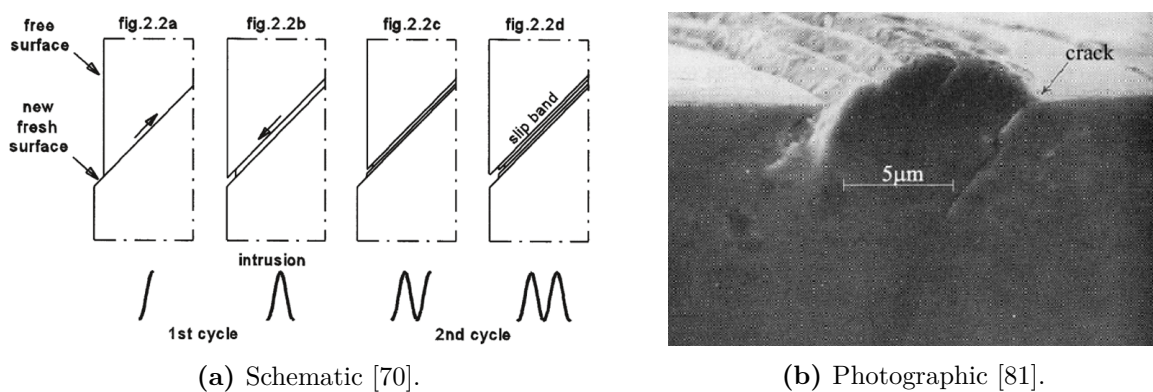


Figure 1: Crack initiation by formation of slip bands.

The total fatigue life N_f is thus composed of two distinct phases, a crack initiation phase N_i and a crack propagation phase N_p

$$N_f = N_i + N_p \tag{1.1.1}$$

The length of the initiation phase is highly dependent on the surface condition and the material strength. In the crack propagation phase on the other hand, the surface condition is insignificant, and the crack propagation rate is not so much dependent on the material strength as it is on the material elastic modulus.

It is important to distinguish between the two phases, since they are driven by different mechanisms. Unfortunately, no generally accepted quantitative measure exists describing when one phase is over and the next begins. As indicated in Fig. 1 a single cycle may be sufficient to create a microscopic crack.

In practice however, a visible/measurable crack length of $a \approx 0.1 - 1.0\text{mm}$ is often used to distinguish the initiation and propagation phase.

For machine components the crack initiation phase covers most of the life. For welded structures on the other hand, small crack-like defects are generally present already at production, so the entire life is considered to be spent in the propagation phase. A crude, but illustrative example is give in Table 1.

Table 1: Distribution of fatigue life.

	Crack initiation, N_i	Crack propagation, N_p
Machine components	90 – 100%	0 – 10%
Welded components	0 – 10%	90 – 100%

1.2 Fatigue loading

As already mentioned fatigue occurs due to cyclic or varying loads. An example of such is shown in Fig. 2 which shows two categories of loading; constant amplitude (CA) and variable amplitude (VA) loading, respectively. For now, we consider only CA loading.

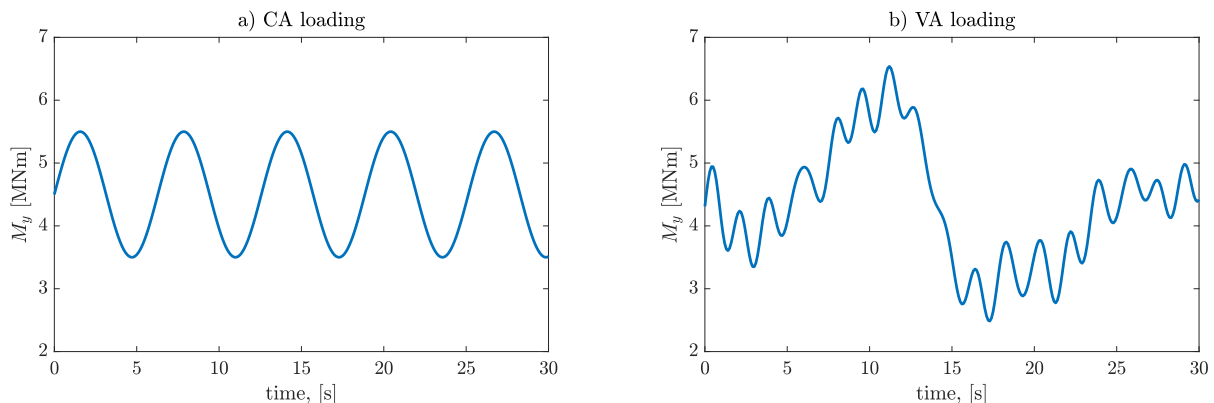


Figure 2: Fatigue loading example: wind turbine mainshaft bending moment.

Fatigue loads are usually established in one of the following ways:

1. Agreement with customer; e.g. maximum load capacity and minimum service life
2. Requirements from code or tradition
3. Simulations including dynamic effects, e.g. vibrations, inertial loads
4. Measurements from load cells or strain gauges on existing component, maybe scaled

It should be noted that the actual shape of the load-time series between the peaks is insignificant in most practical cases. The same goes for the timing/frequency of the loads. The only relevant parameters are the magnitude of the mean and peak loadings.

The fatigue load is used to calculate the fatigue stresses. Handling variable load-time histories as in Fig. 2 can be quite cumbersome, as the stresses needs to be calculated over time for each location of interest in the component.

When dealing with such load-time series, fatigue software is usually applied. Alternatively, a damage equivalent load (DEL) may be calculated. This single cycle equivalent load should then lead to the same fatigue damage as would be found using the entire load-time series. Load-time series and equivalent loads will be dealt with later in chapter 5. Initially, we consider constant amplitude loading and fatigue stress in general.

1.3 Fatigue stress

Fatigue damage is governed by the fluctuations in stresses rather than the maximum stress; hence the stress amplitude σ_a (or range $\Delta\sigma$) and the mean stress σ_m are the most significant parameters in a fatigue assessment.

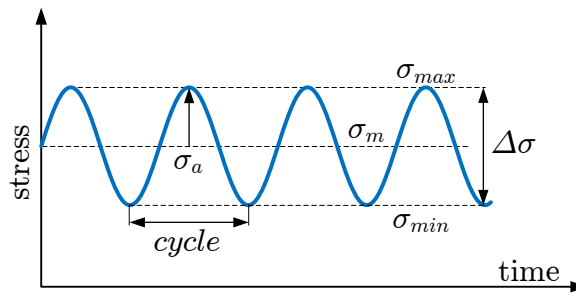


Figure 3: Stress related notation.

The stress range is found as the difference between the minimum and maximum stress in a cycle.

$$\Delta\sigma = \sigma_{max} - \sigma_{min} = 2\sigma_a \quad (1.3.1)$$

The stress range or amplitude can be established in terms of nominal or local stresses. Additionally, various directional stress components (e.g. σ_x) or principal stresses (e.g. σ_1) can be used. With so many choices, it necessary to explain in text or using subscripts which particular stress, the range or amplitude relates to.

It is traditional to use stress amplitudes for machine components and stress ranges for welded components, a tradition we will follow in this document.

In practice, the mean stress is often related to the stress amplitude, such that if the amplitude is increased, so is the mean stress. This condition may be expressed through a constant stress ratio

$$R = \frac{\sigma_{min}}{\sigma_{max}} = \frac{\sigma_m - \sigma_a}{\sigma_m + \sigma_a} \quad (1.3.2)$$

Referring to Fig. 4, the most commonly applied stress ratios in fatigue tests are $R = -1$ (fully reversed loading, e.g. rotating bending) and $R = 0$ (pulsating tension).

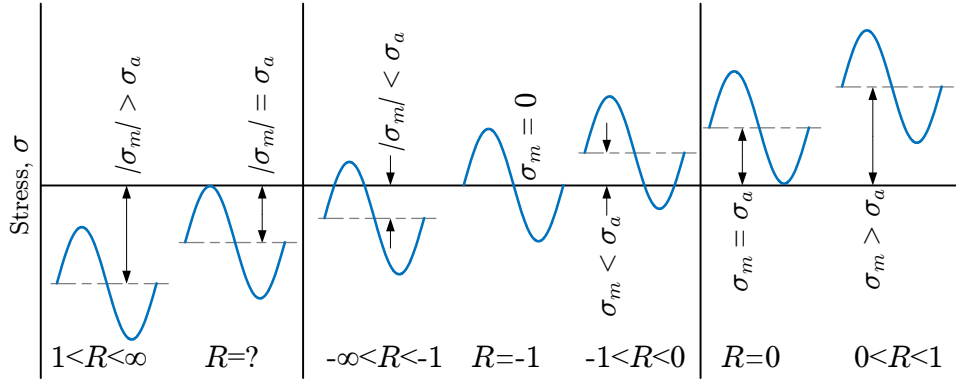


Figure 4: Example relations between mean stress and stress amplitude and the associated stress ratios, after Radaj and Vormwald [67].

A number of useful formulas can be deduced from Fig. 3 and the stress ratio [67]

$$\sigma_m = \frac{1}{2}(\sigma_{max} + \sigma_{min}) = \frac{1}{2}\sigma_{max}(1 + R) = \sigma_a \frac{1 + R}{1 - R} \quad (1.3.3)$$

$$\sigma_a = \frac{1}{2}(\sigma_{max} - \sigma_{min}) = \frac{1}{2}\sigma_{max}(1 - R) = \sigma_m \frac{1 - R}{1 + R} \quad (1.3.4)$$

$$\sigma_{max} = \sigma_m + \sigma_a = \frac{2\sigma_m}{1 + R} \quad (1.3.5)$$

$$\sigma_{min} = \sigma_m - \sigma_a = \frac{2\sigma_m R}{1 + R} \quad (1.3.6)$$

Since fatigue is a highly directionally dependent phenomenon, we usually apply a directional stress component, e.g. $\sigma_x/\sigma_y/\sigma_z$ (depending on the orientation of the coordinate system) or the principal stress σ_1/σ_3 to calculate the stress amplitude, rather than a combined stress such as the von Mises equivalent stress σ_{vM} .

1.4 Fatigue strength

For high cycle fatigue, the fatigue strength is commonly expressed through an SN curve. Many similar variants of SN curves are used in the literature, e.g. linear, bilinear or nonlinear. Usually they are plotted on double-logarithmic axes, but sometimes the stress axis is linear. Furthermore, the stress axis may be given in either ranges or amplitudes. They are conceptually identical in that they describe “what is the expected life at a given stress amplitude”. In this text we generally use the bilinear form shown in Fig. 5.

1.4.1 SN curve definition

The SN curve is divided in a primary part (to the left of the knee) and a secondary part (after the knee). It is defined by the endurable stress amplitude at the knee point $\sigma_{R,D}$ and the primary slope m_1 . We use subscript R to denote *resistance*.

The knee point is located at some specified number of cycles N_D , typically 10^6 to 10^7 after which the slope changes to m_2 . The value m is called *the slope*, however, it is really the negative reciprocal of the slope. It is typically in the range of 3 – 10 for the primary part of the SN curve.

The fatigue strength may be given either in terms of ranges or amplitudes.

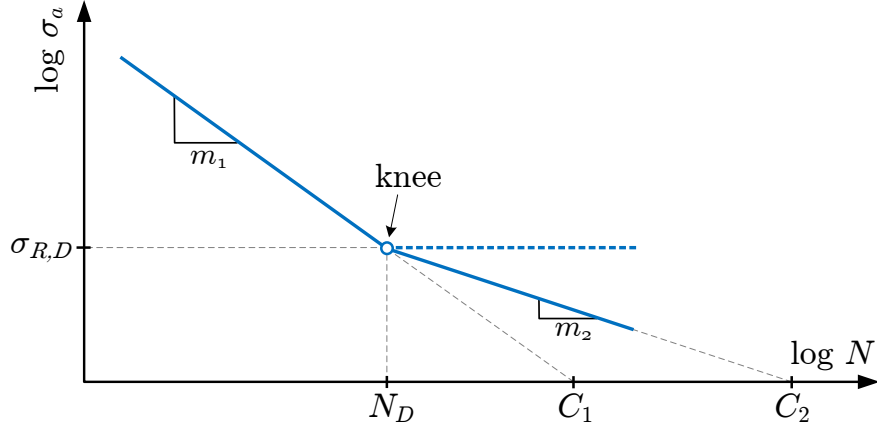


Figure 5: Definitions of the bilinear SN curve.

$$\Delta\sigma_R = 2\sigma_R \quad (1.4.1)$$

As indicated in Fig. 5, the behavior of the SN curve after the knee may take two forms. It may either flatline or continue decreasing at some slower rate. The first is typically what is observed in laboratory tests, whereas the second probably represents a more realistic scenario.

For the flatline case, the fatigue strength may also be referred to as the *fatigue limit* or the constant amplitude fatigue limit (CAFL), because it may not be present under variable amplitude loading. Also, some materials do not exhibit a fatigue limit at all or under certain conditions (e.g. in a corrosive environment).

Any part of an SN curve is described by the following relationship

$$N \cdot \sigma_a^m = C \quad (1.4.2)$$

Typically it is divided in a primary and the secondary (post-knee) part as described by

$$\begin{aligned} N \cdot \sigma_a^{m_1} &= C_1 \\ N \cdot \sigma_a^{m_2} &= C_2 \end{aligned} \quad (1.4.3)$$

Here, C is the fatigue capacity which can be calculated from any known point on the curve, e.g. $(\sigma_{R,D}, N_D)$

$$C_1 = N_D \cdot \sigma_{R,D}^{m_1} \quad (1.4.4)$$

The fatigue capacity describes the intercept of the SN curve with the primary axis (N) at a stress amplitude of $\sigma_a = 1$, i.e. it will be a very large number. Knowing the fatigue capacity, it is possible to determine the fatigue life for a given stress amplitude

$$N = \frac{C_1}{\sigma_a^{m_1}} \quad (1.4.5)$$

Alternatively, given a required life N , the allowable stress amplitude can be found

$$\sigma_a = \sqrt[m_1]{\frac{C_1}{N}} \quad (1.4.6)$$

The above equations can of course be used for both the primary and secondary part of the SN curve using the respective values for C and m .

For the sake of understanding the "slope" m we can rewrite eq. (1.4.6) to show an alternative form of the equation for the SN curve

$$\sigma_a = A \cdot N^b \quad (1.4.7)$$

where $A = \sqrt[m]{C_1}$ is the intercept with the stress axis at $N = 1$ and $b = -1/m_1$ is the real slope. Both eq. (1.4.2) and (1.4.7) describes the same straight line in a log-log plot.

We distinguish between the following types of SN curves:

- Experimental: An SN curve fitted to experimental fatigue data. These are the best. They describe the fatigue strength of the specimens to the best possible degree.
- Synthetic: An SN curve generated from a textbook framework. The accuracy is typically unknown, but since the framework may cover a wide variety of materials and conditions, it can be expected to be relatively low.
- Codified: an SN curve from a code (e.g. Eurocode 3 [11]). These are generally quite conservative because they take into account worst case detrimental effects that *may* arise for the component at hand.

Which type of SN curve to use depend on the problem at hand.

1.4.2 SN curve derivation from experiments

Fatigue testing is typically carried out on small specimens with some well-defined characteristics or using specimens cut out of an actual component. Very often series of tests are carried out in order to assess the effect of some parameter, e.g. the surface roughness. For each specimen the stress amplitude and resulting fatigue life is recorded. Statistical analysis can then be used to establish the SN curve, once a sufficient number of specimens n have been tested.

The test data is plotted in a log-log diagram as exemplified in Fig. 6, which also shows the definition of the mean (50%) and design (95%) SN curves. A peculiarity of SN plots is that the dependent variable N is plotted on the primary axis, and the independent variable σ_a on the secondary axis. This is not the typical way plots are constructed, but deeply rooted in tradition.

Distinguishing the dependent and independent variables is important when fitting the SN curve, i.e. the scatter to be minimized is in terms of the dependent variable. That the life is the dependent variable is easily understood when considering the fatigue test; a specimen is loaded at some given stress amplitude, i.e. the resulting fatigue life is a function of this - not the other way around.

The following procedure is equally applicable to stress ranges and amplitudes, but C will take different values. If we take the logarithm (base-10) on both sides of eq. (1.4.2), we get the following linear expression

$$\log C = \log N + m \cdot \log \sigma_a \quad (1.4.8)$$

The slope m is then calculated by linear regression using the stress amplitude as the independent variable [9], i.e. by minimizing the squared distance between the data points and the fitted mean SN curve

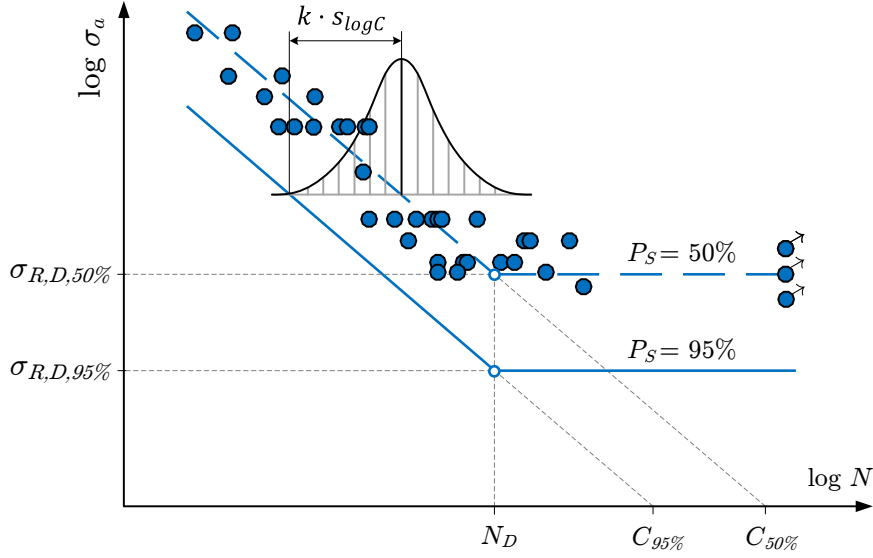


Figure 6: Mean and design SN curves derived from fatigue test results.

$$m = - \frac{\sum(\log \sigma_{a,i} \cdot \log N_i) - \frac{1}{n} \sum \log \sigma_{a,i} \cdot \sum \log N_i}{\sum(\log \sigma_{a,i})^2 - \frac{1}{n} \cdot (\sum \log \sigma_{a,i})^2} \quad (1.4.9)$$

When calculating the primary slope m_1 , it is important to exclude data points that should not affect it, e.g. data points after the knee (they relate to m_2), run-outs and outliers. The secondary slope is typically calculated as a function of m_1 rather than directly from test data (section 2.6). The position of the knee-point N_D is typically determined simply by looking at the data and estimating an appropriate value.

In many cases the data set is not sufficiently large to determine the slope properly, in such cases a specified slope may be used, which can be obtained from other similar tests on larger data sets. For example, $m = 3$ is typically used for welded joints.

The logarithm of the mean fatigue capacity is found by averaging the fatigue capacity calculated for each specimen using eq. (1.4.8)

$$\log C_{50\%} = \frac{1}{n} \sum_{i=1}^n \log C_i \quad (1.4.10)$$

where $C_i = N_i \cdot \sigma_{a,i}^m$. The logarithm of the mean fatigue strength at N_D cycles can now be determined, again using eq. (1.4.8)

$$\log \sigma_{R,D,50\%} = \frac{\log C_{50\%} - \log N_D}{m} \quad (1.4.11)$$

This corresponds to a survival probability of $P_S = 50\%$. For design purposes it is usually desired to ensure a much higher survival probability, typically $P_S = 95\%$ or higher. An additional partial safety factor γ_{Mf} is also added on top of this.

To determine the design fatigue strength, e.g. corresponding to a 95% survival probability, we start by calculating the associated design fatigue capacity. This is typically done by assuming a log-normal distribution of the test data around the mean, as shown in Fig. 6. In many cases,

this is a poor fit, or there may be insufficient data to justify it, however it is still the prevailing approach.

$$\log C_{95\%} = \log C_{50\%} - k \cdot s_{\log C} \quad (1.4.12)$$

Here $s_{\log C}$ is the standard deviation of $\log C$ and k is the number of standard deviations that need to be subtracted to get to the 95% fractile¹. Often k is taken as a function of the number n of test specimens [27], e.g.

n	10	15	20	25	30	40	50	100
k	2.7	2.4	2.3	2.2	2.15	2.05	2.0	1.9

The design fatigue strength is now found as in eq. 1.4.11

$$\log \sigma_{R,D,95\%} = \frac{\log C_{95\%} - \log N_D}{m} \quad (1.4.13)$$

Lastly, of course, the logarithm needs to be lifted.

$$\sigma_{R,D,95\%} = 10^{\log \sigma_{R,D,95\%}} \quad (1.4.14)$$

When dealing with SN curves, it is important to remember the associated probability of survival, e.g. when comparing. Estimating outcomes of experiments is best done using the 50% curve, whereas comparing against codes must be done using the same probability of survival as in the code, e.g. 95%.

1.5 Summary

This chapter introduced the fatigue phenomenon in terms of the two distinct phases; crack initiation and crack propagation. It also presented the SN curve, which is the main concept used for fatigue design. Application of the SN curve for estimating fatigue life or determining allowable stress amplitudes was discussed. Lastly, we discussed derivation of mean and design SN curves from fatigue test results.

¹In general, $\log C_p$ may be determined for any probability $p = 1 - P_S$ [0-1] from the inverse cumulative distribution function. For example in Matlab, this may be achieved using $\log C_p = \text{icdf}(\text{'Normal'}, p, \log C_{50\%}, s_{\log C})$.

Part I

Machined components and general concepts

2 Fatigue strength modifications

As will become painfully clear in this chapter, fatigue is not controlled by the material alone. The fatigue strength and course of the SN curve is highly dependent on many other factors besides just the material. This chapter presents an overview of the dominating features controlling fatigue strength, discusses the physical reasons behind and lastly presents recommendations for design.

The best way to obtain a good SN curve is of course to do full-scale testing on a large number of components using realistic loading conditions. This is rarely possible however, so instead an SN curve is generated from small scale specimens often tested under idealized conditions. In order to apply the knowledge obtained this way, we imagine that the small scale specimens represent the critical location of the component. Ideally everything should be identical, i.e. material, size, surface, etc.

When the available SN curve does not represent a component sufficiently well, e.g. the surface roughness is different, we need to correct for it. This means scaling the fatigue strength using corrections derived from series of fatigue tests, preferably derived from tests under conditions matching the component as far as possible.

Examples of effects which imply corrections to the SN curve (if the curve does not already include these) are shown in Fig. 7. If one of these parameters is different between the component and the specimens from which the SN curve is derived, a correction is needed.

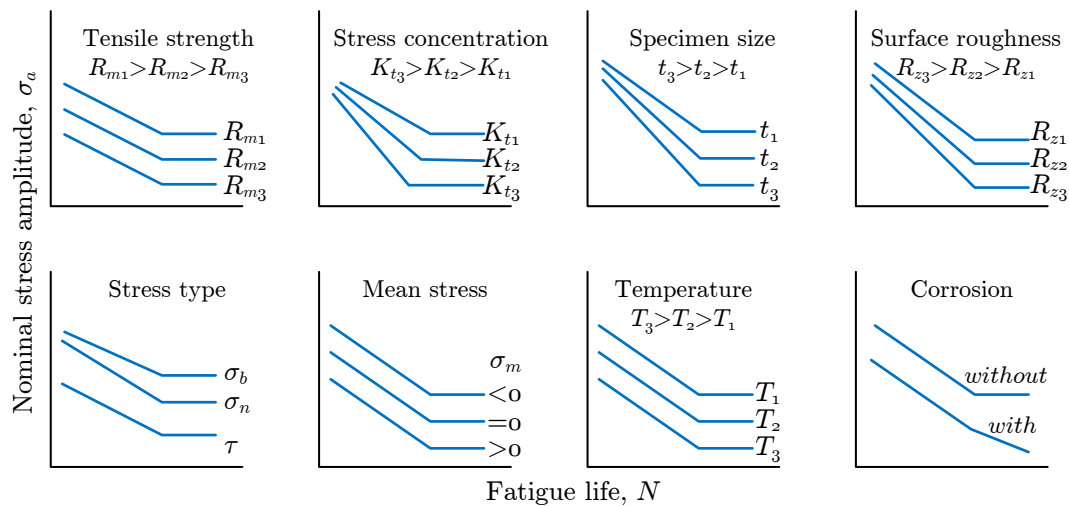


Figure 7: Factors affecting the fatigue strength, after [22], slightly modified.

The influence of these effects is discussed in the following, where also suggestions for corrections are given. It should be noted, that the effects are generally not independent, e.g. the material strength effect will be dependent on the surface roughness and so forth. Such dependencies are generally disregarded though.

2.1 Material strength effect

The material strength (yield strength R_e or tensile strength R_m) is highly influential on the fatigue strength in the crack initiation phase, but not in the crack propagation phase. Indeed, it has been shown that the crack propagation rate is much more dependent on the modulus of elasticity E [39].

This difference is indicated in Fig. 8, where e.g. the fatigue strength of welded joints (which spend most of their life in the crack propagation phase) does not depend much on the material strength.

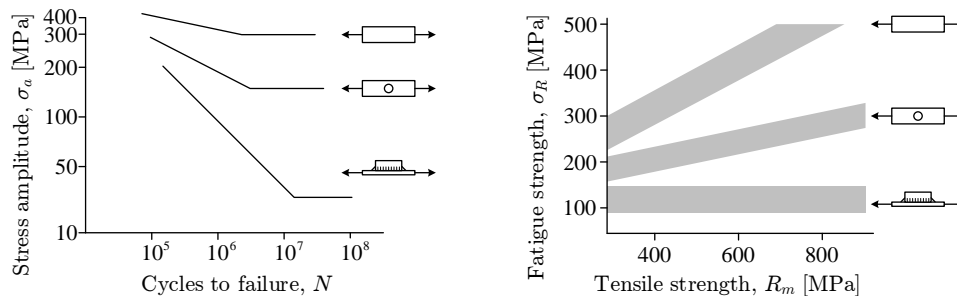


Figure 8: Left: the fatigue strength of notched and welded specimens is lower than for plain specimens. Right: only cases with significant crack initiation phase benefits from higher material strength [46].

As a starting point, the knee point fatigue strength of small un-notched, polished specimens in rotating bending (zero mean stress) can be estimated from the ultimate tensile strength for several engineering metals. This reference is called the *material fatigue strength*, denoted by an asterisk(*).

$$\sigma_{R,D}^* = \alpha_0 \cdot R_m + \beta_0 \quad (2.1.1)$$

The constant α_0 is in the range of 0.3-0.6 for typical engineering metals, e.g. $\alpha_0 \approx 0.5$ and $\beta_0 = 0$ for steel, see Fig. 9. It should be noted, that this is the mean fatigue strength, i.e. leading to 50% survival probability. All fitting parameters will be denoted α and β in the following, please refer to Table 3 for numerical values.

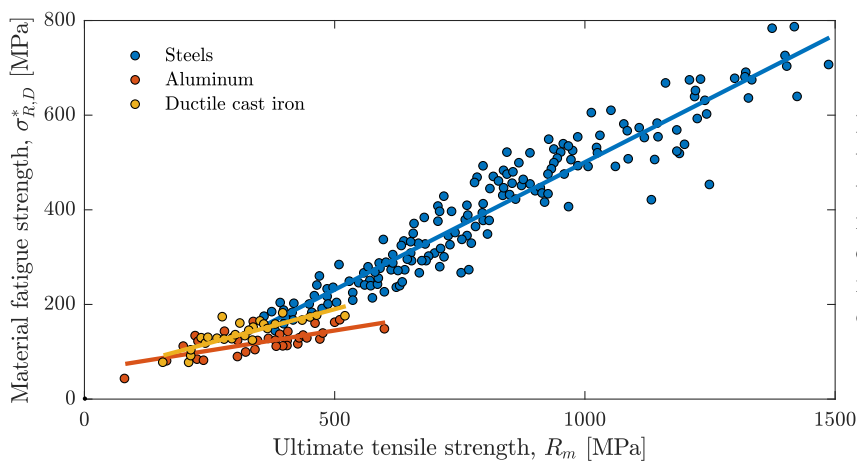


Figure 9: Relationship between tensile strength and fatigue limit for small, un-notched, polished specimens of steel subjected to rotating bending (zero mean stress), data from [70].

2.2 Mean stress effect

It is found from tests, that the fatigue strength decreases with increased mean stress. An example of this dependency for ductile cast iron is shown in Fig. 10. Most materials show similar behavior; that for increased mean stress, the fatigue strength diminishes. The opposite also holds; in case of compressive mean stresses, the fatigue strength increases.

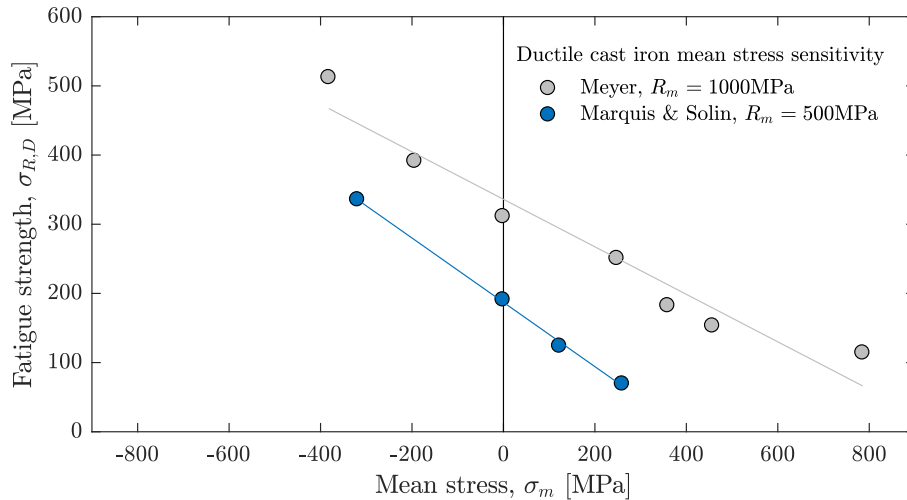


Figure 10: Mean stress dependency for ductile cast iron (GJS), data from [42, 45].

The effect of mean stresses can be handled by several corrections; common for all is that the allowable stress amplitude is scaled down in the presence of tensile mean stress. For compressive mean stresses, it is often reasonable to extrapolate the correction line, as illustrated by the dashed lines in Fig. 11. It is of course more conservative not to do this, however many experiments have shown it is safe [70].

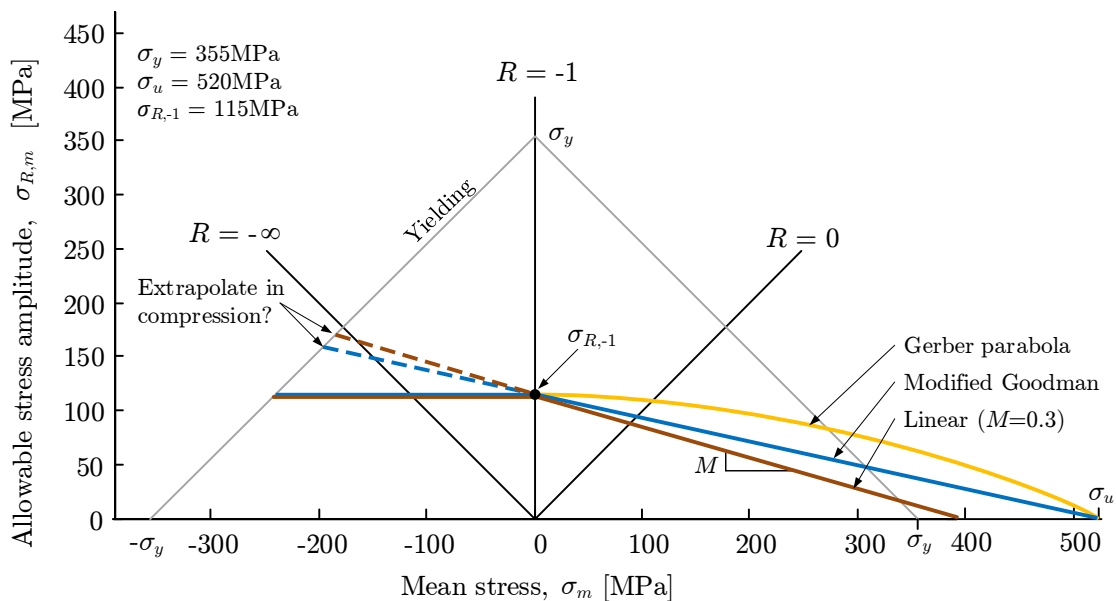


Figure 11: Haigh diagram showing different mean stress corrections.

Residual stresses can be treated as mean stresses, as long as these are known and stable (which they are typically not). Introduction of compressive residual stresses by peening or deliberate overloading is a common trick to increase the fatigue strength of a component. In such cases the stability of these residual stresses must be ensured, i.e. no localized yielding may occur in the treated area, ever! Otherwise, the residual stresses will relax or maybe even become tensile.

In the following subscripts on the fatigue strength indicate the associated stress ratio, e.g. $\sigma_{R,-1}$ is the fatigue strength at zero mean stress ($R = -1$). The fatigue strength at a given mean stress σ_m is then determined using a correction factor k_{mean} as follows

$$\sigma_{R,\sigma_m} = k_{mean} \cdot \sigma_{R,-1} \quad (2.2.1)$$

2.2.1 Linear correction

The linear mean stress correction reduces the allowable stress amplitude depending on a single parameter M called the mean stress sensitivity [68]

$$k_{mean} = 1 - \frac{M\sigma_m}{\sigma_{R,-1}} \quad (2.2.2)$$

The mean stress sensitivity M is determined from experiments and is defined as follows. It corresponds to the slope of the green line in Fig. 11. The value of M is typically in the range of 0.3.

$$M = \frac{\sigma_{R,-1}}{\sigma_{R,0}} - 1 \quad (2.2.3)$$

This correction is popular in the German literature, e.g. Gudehus and Zenner [22].

2.2.2 Modified Goodman

The Modified Goodman correction is equivalent to the Linear mean stress correction in that the reduction of the allowable stress amplitude is linear. Indeed, M can be selected in such a way, that the two corrections are identical. This correction is recommended for high-strength/low-ductility materials and requires only one material parameter, the tensile strength R_m [70].

$$k_{mean} = 1 - \frac{\sigma_m}{R_m} \quad (2.2.4)$$

2.2.3 Gerber parabola

The Gerber correction is mathematically similar to the Modified Goodman correction, except that the last term is squared, causing it to describe a parabola in the Haigh diagram. It is thus less conservative compared to the Modified Goodman correction. This option is recommended for *reasonably ductile* materials [70]. It only makes sense for tensile mean stresses, $\sigma_m > 0$.

$$k_{mean} = 1 - \left(\frac{\sigma_m}{R_m} \right)^2 \quad (2.2.5)$$

2.3 Surface roughness effect

As already explained, the surface roughness has a large influence on the fatigue strength in the crack initiation part of the fatigue life. The microscopic ridges in the surface typically obtained after machining will act as crack initiation locations. Typically a correction factor is applied to the fatigue strength of polished specimens, defined as

$$k_{surf} = \frac{\sigma_{R,rough}}{\sigma_{R,polished}} \quad (2.3.1)$$

It is found that higher strength materials are more sensitive to surface roughness, so k_{surf} depends on the material tensile strength R_m and the surface roughness R_z , see Fig. 12.

Additional effects of the surface condition, e.g. whether it is rolled, forged or machined may also influence the fatigue strength. Unfortunately, the effect is not well investigated and often a correction based on machined steel specimens is used in the absence of more material specific knowledge.

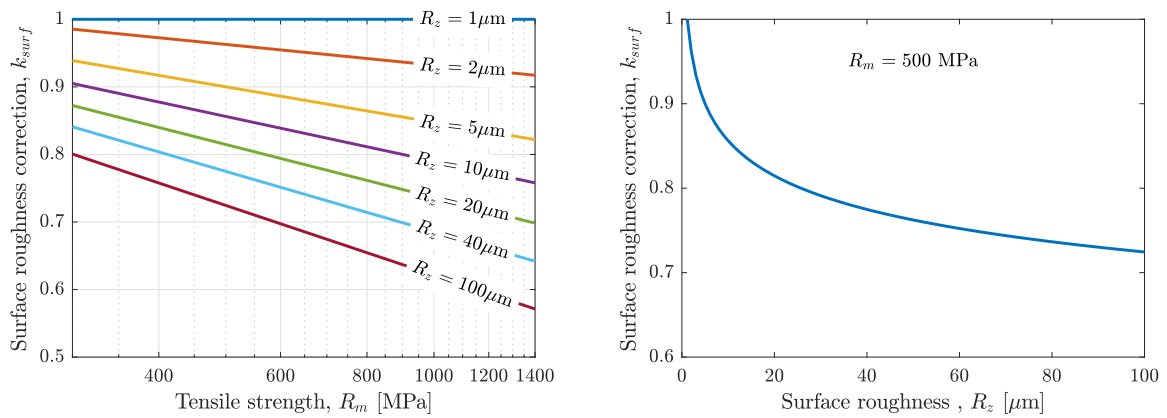


Figure 12: Correction factor for surface roughness, after [22].

2.4 Size/thickness effect

Tests show that larger specimens have lower fatigue strength than smaller ones as shown in Fig. 13. This is called the size/thickness effect. It is comprised by three sub-effects; the so-called geometric-, statistical- and technological size effects, as explained in the following.

Unfortunately, it is difficult to separate the effects and a single correction factor is typically applied to account for all sub-effects, as in eq. 2.4.1.

The fatigue strength of a component of thickness t can be estimated from that of small scale specimens of thickness t_{ref} using the following expression.

$$k_{size} = \left(\frac{t_{ref}}{t} \right)^{\alpha_t} \quad (2.4.1)$$

Here, α_t is called the thickness correction exponent. It is typically in the range of 0.1 – 0.3. For round components use the diameter instead of the thickness.

This effect is linked to the thickness of components per tradition, however, it would probably be more reasonable to consider the volume instead.

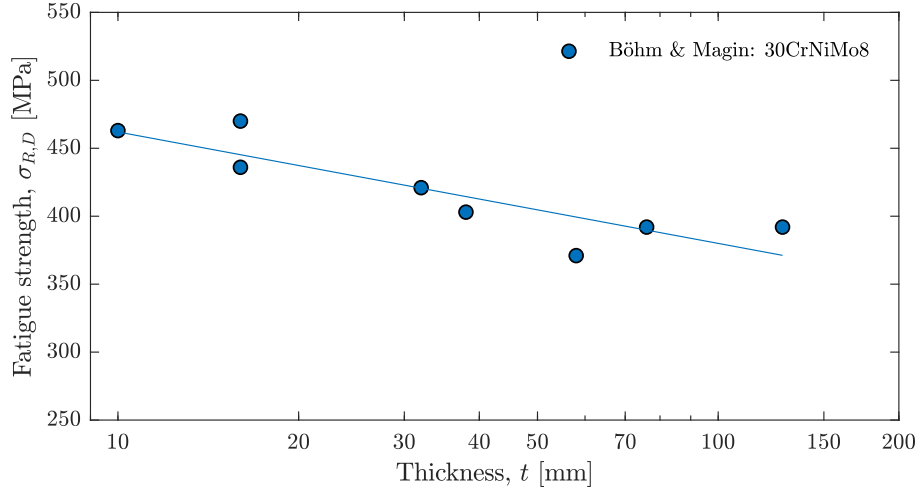


Figure 13: Experimental investigations of the size effect, data from [26].

2.4.1 Geometric size effect

The geometric size effect relates to the stress gradient due to stress concentrations and direct or superimposed bending, which becomes steeper when the joint become thinner, see Fig. 14. The combined stress field at the crack tip of a given crack size a_i will thus be less intense for a thin joint compared to a thick joint, i.e. for $t_1 < t_2$, we get $\sigma_1 < \sigma_2$, when the nominal surface stress is the same.

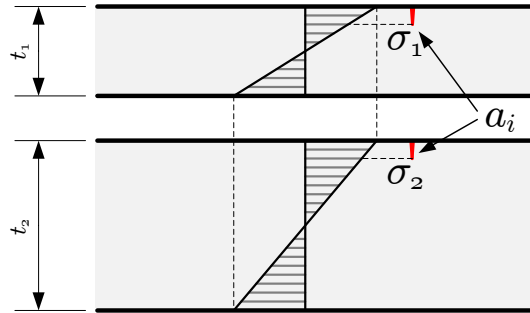


Figure 14: Geometric size effect.

The stress gradient effect do not only occur in case of bending, similar tendencies are observed below notches in pure tension. This effect is strongly linked to the notch support effect, see Chapter 3.

2.4.2 Statistical size effect

The statistical size effect considers that the probability of a severe defect occurring is higher in a large volume (thick joints) than in a small volume (thin joints).

Some materials are more prone to this effect than others. Steel, for example, which has a very nice homogeneous microstructure usually fails from defects on the surface, and is thus not not as affected by this. Cast iron, on the other hand, usually fails from embedded/internal defects and therefore will be very affected.

Referring to Fig. 15, imagine that we have some material containing a severe defect (red). If we

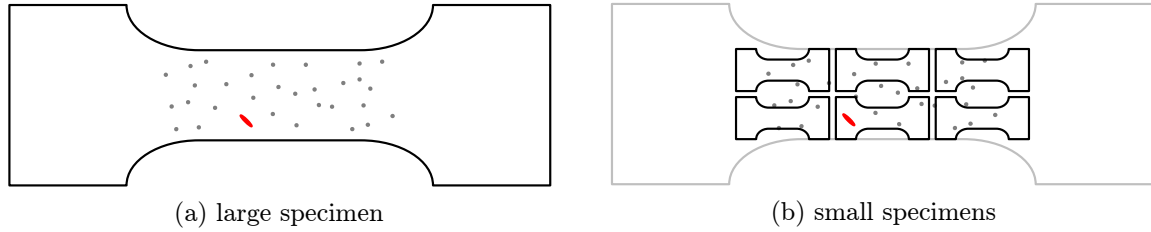


Figure 15: Statistical size effect.

make one large specimen from all the material, it will necessarily contain the severe defect and, when tested, it will show low fatigue strength.

If instead we made 6 small specimens from the same material, only one of them will contain the severe defect. So when testing, one of the resulting data points will show low fatigue strength, while the other 5 will show much higher fatigue strength.

2.4.3 Technological size effect

The technological size effect refers to the rougher manufacturing conditions typically applied for larger structures. It also accounts for differences in residual stresses, surface roughness and microstructure.

It is well known that the cooling rate of thicker sections is slower, e.g. during casting, which leads to lower static strength and hence lower fatigue strength according to section 2.1.

This effect can be considered either by applying eq. 2.4.1 or by measuring and applying the tensile strength R_m of the material thickness in question in eq. 2.1.1 [20]. In the latter case, it is important to remember, that the geometrical and statistical size effects are not covered.

2.5 Environmental effects

2.5.1 Temperature

The effect of temperature is typically not necessary to consider, as long as the temperature does not affect the material properties, e.g. $-25^\circ\text{C} < T < 60 - 100^\circ\text{C}$. In case of temperatures exceeding this range, corrections can be found in [15] or derived based on the reduced material strength and stiffness at the given temperature.

2.5.2 Corrosion

For components operating in a corrosive environment on the other hand, this can have a dramatic effect on the fatigue strength. In the crack initiation phase, corrosion pits will act as crack initiation sites. Similarly, in the crack propagation phase, corrosion will usually accelerate crack growth.

In a corrosive environment, the cut-off on the SN curve tends to vanish, and the fatigue strength may be severely reduced.

2.6 Variable amplitude loading

The long life fatigue strength is different between constant- and variable amplitude loading. As seen in Fig. 16, especially the post-knee part of the SN curve deviates.

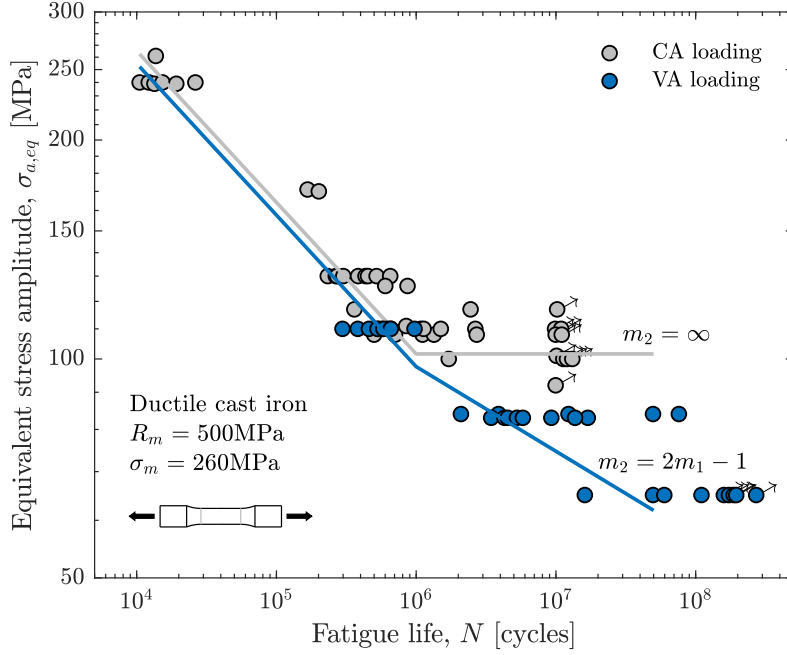


Figure 16: Effect of variable loading, data from [42].

For constant amplitude loading a *fatigue limit* (SN curve flat-lining, $m_2 = \infty$) is typically observed in laboratory tests, i.e. below some stress amplitude, cracks do not initiate and the fatigue life is in principle infinite. If the same tests are carried out under variable amplitude loading, on the other hand, the post-knee part of the SN curve typically tends to decline at some slope $m_2 > m_1$. This is because a large stress amplitudes in VA loading may be sufficient to initiate a crack, and subsequent small stress amplitudes may be sufficient to propagate the crack.

Many proposals have been made for estimating the secondary slope in VA loading. The most commonly applied is that of Haibach [25], estimating m_2 from

$$m_2 = 2m_1 - 1 \quad (2.6.1)$$

As is also evident from Fig. 16 the pre-knee part of the SN curve may also be slightly lower for VA loading, however, this is generally ignored.

2.6.1 Summary

This chapter presented some of the main features which may modify the fatigue strength. Experimental observations have been presented and discussed along with explanations of the physical reasons for the observed behavior and preliminary approaches for design calculations. Chapter 4 will present a systematic way of including all potential effects in order to estimate the fatigue strength of an arbitrary component.

There is one more extremely influential feature which often governs the fatigue strength, notches. Notches have both positive and negative effects on a component, so their effect is quite complex, which is why the entire next chapter is devoted to this topic.

3 Effect of notches

In this chapter we investigate the influence of notches on the fatigue strength. Notches may cause very severe reductions in fatigue strength and are among the most difficult to correct for. Important factors such as the stress concentration factor and fatigue notch factor will be introduced. The latter may be estimated using one of several notch support concepts.

3.1 Stress concentrations

The stress concentration factor (SCF or K_t) describes the increase in stress level due to changes in the geometry. It is therefore sometimes called the geometric or theoretical stress concentration factor (hence the subscript t). It is given as the ratio of local notch stress σ_k (e.g. obtained from FE) to the nominal stress σ_n in the section.

$$K_t \equiv \frac{\sigma_k}{\sigma_n} \quad (3.1.1)$$

The SCF primarily depends on the root radius of the notch, secondarily on other geometric parameters of the notch (e.g. opening angle) and loading type (tension/bending). The nominal stress (sometimes also called engineering stress) is easily determined for uniaxially loaded specimens as either the axial or bending stress

$$\sigma_n = \frac{F}{A} \quad (3.1.2)$$

or

$$\sigma_n = \frac{My}{I} \quad (3.1.3)$$

or similar expressions, or maybe a combination. In many practical cases, however, the nominal stress can be very difficult to determine due to complex geometry or loading.

An initial estimate of the fatigue strength of a notched component could be

$$\sigma_{R,notched} = \frac{\sigma_{R,smooth}}{K_t} \quad (3.1.4)$$

However, the effect of a notch on the fatigue strength cannot be fully described by the stress increase due to geometry alone, other factors also contribute. Typically, eq. 3.1.4 will give very conservative values, especially in the case of sharp notches.

A fatigue notch factor (or fatigue effective stress concentration factor) is therefore introduced, which relates the fatigue strength of a smooth specimen to that of a notched specimen.

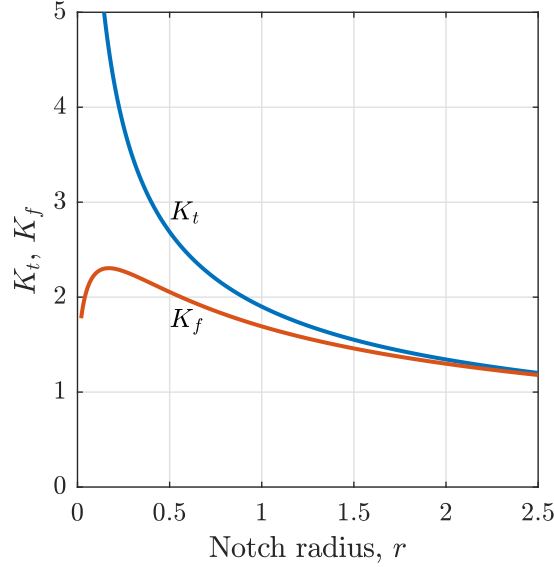


Figure 17: Example relationship between K_t and K_f .

$$K_f \equiv \frac{\sigma_{R,smooth}}{\sigma_{R,notched}} \quad (3.1.5)$$

It thus describes the reduction in fatigue strength due to the notch. It can only be determined accurately from experiments and thus includes both the effect of the geometric stress concentration, but also any other effects, e.g. due to notch support and so forth. Many researchers have tried establishing a relation between K_t and K_f in order to calculate it, with some success, but large deviations are often seen. One thing is clear regarding the magnitude though

$$1 \leq K_f \leq K_t \quad (3.1.6)$$

At mild notches we have $K_f \approx K_t$, whereas for sharp notches $K_f < K_t$, see Fig. 17. It is also seen that the geometric stress concentration approaches infinity as the notch radius approaches zero, whereas the effect on the fatigue notch factor is more moderate.

Methods for estimating K_f are discussed in the following section. Once it is determined, we can use it to correct the fatigue strength for the notch effect

$$\sigma_{R,notched} = \frac{\sigma_{R,smooth}}{K_f} \quad (3.1.7)$$

Figure 18 shows examples of fatigue tests plotted using different stresses on the secondary axis. Firstly using nominal stresses, Fig.18a - as expected the SN curve of the notch specimens are lower than that for the smooth. Fig. 18b then shows the same data in terms of local stresses. This results is more puzzling - suddenly, the notched specimens can endure higher local stresses? This is rather counter-intuitive. It just shows, however, that the local stress alone do not correlate well with the fatigue life. Indeed we need something more to properly describe the effect of the notch. The missing factor is of course K_f . If we instead plot the data in terms of fatigue effective stresses, Fig. 18c, the data collapses in a narrow scatterband, indicating that what we have on the secondary axis fully describe the difference in the data.

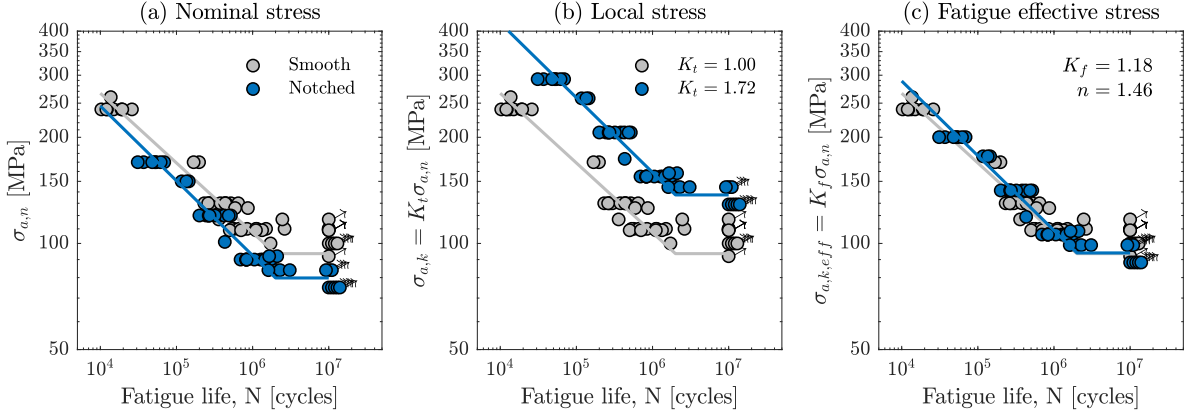


Figure 18: The same fatigue test results plotted using different stresses, data from [43].

3.2 Notch support effect

The main reason for the difference between K_t and K_f is to the so-called notch support effect. Many attempts have been made to establish an approximate relationship between the two, such that K_t is scaled down by a notch support factor n

$$K_f = \frac{K_t}{n} \quad (3.2.1)$$

Here we discuss three of the most common approaches. Generally they are related to the steepness of the stress gradient below the notch, as illustrated in Fig. 19. These concepts can be applied to describe the difference between axial and bending fatigue test results due to the stress gradient also. Furthermore, it should be noted, that the first two concepts are two-dimensional in their nature, whereas the highly stressed volume is the only concept that can be used to describe differences in fatigue strength due to spatial differences in the stress field.

An example of the latter is rotating bending compared to in-plane bending. Here, the highly stressed volume of the rotating specimen is larger compared to the stationary specimen, which can explain why the fatigue strength is lower for the rotating specimen.

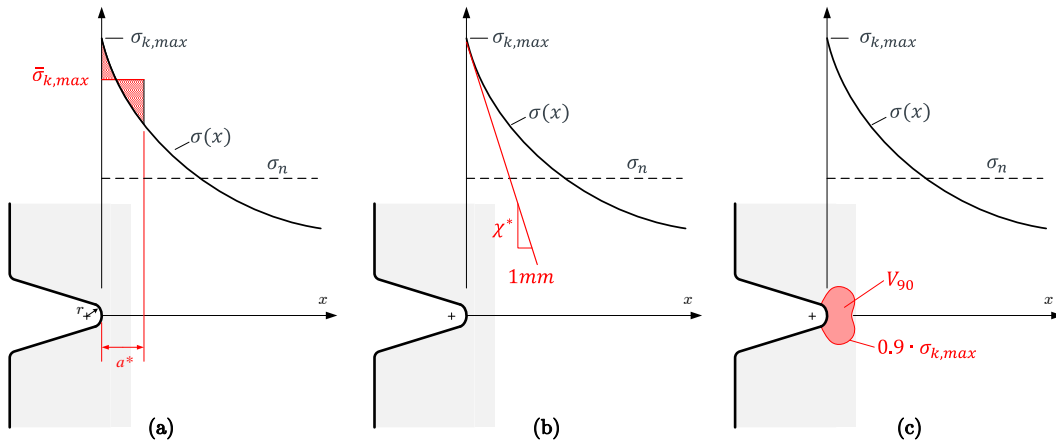


Figure 19: Notch support concepts: a) stress averaging, b) stress gradient and c) highly stressed volume.

It should be noted, that the notch support effect and the size effect are closely linked, and care should be taken when correcting for both. It is conservative to leave out the notch support effect. For all concepts, relevant material parameters can be found in the literature for a relatively small selection of engineering materials. Often these values are used for different materials with unknown success. In critical applications it is therefore recommended to derive specific material parameters for the case at hand, if these are not readily available.

3.2.1 Stress averaging approach

According to Neuber [47] there is a limit to how large stresses can exist in a notch. Accordingly the fatigue notch factor can be calculated equivalently to the stress concentration factor, using an averaged value of the notch stress over a material dependent length a^* , Fig. 19a.

$$K_f = \frac{\bar{\sigma}_{k,max}}{\sigma_n} \quad (3.2.2)$$

It will thus be slightly lower than K_t . Instead of the averaging procedure, Neuber also derived a trick, using a fictitiously enlarged notch radius, see section 10.2.

As yet another alternative K_f can be calculated from K_t as

$$K_f = 1 + q(K_t - 1) \quad (3.2.3)$$

where q is called the notch sensitivity, determined as

$$q = \frac{1}{1 + \sqrt{a^*/r}} \quad (3.2.4)$$

Values of q and a^* can be found in textbooks, e.g. [50]. Limit values are $q = 0$ corresponding to no notch sensitivity at all, i.e. $K_f = 1$, and $q = 1$ indicating full notch sensitivity, i.e. $K_t = K_f$.

3.2.2 Stress gradient approach

In the stress gradient approach, the fatigue notch factor is calculated from the stress gradient below the notch, Fig. 19b, or rather the maximum normalized stress gradient χ^* [22].

$$\chi^* = \frac{1}{\sigma_{k,max}} \frac{d\sigma}{dx} \quad (3.2.5)$$

It has the unit $[\text{mm}^{-1}]$ and can be thought of as *if the stress is 1 at the notch root, what have they fallen to at 1mm depth*. It is a measure of how fast the stress field is decreasing under the notch and thus how much material is subjected to a *high level of stress*.

A support factor n is then introduced as

$$n = 1 + \alpha_n \chi^{*\beta_n} \quad (3.2.6)$$

Here, α_n and β_n are material constants e.g. available in [22] along with analytical approximations for χ^* for simple geometries. Finally, the fatigue notch factor can be determined by scaling down the stress concentration factor with the support factor.

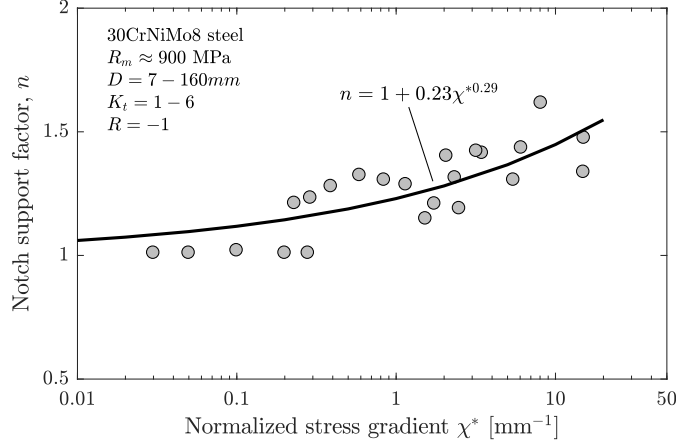


Figure 20: Correlation between the notch support factor and the stress gradient [26].

$$K_f = \frac{K_t}{n} \quad (3.2.7)$$

Determining the stress gradient $\frac{d\sigma}{dx}$ for an arbitrary geometry can be relatively cumbersome, but using FEA and mapping the stress to a path under the notch can help. Experimental data in Fig. 20 show how the notch support factor increases with increased stress gradient.

3.2.3 Highly stressed volume approach

The highly stressed volume is defined as that subjected to a stress higher than some percentage of the maximum notch stress, typically 90%, hence denoted V_{90} , see Fig. 19c.

$$V_{90} = V_{\sigma_k > 0.9\sigma_{k,max}} \quad (3.2.8)$$

Kuguel [33] discovered that this highly stressed volume correlated well with the local fatigue strength as shown in Fig. 21. Thus one can estimate the fatigue strength for a component with an arbitrary V_{90} from

$$\sigma_{R,D,k} = \alpha_h \cdot V_{90}^{-\beta_h} \quad (3.2.9)$$

This volume can be calculated based on the stress gradient for simple geometries or using FEA for arbitrary cases. The idea is that the different fatigue strength obtained for similar specimens with different notches and/or loading can attributed to the difference in highly stressed volume, such that

$$\frac{\sigma_{R,k,1}}{\sigma_{R,k,2}} = \left(\frac{V_{90,1}}{V_{90,2}} \right)^{-\beta_h} \quad (3.2.10)$$

The exponent β_h is a material parameter in the order of 0.03. Using this concept, the fatigue strength of an un-notched (smooth) specimen can be related to that of a notched specimen, and we get

$$K_f = \left(\frac{V_{90,K_t=1}}{V_{90,K_t>1}} \right)^{-\beta_h} \cdot K_t \quad (3.2.11)$$

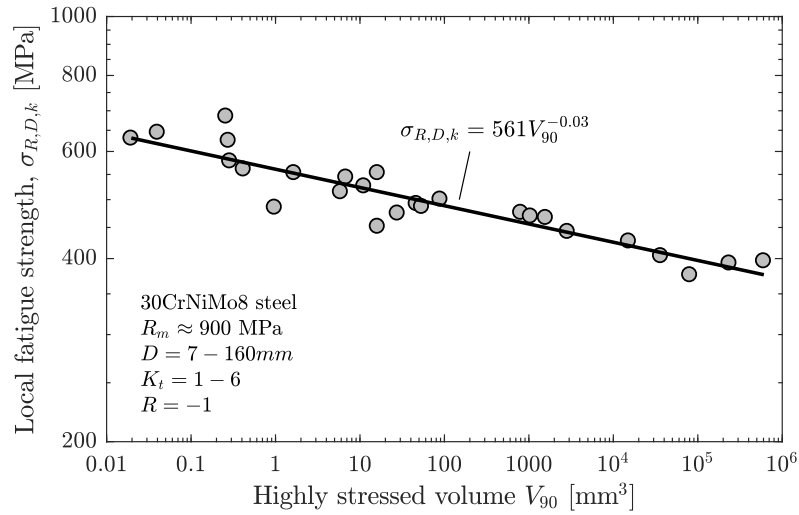


Figure 21: Correlation between the highly stressed volume and the local fatigue strength[26].

Material parameters for this concept are scarcely available, see e.g. [3, 19, 31, 68] and the volume is typically cumbersome to determine. However, it has been found that this approach offers the best predictive capability, compared to the other two approaches discussed here [26].

4 Synthetic SN curves

This chapter describes a systematic way of constructing an SN curve without test data. This is approach usually taken in practical machine design, i.e. estimating the SN curve from material properties and properties of the component in the location of interest.

Many approaches exist for constructing or *synthesizing* an SN curve, in fact any decent textbook on machine design features a system for this, e.g. Shigley's [7], Norton [50], Gudehus & Zenner [22], Rolof/Matek [87] or the FKM guideline [15].

All approaches takes their starting point in the *material fatigue strength*, i.e. the fatigue strength of small, polished specimens tested in rotating bending. Then subjecting it to a number of corrections in order to estimate the SN curve of the component as shown in Fig. 22.

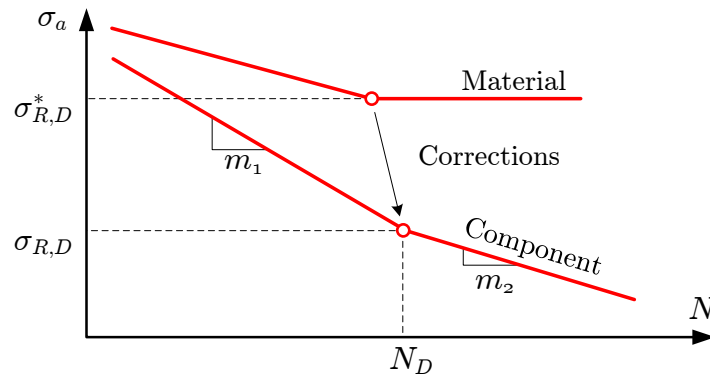


Figure 22: Synthesizing of component SN curve from material SN curve.

An SN curve can be established for either nominal or local stresses. Here we consider first the nominal stresses and later the local stresses. Stress amplitudes σ_a and strength values $\sigma_{R,D}$ are implicitly given in terms of nominal stresses. Sometimes we append a subscript $\sigma_{a,n}$ for emphasis. Local quantities are always denoted by a subscript $\sigma_{a,k}$ though.

In the following an approach is given, which is primarily based on Gudehus & Zenner [22], which is again based on Hück et al. [28]. The approach is modified and expanded however, using elements from Shigley's and the FKM guideline. A number of fitting parameters are needed in the system denoted α_x and β_x . Numerical values for all fitting parameters are given in Table 3.

Note that all SN curves are specific to a single location/notch in the component, i.e. several SN curves are typically needed when assessing a component.

4.1 Nominal stress SN curve

4.1.1 Material fatigue strength

The material fatigue strength (or limit) $\sigma_{R,D}^*$ is the starting point and is found from the ultimate tensile strength of the material

$$\sigma_{R,D}^* = \alpha_0 \cdot R_m + \beta_0 \quad (4.1.1)$$

where R_m is the ultimate tensile strength of the material and α_0 and β_0 are fitting parameters listed in Table 3 for a selection of engineering metals.

4.1.2 Component SN curve

The component fatigue limit is found from the material fatigue limit by applying relevant correction factors as follows

$$\sigma_{R,D} = k_{reliab} \cdot k_{mean} \cdot k_{size} \cdot k_{env} \cdot k_{treat} \cdot \frac{\sigma_{R,D}^*}{\sqrt{K_f^2 - 1 + 1/k_{surf}^2}} \quad (4.1.2)$$

The denominator can be assembled in yet another factor

$$k_{crack} = \sqrt{K_f^2 - 1 + 1/k_{surf}^2} \quad (4.1.3)$$

which describes the susceptibility to crack initiation. This is mainly dominated by the sharpness of the notch (K_t and thus K_f) and the roughness of the surface (k_{surf}). As seen, eq. 4.1.3 resembles the vector sum of these two factors. The primary slope is determined from this factor and material parameters

$$m_1 = \frac{\alpha_k}{k_{crack}^2} + \beta_k \quad (4.1.4)$$

So for high values of K_t or low values of k_{surf} we get steep SN curves, i.e. small m_1 . The knee-point number of cycles is found from the slope as

$$N_D = 10^{\alpha_N - \frac{\beta_N}{m_1}} \quad (4.1.5)$$

The secondary slope can be taken as

$$m_2 = \begin{cases} \infty & \text{for } CA - \text{loading} \\ 2m_1 - 1 & \text{for } VA - \text{loading} \\ m_1 & \text{for } \text{corrosion} \end{cases} \quad (4.1.6)$$

4.1.3 Fatigue notch factor, K_f

The fatigue notch factor is found from the stress concentration factor. In case of complex geometry, where it is not possible to accurately determine a nominal stress and thus K_t , it is necessary to make an estimate.

$$K_f = \frac{K_t}{n} \quad (4.1.7)$$

The notch support factor n is determined from the normalized stress gradient χ^* in $[mm^{-1}]$

$$n = 1 + \alpha_n \chi^{*\beta_n} \quad (4.1.8)$$

Alternative measures for finding the fatigue notch factor could also be considered, see section 3.2.

4.1.4 Mean stress correction, k_{mean}

The mean stress sensitivity is estimated from

$$M = \alpha_m \cdot R_m + \beta_m \quad (4.1.9)$$

The mean stress correction k_{mean} can then be found from eq. 2.2.2 or using any other of the mean stress corrections in section 2.2.

4.1.5 Surface roughness correction, k_{surf}

The surface roughness factor is found as

$$k_{surf} = 1 - 0.22(\log R_z)^{0.64} \cdot \log R_m + 0.45(\log R_z)^{0.53} \quad (4.1.10)$$

where the surface roughness R_z is in $[\mu m]$ and the tensile strength R_m is given in $[MPa]$. Remember to use the base-10 logarithm. For rolled, forged or cast surfaces, set $R_z = 200\mu m$ [15]. For the case of forged steel, the surface correction factor may be modified by including a so-called technology factor depending on the type of forging [22]. For laminar cast iron on the other hand, one may set $k_{surf} = 1$, because fatigue cracks will come from internal defects rather than the surface.

4.1.6 Surface treatment, k_{treat}

An increase in fatigue strength is obtained in case of surfaces subjected to hardening or peening or other treatments. The benefit varies significantly from case to case, but is typically in the range of

$$k_{treat} = 1.0 - 3.0 \quad (4.1.11)$$

It is generally necessary to determine the actual improvement experimentally. The expected range of improvement is given in [15]. In case of surface coated aluminum a reduction may be necessary though, i.e.

$$k_{treat} < 1 \quad (4.1.12)$$

4.1.7 Environmental effects, k_{env}

This correction covers the effects of the environment, e.g. high temperature or corrosive environments. For normal operating temperatures, i.e. $-25^{\circ}\text{C} < T < 60^{\circ}\text{C}$ the temperature does not influence the fatigue strength and we use

$$k_{env} = 1 \quad (4.1.13)$$

for higher (or lower) temperatures consult the literature, e.g. [15].

For corrosive environments, the fatigue strength is severely reduced, and also becomes time dependent (exposure time). A tentative correction factor could be [27]

$$k_{env} = 0.7 \quad (4.1.14)$$

4.1.8 Size/thickness correction, k_{size}

For large components, the fatigue strength needs to be reduced due to the size effect as explained in section 2.4. The following correction factor may be adopted from GL recommendations [20].

$$k_{size} = \left(\frac{25}{t}\right)^{\alpha_t} \quad (4.1.15)$$

The thickness correction exponent can be set to $\alpha_t = 0.1$ for rolled and forged components and $\alpha_t = 0.15$ for cast components.

Alternatively the thickness dependent tensile strength R_m of the material can be applied in eq. 4.1.1 to find the material fatigue strength. In that case it should be noted that this only covers the technological size effect and not the two others which must be considered separately, e.g. using the highly stressed volume concept.

4.1.9 Reliability correction, k_{reliab}

The reliability factor is taken from Table 2, depending on the required probability of survival. A typical value could be $P_S = 99.9\%$. These factors are derived assuming a common scatter (standard deviation) in fatigue data.

$P_S\%$	50	90	95	97.7	99	99.9	99.99	99.999	99.9999
k_{reliab}	1.000	0.897	0.868	0.840	0.814	0.753	0.702	0.659	0.620

Table 2: Reliability factor [7].

4.1.10 Material data

All material specific fitting constants are listed in Table 3. For materials not included in the table, e.g. aluminum, please refer to [15, 87].

4.1.11 Example

Figure 23 shows an example of a synthetic SN curve compared against experimental results. In this case, the agreement between the curve and the data is quite good, but often relatively large deviance is seen.

Material	α_0	β_0	α_n	β_n	α_m	β_m	α_N	β_N	α_k	β_k
Rolled steel	0.45	0	0.45	0.30	0.00035	-0.10	6.4	2.5	12	3
Cast steel (GS)	0.27	85	0.33	0.65	0.00035	0.05	6.8	3.6	5.5	6
Ductile cast iron (GJS)	0.27	100	0.32	0.77	0.00035	0.08	6.8	3.6	5.5	6
Laminar cast iron (GJL)	0.27	110	0.39	0.58	0.00035	0.13	6.8	3.6	5.5	6
Mallable cast iron (GTS)	0.39	0	0.43	0.68	$M = 0.5$		6.4	2.5	7.5	2.5

Table 3: Material values from Gudehus & Zenner [22].

The input data needed for generating the SN curve is given in the lower left and the resulting specification of the SN curve is given in the upper right part of the figure.

Of course, the engineer rarely have actual fatigue data for the component at hand, so such comparison is not possible. It is however possible to find *some fatigue data* that resembles the component to be designed to some extend and then do a comparison with the synthetic curve, and this is highly recommended.

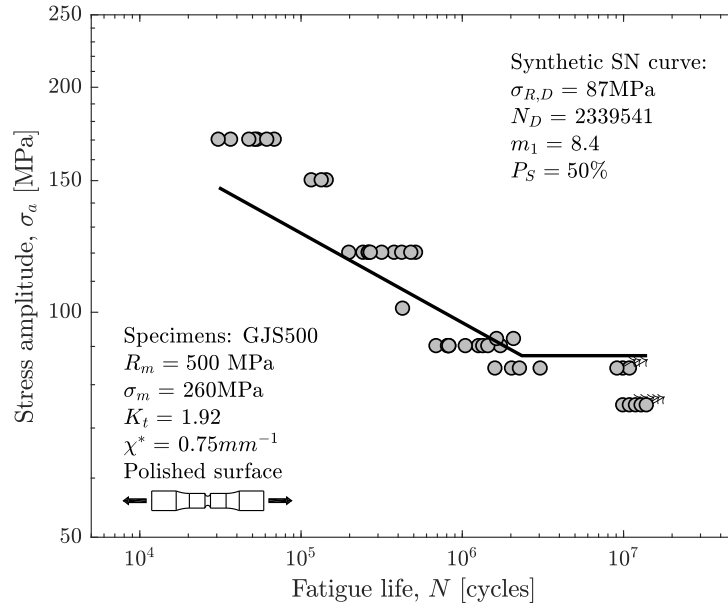


Figure 23: Example synthetic SN curve compared with experimental data from [42].

4.2 Comparison of synthesis frameworks

The system for deriving a component SN curve presented in this chapter is compared qualitatively against similar systems from textbooks. Only the overall trends in the systems are discussed, for details please refer to the sources.

The correction factors are more or less identical, except that they are established using different fitting parameters (α and β). It varies how many, and which, corrections are included.

4.2.1 Norton [50] and Shighley's [7]

This system is probably the simplest system. It is used in terms of fatigue effective stresses $\sigma_{a,eff} = K_f \sigma_a$, rather than nominal stresses. Here, it is rewritten in terms of nominal stresses for the purpose of comparison.

$$\sigma_{R,D} = k_{reliab} \cdot k_{load} \cdot k_{mean} \cdot k_{size} \cdot k_{temp} \cdot k_{surf} \cdot \frac{\sigma_{R,D}^*}{K_f} \quad (4.2.1)$$

Interestingly, different loadings are considered through k_{load} , which takes the following values

$$k_{load} = \begin{cases} 1.0 & \text{for bending} \\ 0.85 & \text{for axial} \\ 0.59 & \text{for torsion} \end{cases} \quad (4.2.2)$$

The knee point is generally fixed at $N_D = 10^6$ cycles, however with modification for some materials. The slope is calculated between two points; the knee point ($N_D, \sigma_{R,D}$) and an upper transition point to LCF ($10^3, \alpha_S \cdot R_m$).

$$m_1 = \frac{3}{\log \frac{\alpha_S R_m}{K_f \sigma_{R,D}}} \quad (4.2.3)$$

where $\alpha_S = 0.9$ for bending and 0.75 for axial loading.

4.2.2 Rolof-Matek [87] and FKM guideline [15]

This system is very elaborate and contains corrections for everything.

$$\sigma_{R,D} = k_{mean} \cdot k_{temp} \cdot k_{treat} \cdot \frac{\sigma_{R,D}^*}{K_f - 1 + 1/k_{surf}} \quad (4.2.4)$$

The slope is fixed at $m_1 = 5$ for normal stress and the knee point at $N_D = 10^6$ cycles.

4.2.3 Gudehus & Zenner [22]

This is basically the same system as presented in this chapter, except that many of the corrections are not explicitly included.

$$\sigma_{R,D} = k_{mean} \cdot \frac{\sigma_{R,D}^*}{\sqrt{K_f^2 - 1 + 1/k_{surf}^2}} \quad (4.2.5)$$

The slope and knee point no. cycles are determined as in eq. 4.1.4 and 4.1.5. In this system, the material fatigue strength $\sigma_{R,D}^*$ is calculated either from the measured/actual tensile strength R_m (if available) or from the required minimum tensile strength scaled up slightly, i.e. $R_m = 1.06 \cdot R_{m,min}$ (e.g. from code).

4.3 Local stress SN curve

The nominal stress SN curve developed in the previous section using eq. 4.1.2 must of course be used for evaluation of nominal stress amplitudes, i.e. for some number of cycles N we require that

$$\sigma_{a,n} \leq \sigma_{R,D,n} \quad (4.3.1)$$

in order to avoid fatigue failure. In many practical cases, however, it is impossible to determine nominal stresses e.g. due to complex geometry or loading. The engineer is thus left with a dilemma where he can calculate very precise local stresses using FE, but is in trouble when the SN curve is defined in terms of nominal stresses. A method for establishing SN curves in terms of local stresses from FE is therefore needed.

Two approaches exist for this; we can scale the nominal SN curve using K_t or we can synthesize a local SN curve straight away.

4.3.1 Scaling SN curve to local stresses

Scaling to local stresses is straightforward using K_t , considering

$$\sigma_k = K_t \cdot \sigma_n \quad (4.3.2)$$

so by pre-multiplication of K_t in eq. 4.3.1 we get

$$K_t \cdot \sigma_{a,n} \leq K_t \cdot \sigma_{R,D,n} \quad (4.3.3)$$

or

$$\sigma_{a,k} \leq \sigma_{R,D,k} \quad (4.3.4)$$

where $\sigma_{R,D,k}$ is the local fatigue strength. The procedure is illustrated in Fig. 24, where the nominal stress SN curve is shifted parallel upwards by K_t . The local stress SN curve can then be used to evaluate stresses from FEA.

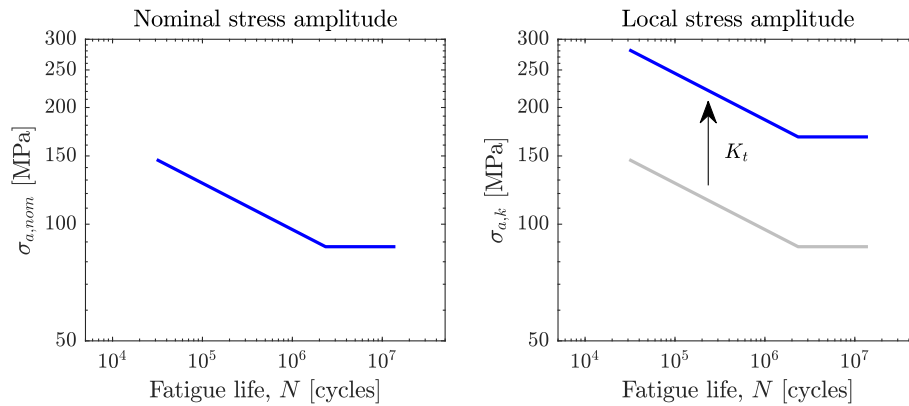


Figure 24: Nominal stress SN curve converted to local stresses.

A major drawback of the scaling approach is that we need K_t which is calculated from the nominal stresses, eq. 3.1.1. K_t is used both for synthesizing the SN curve using eq. 4.1.2 and also for scaling in eq. 4.3.3.

An estimate of K_t can be made without relying on nominal stresses though. The two main ingredients needed for determining the stress concentration factor is the notch radius r and wall thickness t . In case the notch radius is not well defined, e.g. not circular, an estimate (or reference) notch radius can be found from the normalized stress gradient [15]

$$r_{ref} \approx \frac{2}{\chi^*} \quad (4.3.5)$$

Analytical estimates for stress concentration factors \tilde{K}_t depending only on geometry can then be found in textbooks, e.g.

$$\tilde{K}_t = 10^{0.066 - 0.36 \cdot \log \frac{r_{ref}}{t}} \quad (4.3.6)$$

Figure 25 shows the resulting stress concentration factor for various radii and wall thicknesses. The main influence of the stress concentration factor on the local SN curve is in the slope (see eq. 4.1.4).

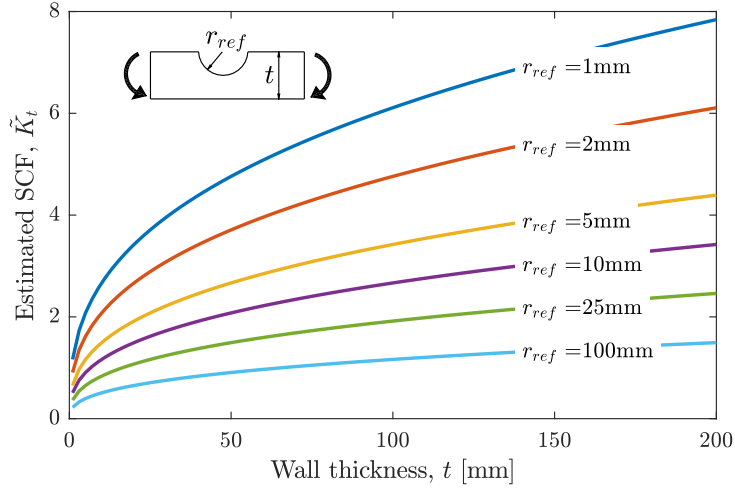


Figure 25: Stress concentration factor estimate, after [15].

4.3.2 Synthesizing local SN curves

In order to synthesize a local SN curve straight away, we insert eq. 4.1.2 into 4.3.3 to get

$$\sigma_{a,k} \leq K_t \cdot k_{reliab} \cdot k_{mean} \cdot k_{env} \cdot k_{treat} \cdot k_{size} \cdot \frac{\sigma_{R,D}^*}{\sqrt{K_f^2 - 1 + 1/k_{surf}^2}} \quad (4.3.7)$$

If we disregard the dependence between K_f and k_{surf} (inspired by eq. 4.2.1) we can write the local fatigue strength (right hand side) as

$$\sigma_{R,D,k} = k_{reliab} \cdot k_{mean} \cdot k_{env} \cdot k_{treat} \cdot k_{surf} \cdot k_{size} \cdot \frac{K_t}{K_f} \cdot \sigma_{R,D}^* \quad (4.3.8)$$

which can be simplified using eq. 3.2.1

$$\sigma_{R,D,k} = k_{reliab} \cdot k_{mean} \cdot k_{env} \cdot k_{treat} \cdot k_{surf} \cdot k_{size} \cdot n \cdot \sigma_{R,D}^* \quad (4.3.9)$$

The local fatigue strength can thus be determined without K_t and K_f - we just need the notch support factor n . Luckily, this can be estimated from stress analysis of the local geometry, e.g. using the stress gradient- or highly stressed volume concept of section 3.2.

Recalling from section 3.2.3 that the local fatigue strength can be estimated nicely from a given highly stressed volume as

$$\sigma_{R,D,k}^{**} = \alpha_h \cdot V_{90}^{\beta_h} \quad (4.3.10)$$

which include both size effect (at least most of k_{size} , except for the technological size effect k_{tech}) and notch support effect n . We can then rewrite 4.3.9

$$\sigma_{R,D,k} = k_{reliab} \cdot k_{mean} \cdot k_{env} \cdot k_{treat} \cdot k_{surf} \cdot k_{tech} \cdot \sigma_{R,D,k}^{**} \quad (4.3.11)$$

Eichlseder [10] devised a similar system which can establish the local fatigue strength based on the stress gradient. Such systems lend themselves well to implementation in an FE context and Eichlseder's is used as the basis for the fatigue software FEMFAT.

The slope and knee point still need to be determined somehow without using K_t and/or K_f , e.g. using the FKM approach and assuming these fixed at $m_1 = 5$ and $N_D = 10^6$.

5 Variable amplitude loading

In the case of variable amplitude (VA) loading, such as Fig. 26, the time series needs to be broken down into single cycles which can be handled individually. This is achieved using cycle counting techniques. Subsequently, the damage of each individual stress cycle must be accumulated in order to estimate the total damage. This is typically done using the Palmgren-Miner linear damage accumulation rule.

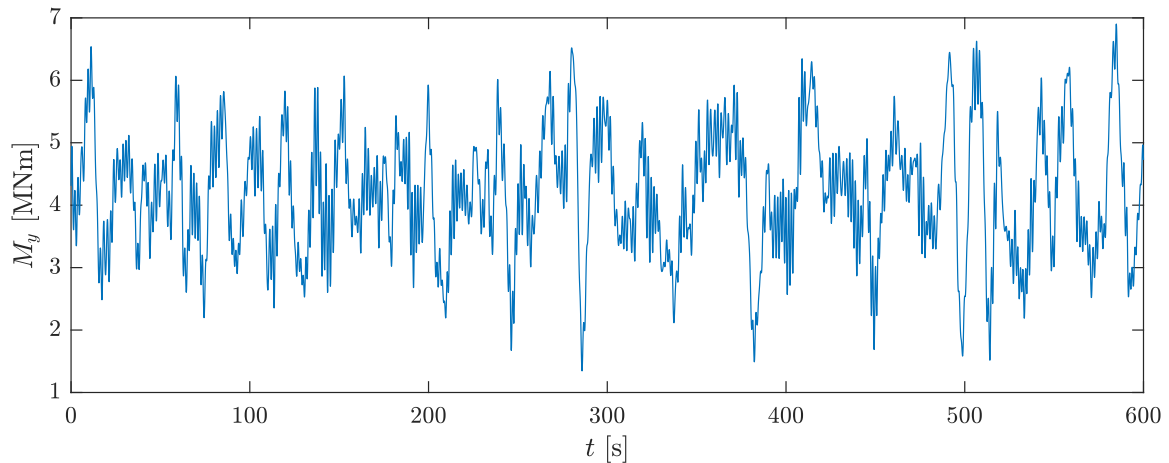


Figure 26: Example VA loading: Simulated main shaft bending moment in 5MW wind turbine.

5.1 Stress-time series generation

In order to perform a fatigue analysis, the load-time series, e.g. Fig. 26, must be converted to a stress-time series for the location (hotspot) under investigation (e.g. a single node in an FE model).

The stress-time history, i.e. the time varying stress tensor $\sigma(t)$, is usually generated from superposition of scaled FE stresses from unit load cases. For multiple loads, a number of unit LC stresses $\sigma_i(L_{FE,i})$ (nodal stresses at unit load i) may be scaled with the associated load-time history $L_i(t)$ and combined according to the principle of superposition.

$$\sigma(t) = \sum \sigma_i(L_{FE,i}) \cdot \frac{L_i(t)}{L_{FE,i}} \quad (5.1.1)$$

The time dependent stress tensor can then be established.

$$\boldsymbol{\sigma}(t) = \begin{bmatrix} \sigma_x(t) & \tau_{xy}(t) & \tau_{xz}(t) \\ \tau_{xy}(t) & \sigma_y(t) & \tau_{yz}(t) \\ \tau_{xz}(t) & \tau_{yz}(t) & \sigma_z(t) \end{bmatrix} \quad (5.1.2)$$

5.1.1 Fatigue stress determination

For fatigue analysis, in particular the cycle counting process, only one stress component must be selected or a fatigue effective stress must be calculated. Selecting a stress component, e.g. σ_x is straight forward, however this is only meaningful in certain cases where the coordinate system is appropriately oriented in relation to the fatigue critical location.

In other cases, a fatigue effective stress can be used such as the (signed) von Mises, principal stress or maximum shear stress, which will be explained in the following.

(Signed) von Mises

Two versions of the von Mises equivalent stress may be used; the standard strictly positive and the so-called signed von Mises, which can take negative values.

The first is generally a poor choice for fatigue assessment because the range calculated from the strictly positive history of the von Mises stress does not include any potentially negative part of the stress cycle.

In two dimensions we use

$$\sigma_{vm} = \sqrt{\frac{1}{2} (\sigma_x^2 - \sigma_x \sigma_y + \sigma_y^2 + 3\tau_{xy}^2)} \quad (5.1.3)$$

$$= \sqrt{\frac{1}{2} (\sigma_1^2 - \sigma_1 \sigma_2 + \sigma_2^2)} \quad (5.1.4)$$

whereas in three dimensions

$$\sigma_{vm} = \sqrt{\frac{1}{2} ((\sigma_x - \sigma_y)^2 + (\sigma_y - \sigma_z)^2 + (\sigma_z - \sigma_x)^2 + 6(\tau_{xy}^2 + \tau_{yz}^2 + \tau_{xz}^2))} \quad (5.1.5)$$

The signed von Mises σ_{svm} is used to mediate this shortcoming, i.e. by applying the sign of the first stress invariant.

$$\sigma_{svm} = \text{sign}(I_1) \cdot \sigma_{vm} \quad (5.1.6)$$

where $I_1 = \sigma_x + \sigma_y + \sigma_z$. Then σ_{svm} can take both positive and negative values.

Principal stresses

In two dimensions, the principal stresses can be found from

$$\sigma_{1,2} = \frac{\sigma_x + \sigma_y}{2} \pm \sqrt{\left(\frac{\sigma_x - \sigma_y}{2}\right)^2 + \tau_{xy}^2} \quad (5.1.7)$$

by rotating the coordinate system θ_p into an orientation where the shear stress vanish as shown in Figure 27. The algebraically largest stress is σ_1 and the smaller is σ_2 .

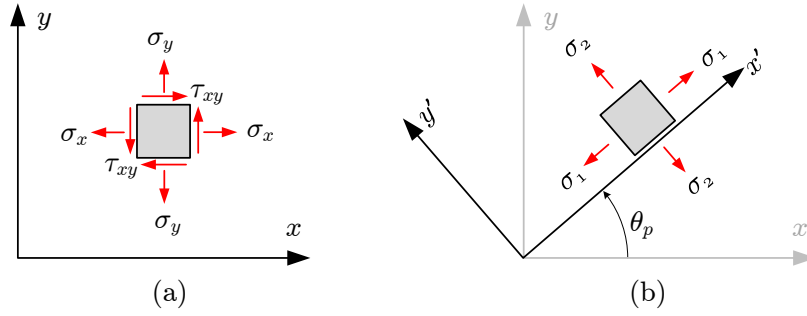


Figure 27: Principal stresses in 2D.

In three dimensions, the determination of principal stresses in 3D corresponds to finding the eigenvalues of the stress tensor for each time step.

$$[\sigma_1 \ \sigma_2 \ \sigma_3] = \text{eig}(\boldsymbol{\sigma}) \quad (5.1.8)$$

The principal stresses are arranged by their algebraic magnitude, i.e. $\sigma_1 > \sigma_2 > \sigma_3$.

Due to the way the principal stresses are defined, none of them are suitable for fatigue assessment alone. Therefore, the numerically largest principal stress is used

$$\sigma_{pmax} = \begin{cases} \sigma_1 & \text{for } |\sigma_1| \geq |\sigma_3| \\ \sigma_3 & \text{for } |\sigma_1| < |\sigma_3| \end{cases} \quad (5.1.9)$$

This is probably the most commonly applied fatigue effective stress. It is not fool-proof for multiaxial loading though, as will be discussed later.

5.2 Cycle counting

Many techniques exist for extracting cycles from a load/stress-time series such as in Fig. 26. The most common is the Rainflow counting technique which exist in several variants, see ASTM E1049-85 [2].

5.2.1 Preparing the signal

Before any cycle counting can be carried out, the stress signal needs to be reduced to a series of peaks and valleys. The process is illustrated in Fig. 28 using the first 30 seconds of data from Fig. 26. The original signal typically contains many sample points between the peaks, Fig. 28a, which must be eliminated.

The peaks (and valleys) are detected based on the gradient of the signal, Fig. 28b, i.e. by checking for each point whether the two neighboring points on both sides are either higher or lower than the current point. The final signal, Fig. 28c, can then be fed into a cycle counting algorithm.

Some cycle counting algorithms also require the signal to be re-arranged, such that it begins and ends with the highest peak [39]. This is accomplished by moving the part of the stress-time history prior to the highest peak to the end of the stress history.

Some kind of filtering is often used for a noise signal, e.g. *low-pass filtering* or in particular *racetrack filtering*, in which cycles smaller than some fraction of the maximum is removed.

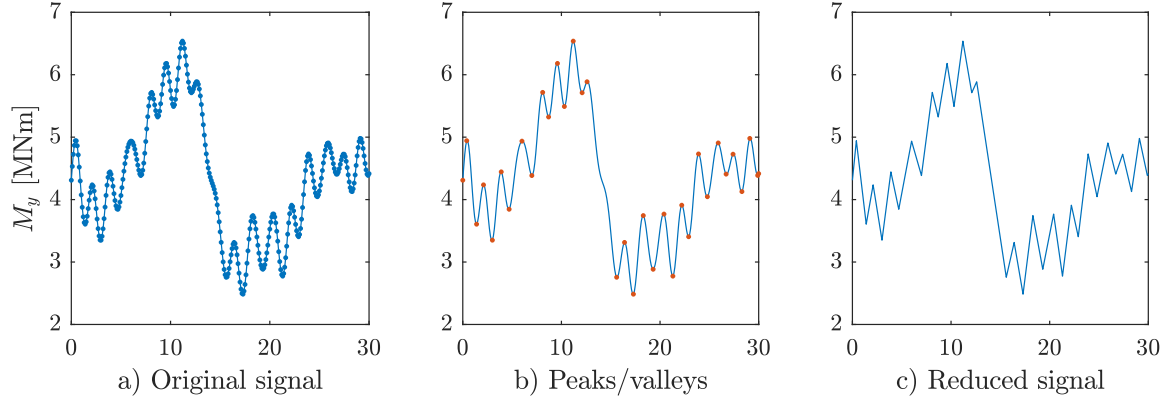


Figure 28: Preparing a signal for cycle counting.

5.2.2 Reservoir counting

In order to use this method, the stress-time history is rearranged to start with the highest peak (i.e. moving *A* in Fig. 29). The stress-time history is then imagined to be filled with water and subsequently drained, one valley at the time, starting from the lowest one.

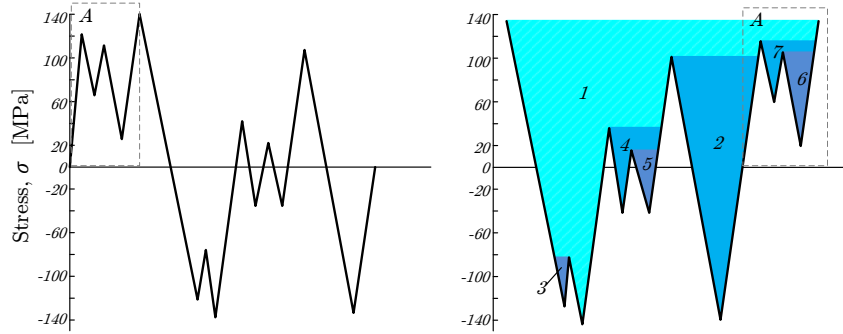


Figure 29: Reservoir counting principle, after [39].

The height of the water that is drained corresponds to the stress range. Each draining procedure results in one full stress cycle, i.e. stress range and mean stress. The stress-time history given in Fig. 29 will thus be counted as 7 cycles, as listed in Table 4. Reservoir counting is recommended for short time series [39].

Table 4: Reservoir counting results.

Draining	$\Delta\sigma$ [MPa]	σ_m [MPa]
1	280	0
2	240	-20
3	40	-100
4	80	0
5	60	-10
6	80	60
7	40	90

5.2.3 Rainflow counting

The signal is rotated clockwise and is imagined to be a series of pagoda roof tops (Japanese style roofs). Water (rain) is then dripping from one to the next and the length of the run of each

drop can be taken as the stress range. The counting is performed in two steps; firstly counting the positive half-cycles and secondly the negative half-cycles. For the positive case, Fig. 30a, a drop is stopped if it passes a more negative valley than it started at. It is also stopped if it encounters the run of an existing drop. The negative cycles are counted similarly, Fig. 30b.

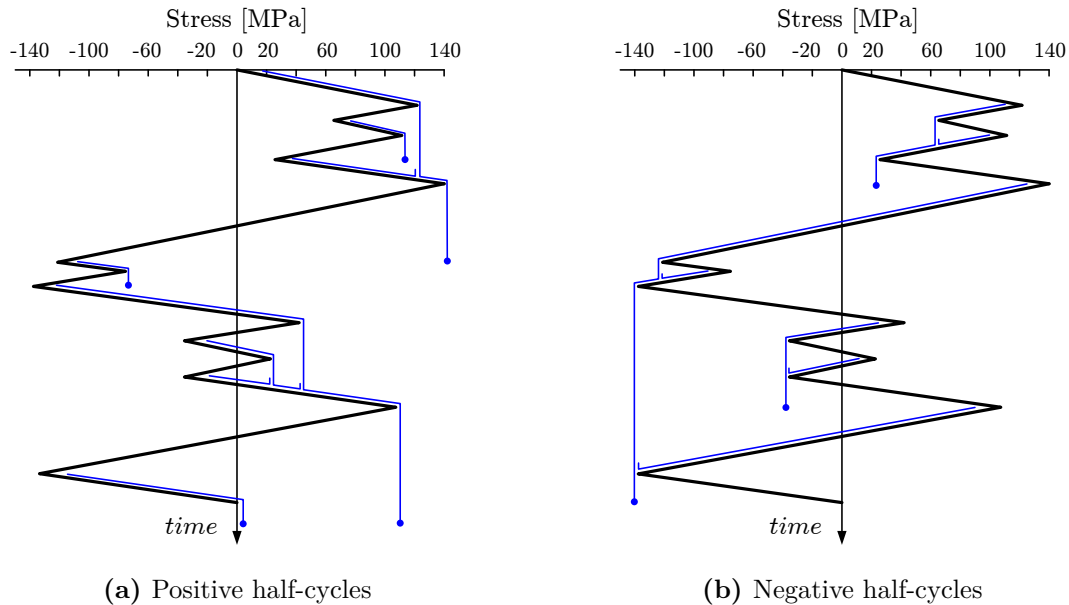


Figure 30: Rainflow counting, after [39].

The Rainflow counting algorithm is different from the Reservoir counting algorithm in that it counts half-cycles, which are subsequently paired up to full cycles. However, there will generally be some half-cycles which are left un-matched. These are called residue and can be handled in two ways; either they can be *closed* to form full cycles, or they can be included in the damage sum as they are.

The half-cycles counted from Fig. 30 are listed in Table 5. It is clear that not all half-cycles can be paired up.

Table 5: Rainflow counting results: positive half-cycles (left), negative half-cycles (right).

Drop	$\Delta\sigma$ [MPa]	σ_m [MPa]	Drop	$\Delta\sigma$ [MPa]	σ_m [MPa]
1	140	70	1	100	70
2	40	80	2	50	85
3	120	80	3	280	0
4	40	-100	4	40	-100
5	240	-20	5	80	0
6	80	0	6	60	-10
7	60	-10	7	240	-20
8	140	-70			

The Rainflow counting algorithm is considered the best choice for long stress-time series. In such cases, most half-cycles will be paired up, and the residual amount of half-cycles relative to the total number of cycles is insignificant. It should be noted though, that the very largest (half-) stress cycles will usually be in the residue.

5.2.4 Binning

Having completed the cycle counting procedure as described above, it is common to bin the results and plot the resulting histograms, as in Fig. 31. The leftmost figure depicts the distribution of load/stress ranges and is sometimes referred to as a load spectrum. The rightmost figure displays the number of cycles as a function of both mean and range.

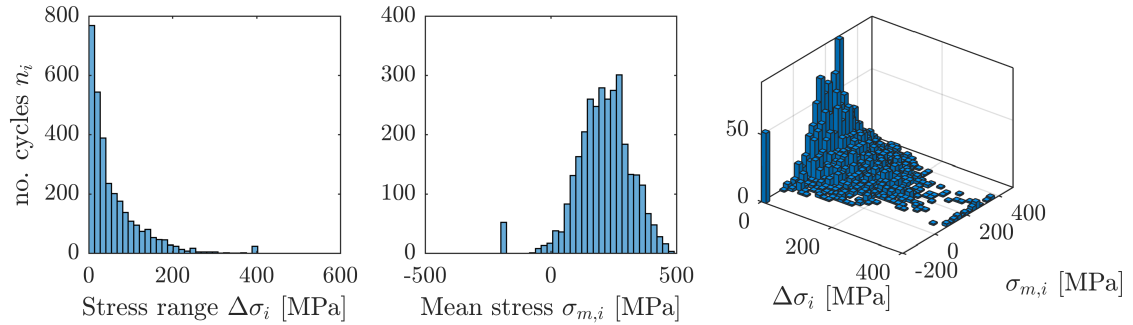


Figure 31: Binning of the load cycles extracted from Fig. 26.

The data in Fig. 31 (right) is often used as basis for fatigue design. It may be listed in a so-called *Markov matrix*, i.e. in the format of Table 6. Traditionally, this format is used for presenting loads.

Each bin of course covers a range of stresses, e.g. the first one $\Delta\sigma_1 = [0; 40]$ MPa and $\sigma_{m,1} = [-200; -167]$ MPa. For the later calculations, we use only the highest values of these ranges in order to be conservative.

$\Delta\sigma_i$ [MPa]	$\sigma_{m,i}$ [MPa]									
	-167	-94	-21	52	125	198	271	344	417	490
40	52	0	14	47	220	405	455	301	149	33
80	0	0	3	17	84	157	192	111	56	11
120	0	0	3	12	39	99	90	63	31	4
160	0	0	0	11	26	52	64	36	22	4
200	0	0	0	5	12	34	40	19	5	0
240	0	0	0	0	5	17	13	11	3	0
280	0	0	0	0	4	13	6	4	0	0
320	0	0	0	0	2	4	4	2	0	0
360	0	0	0	0	0	0	2	1	0	0
400	0	0	0	0	4	6	8	7	2	0

Table 6: Markov matrix; number of cycles (n_i) per bin.

5.3 Damage accumulation

According to the Palmgren-Miner rule, damage is defined as the fraction of life consumed by a stress cycle with range $\Delta\sigma_i$

$$D_i = \frac{1}{N_i} \quad (5.3.1)$$

where N_i is the number of endurable cycles at the given stress range and associated mean stress $\sigma_{m,i}$, determined from an SN curve using eq. 1.4.5. Of course, it should be calculated from the part of the SN curve fitting the stress range at hand (before/after the knee).

The partial damage from each stress cycle can be added, such that the accumulated damage can be expressed as

$$D = \sum D_i = \sum_{i=1}^{n_{cycles}} \frac{1}{N_i} \quad (5.3.2)$$

Typically damage is calculated from binned stress cycles

$$D = \sum_{i=1}^{n_{bins}} \frac{n_i}{N_i} \quad (5.3.3)$$

where, n_i is the number of repetitions of the cycle with stress range $\Delta\sigma_i$ in bin i . The calculation process is illustrated in Fig. 32.

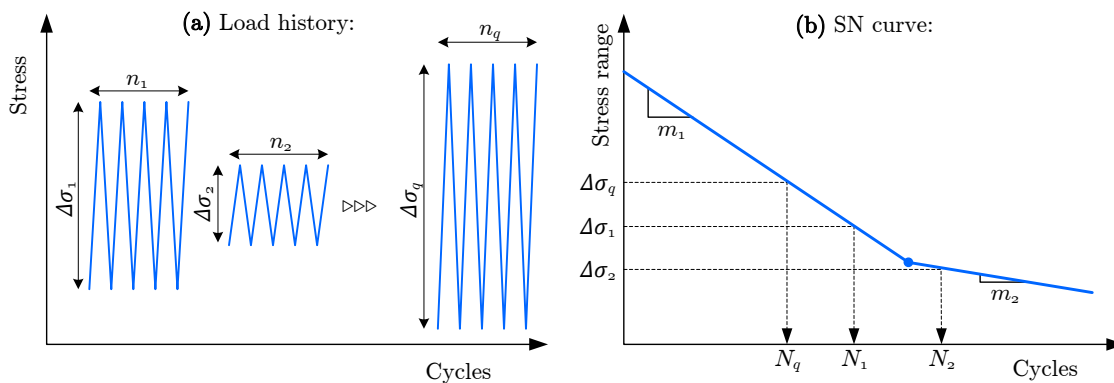


Figure 32: Loading blocks used for damage accumulation, after [39].

Each of the blocks constitutes a partial damage contribution, which when added gives the total damage or damage sum D . Failure is usually assumed at a damage sum of $D = 1.0$, however it is commonly acknowledged that the real damage sum can vary greatly, e.g. in the range of 0.1-10.

Several investigations have shown the Palmgren-Miner linear damage accumulation rule to be unreliable, particularly under fluctuating mean stresses or when pronounced sequence effects occur, e.g. repeated compressive overloads. Some codes therefore recommend using only 0.5 or less.

Another issue that is overlooked by the linear damage accumulation is that stress ranges occurring towards the end of the service life is more damaging then in the beginning. Many

more advanced damage accumulation principles have been proposed to remedy these shortcomings [12], however they typically rely on experimental parameters that are not available in an engineering context. Palmgren-Miner is therefore still the most widely used and recognized approach. Understanding the damage D is difficult, except that we can say whether it is above or below 1.0. One option for better relating to the result is to calculate the endurable life (i.e. the number of cycles the component will sustain).

$$N_{endurable} = \frac{N_{applied}}{D} \quad (5.3.4)$$

5.4 Damage equivalent stress range

Instead of calculating damage, it is often preferred to calculate a damage equivalent stress range, which will lead to the same damage as all the loading blocks combined. For a single-slope SN curve the equivalent stress range $\Delta\sigma_{eq}$ at n_{eq} cycles is

$$\Delta\sigma_{eq} = \left(\frac{\sum(\Delta\sigma_i^m n_i)}{n_{eq}} \right)^{1/m} \quad (5.4.1)$$

The number of cycles n_{eq} at which the equivalent stress is calculated can be chosen arbitrarily. Typical values are e.g. $n_{eq} = 2 \cdot 10^6$. This single stress range can then be evaluated against an SN curve. Stress ranges below the cut-off are considered non-damaging and hence ignored. Alternatively, the knee is disregarded and all stress ranges are considered damaging.

In case of a bilinear SN curve it gets slightly more complicated [44]. Here, $(\Delta\sigma_i, n_i)$ refers to stress cycles before the knee point and $(\Delta\sigma_j, n_j)$ stress cycles after the knee

$$\Delta\sigma_{eq} = \left(\frac{\sum \Delta\sigma_i^{m_1} n_i + \Delta\sigma_{R,D}^{m_1-m_2} \cdot \sum \Delta\sigma_j^{m_2} n_j}{n_{eq}} \right)^{1/m_1} \quad (5.4.2)$$

Here $\Delta\sigma_{R,D}$ is the knee-point stress range of the SN curve. Eq. 5.4.1 and 5.4.2 do not take mean stress effects into account. In that case, the stress ranges applied should be corrected to zero mean stress before use in the above equations using k_{mean} .

5.4.1 Damage equivalent loads (DELs)

The same principle can be applied to loads L (force or moment) in order to calculate a single load that will produce the same damage as a time series. Such a load is called a damage equivalent load or DEL. Only the slope of the SN curve is needed.

$$\Delta L_{eq} = \left(\frac{\sum(\Delta L_i^m n_i)}{n_{eq}} \right)^{1/m} \quad (5.4.3)$$

This works when the stress is proportional to the load, i.e. in linear models. In this case, one cannot include the effect of a bilinear SN curve, as in eq. 5.4.2, since the knee point is defined in terms of stress and not load. A typical approach to dealing with this is to assume a mean value of the slope, e.g. $m = (m_1 + m_2)/2$.

5.4.2 Utilization ratio

It is typically preferred to present the results of a fatigue analysis in terms of the utilization ratio on stress level, rather than damage, because people can better relate to this.

The utilization ratio is defined as the ratio of the equivalent stress range at some number of cycles to the fatigue strength at the same number of cycles, typically N_D

$$UR = \frac{\Delta\sigma_{eq@N_D}}{\Delta\sigma_{R,D}} \quad (5.4.4)$$

This ratio describes how close the equivalent stress range is to the allowable, e.g. if $UR = 0.8$ the stress range may be increased by 25%, on the other hand, if $UR = 1.10$, the stress ranges must be brought down to approximately 90% of the current (to lower loads, change design).

It is not always desired to achieve a fully utilized component ($UR = 1.0$), because this leaves no room for problems discovered later on, e.g. slightly higher loads or similar.

6 Multiaxial fatigue

So far, we have been dealing with uniaxial fatigue, i.e. fatigue problems where we can easily identify a single dominating stress component such as σ_x or σ_1 . The difference between uniaxial and multiaxial fatigue is then, that in multiaxial fatigue, we consider multiple stress components, typically a normal stress σ_x and a shear stress τ_{xy} .

6.1 Multiaxial loading

We consider two types of multiaxial loadings; *proportional*- and *non-proportional* loading. Figure 33 illustrates the difference and at the same time indicates why it is necessary to consider multiaxial fatigue. It shows two stress components acting in-phase and out-of-phase, respectively, and the range of principal stress calculated from these situations. The phase shift between the stress components is called δ .

With proportional loading, Fig. 33a, the two stress components are acting in phase and the resulting principal stress range becomes relatively large. For non-proportional loading, Fig. 33b, on the other hand the resulting range of principal stress becomes smaller, because the two stress components are acting out of phase. Thus one could expect longer fatigue life in the case of non-proportional loading, however most experiments shows that the opposite is the case [41].

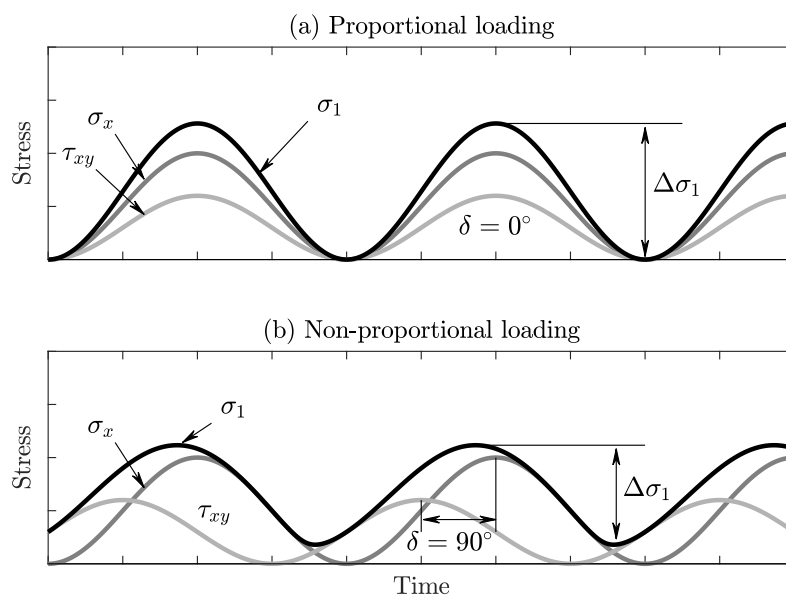


Figure 33: Proportional vs. non-proportional loading, after [41].

This tells us that the principal stress range is a poor choice for multiaxial fatigue assessment. A number of alternatives have thus been proposed, where the most interesting is the critical plane

approach, which will be the topic of the remainder of this chapter.

A good way to think of the two loadings are in terms of the stability of the principal stress directions. For proportional loading, they are constant, while in case of non-proportional loading they may rotate.

6.2 Simple approaches

Figure 34 shows experimental results for multiaxial loading using compiled data from [6]. Each marker represents the normalized fatigue strength obtained from a test carried out at some specific combination of normal and shear stress. It is seen how e.g. for increased normal stress, the allowable shear stress declines.

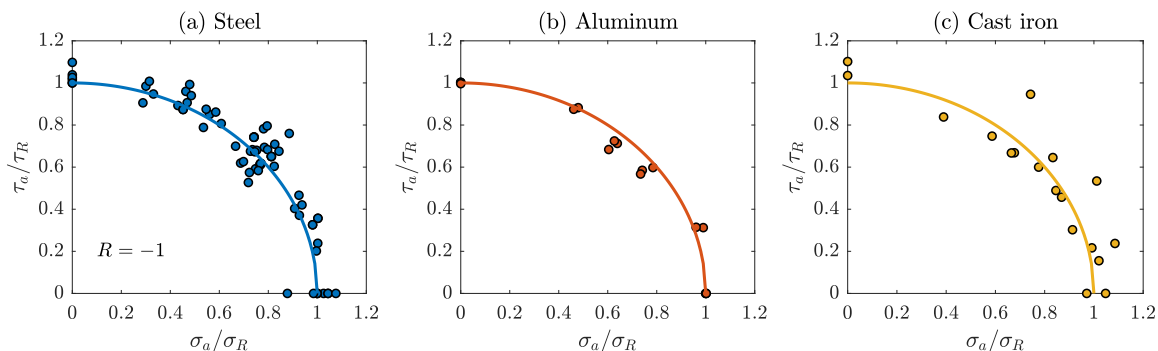


Figure 34: Normalized fatigue strength under multiaxial loading, after [6].

A simple way to address the problem of multiaxiality is to use the Gough-Pollard equation [21]. Referring to Fig. 34, they found that an ellipse fits the experimental data well and proposed the following criterion

$$\left(\frac{\sigma_a}{\sigma_R}\right)^2 + \left(\frac{\tau_a}{\tau_R}\right)^2 = 1 \quad (6.2.1)$$

Equation (6.2.1) can be rewritten to express an equivalent uniaxial stress σ_{GP} which can be evaluate against the uniaxial fatigue strength

$$\sigma_{GP} = \sqrt{\sigma_a^2 + k \cdot \tau_a^2} \leq \sigma_R \quad (6.2.2)$$

where $k = \left(\frac{\sigma_R}{\tau_R}\right)^2$. The mean value of the experiments in Fig. 34 is $k = 2.3$. It is also seen that eq. (6.2.2) resembles the von Mises equivalent stress (if we set $k = 3$).

This approach is only recommended for proportional loading.

6.3 The critical plane approach

In the critical plane approach, a number of search planes intersecting the surface either orthogonally (see Fig. 35) and/or at some inclination are searched for the maximum value of a damage parameter. The plane that maximizes the damage parameter is called the critical plane [62].

Each search plane is defined by its unit normal vector \mathbf{n} , which is again defined by the angle to the local x-axis θ and the inclination angle ϕ as shown in Fig. 36a.

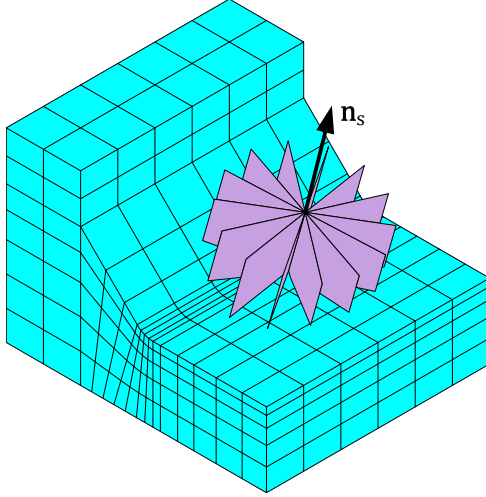


Figure 35: Distribution of search planes around the surface normal.

The stress tensor in the point of investigation (e.g. a node) is needed as the starting point for the analysis, i.e.

$$\boldsymbol{\sigma}(t) = \begin{bmatrix} \sigma_x(t) & \tau_{xy}(t) & \tau_{xz}(t) \\ \tau_{xy}(t) & \sigma_y(t) & \tau_{yz}(t) \\ \tau_{xz}(t) & \tau_{yz}(t) & \sigma_z(t) \end{bmatrix} \quad (6.3.1)$$

This is determined e.g. from FE and is given in some coordinate system $x - y - z$, preferably aligned such that the z -axis is normal to the surface. The stress vector acting on any given search plane can then be calculated

$$\mathbf{S}_n(t) = \boldsymbol{\sigma}(t)\mathbf{n} \quad (6.3.2)$$

The tip of the stress vector describes some curve in stress space, as illustrated in Fig. 36b. It can then be divided in a component normal to the plane, i.e. the normal stress

$$\sigma_n(t) = \mathbf{n}^T \boldsymbol{\sigma}(t)\mathbf{n} \quad (6.3.3)$$

and parallel to the plane, i.e. the shear stress

$$\boldsymbol{\tau}(t) = \boldsymbol{\sigma}(t)\mathbf{n} - \mathbf{n}\mathbf{n}^T \boldsymbol{\sigma}(t)\mathbf{n} \quad (6.3.4)$$

For proportional loading, the shear stress vector $\boldsymbol{\tau}(t)$ has a constant direction; however under non-proportional loading, it describes some trajectory in the search plane, whereas only the magnitude of the normal stress will change, see Figure 36b.

6.3.1 Extraction of stress ranges

Determining the range of normal stress is straight forward for constant amplitude (periodic) loading

$$\Delta\sigma_n = \max \sigma_n(t) - \min \sigma_n(t) \quad (6.3.5)$$

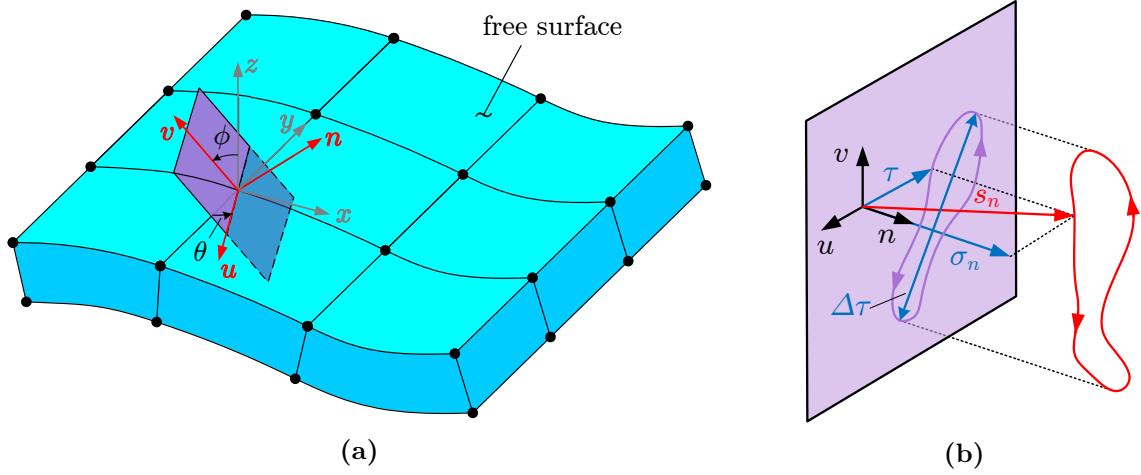


Figure 36: Specification of search plane and extraction of stress ranges [62].

For variable amplitude loading, the cycle counting techniques described in Chapter 5 may be used for the normal stress-time signal of each search plane. The mean normal stress σ_m is found the usual way, eq. (1.3.3).

The shear stress range is much more difficult to handle and many proposals have been made to accomplish this. The simplest is probably the *Longest Chord* method [36]. Here, the longest distance between any two points in the shear stress vector tip trajectory is found from

$$\Delta\tau = \max_{t_i} \left[\max_{t_j} \|\tau(t_i) - \tau(t_j)\| \right] \quad (6.3.6)$$

Here $\|\cdot\|$ indicates the 2-norm and t_i and t_j are instances in time. The above solution is brute force, it requires checking all possible combinations to find the longest chord. The mean shear stress is found from the two time instances that maximize eq. (6.3.6), t_i^* and t_j^* such that

$$\tau_m = \frac{1}{2} \|\tau(t_i^*) - \tau(t_j^*)\| \quad (6.3.7)$$

A multitude of other approaches exist for determining the shear stress range, typically based on fitting various geometrical objects around the trajectory, e.g. circles, ellipses or rectangles, see e.g. Petrucci [66]. In general, they only work for constant amplitude loading.

6.3.2 Setting up search planes

For this purpose, the search planes are best described by their normal \mathbf{n} . Initially, the normals of the search planes are distributed around the surface normal \mathbf{n}_s and from some arbitrary starting direction, e.g. coincident with the x -axis, see Fig. 36a (keeping $\phi = 0^\circ$).

The planes are spaced at e.g. 10 degree intervals, such that $\theta = 0, 10, 20, \dots, 160, 170^\circ$. No plane is specified for $\theta = 180^\circ$, because this will be identical to $\theta = 0^\circ$.

The i th plane normal is then

$$\mathbf{n}_i = \begin{bmatrix} \cos \theta_i \\ \sin \theta_i \\ 0 \end{bmatrix} \quad (6.3.8)$$

These search planes are sufficient to find the plane of maximum normal stress.

The plane of maximum shear stress may be inclined to the surface though, so in order to find this, additional search planes are needed. For each direction θ , a number of inclined search planes are distributed at the same angle interval, but in the range of $\phi = -90, -80, \dots, 0, \dots, 80, 90^\circ$.

The normals for inclined planes can be established using the *Rodrigues rotation formula*

$$\mathbf{n}_j = \mathbf{n}_i \cos \phi_j + (\mathbf{k} \times \mathbf{n}_i) \sin \phi_j + \mathbf{k}(\mathbf{k} \cdot \mathbf{n}_i)(1 - \cos \phi_j) \quad (6.3.9)$$

where \mathbf{k} is the axis or rotation found from the cross product between the current θ -normal and the normal to the surfaces \mathbf{n}_s

$$\mathbf{k} = \mathbf{n}_i \times \mathbf{n}_s \quad (6.3.10)$$

Thus, to find the maximum shear stress plane in e.g. 10° intervals, one needs to search $18 \cdot 19 = 342$ planes per node. Multiply that with the number of nodes and we have a very slow process.

Weber et al. [86] attempted to increase the performance of the process using a more efficient grid of search planes, Fig. 37a. Svärd [82] proposed to use an incremental zone division search, as illustrated in Fig. 37b similar to that of Norberg and Olsson [49].

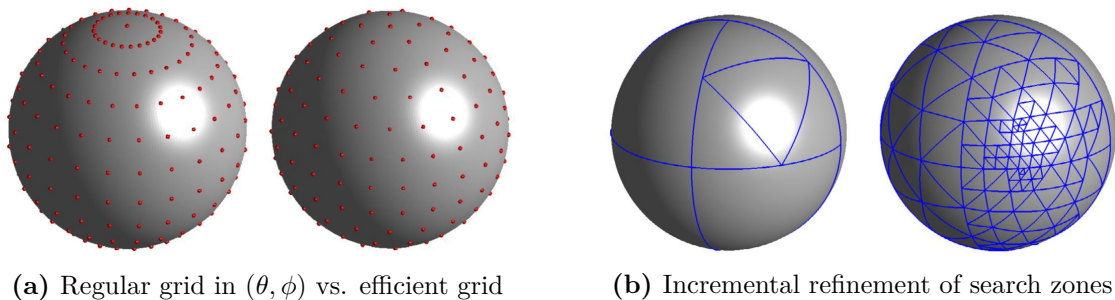


Figure 37: Regular and refined search strategies for finding the critical plane, from [82].

6.4 Multiaxial fatigue criteria

A damage parameter needs to be calculated for each plane in order to determine which plane is the critical one. Many methods exist for this of course, see e.g. [59], here we will concentrate on a few of the most common. The methods are called multiaxial criteria and generally specify an equivalent uniaxial stress range $\Delta\sigma_{uni}$ which can be evaluated against the normal uniaxial fatigue strength

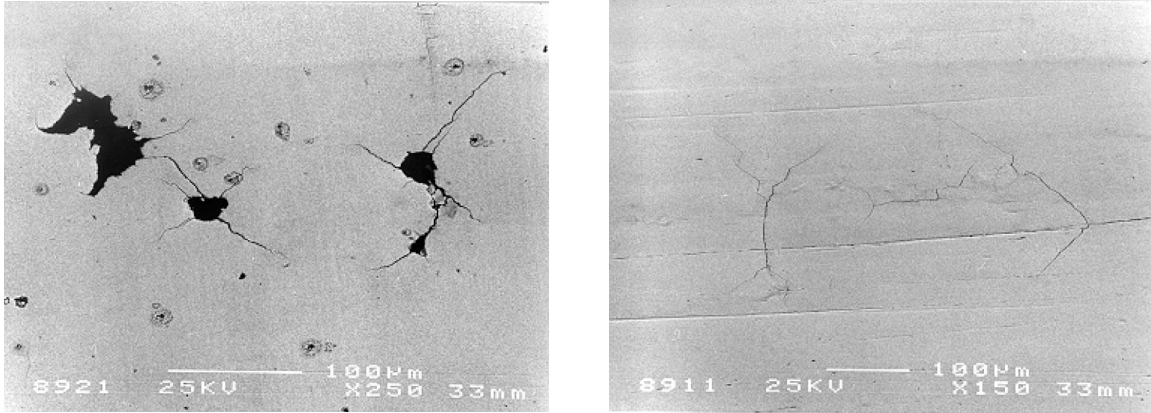
$$\Delta\sigma_{uni} \leq \Delta\sigma_R \quad (6.4.1)$$

The equivalent uniaxial stress range is generally a combination of normal- and shear stress ranges and may include various stress invariants and/or material specific fitting parameters, e.g.

$$\Delta\sigma_{uni} = \alpha\Delta\tau + \beta\Delta\sigma_n \quad (6.4.2)$$

Most criteria for ductile metals are based primarily on the shear stress range, because of experimental observations that the very first part of crack initiation occurs on the plane of maximum

shear, see e.g. Fig. 1. For other materials, e.g. brittle metals and materials with inhomogeneous microstructure, crack initiation typically occur at the plane of maximum normal stress. This difference is illustrated in Fig. 38.



(a) Cast iron: cracking in plane of max normal stress (b) C45 steel: cracking in plane of max shear

Figure 38: Crack initiation under pure shear loading, from [43].

The development of multiaxial criteria is based on attempting to find some parameter that achieves its maximum in the plane where crack initiation is observed experimentally. As evident from Fig. 38 this is material dependent, but besides this fact, not much consensus is found in the literature.

6.4.1 Normal stress criterion

This is the simplest and probably most commonly applied criterion (at least in the Danish Wind industry). Here, we search for the plane that experience the maximum damage calculated from normal stress alone. The normal stress criterion can thus be expressed as

$$\max_{0 \leq \theta \leq \pi} \Delta \sigma_n(\theta) \leq \Delta \sigma_R \quad (6.4.3)$$

According to GL [20], the normal stress criterion is sufficient for assessing ductile cast iron, such as GJS-400-18, because of its semi-ductile nature.

In an investigation by Marquis and Solin [43] on a related material (GRP500 \approx GJS-500-7), they found *that the fatigue limit of this nodular iron was not controlled by crack initiation, but rather by growth of micro-cracks*. Hence, it should be expected to be dominated by mode I crack growth, driven by normal stresses.

6.4.2 Findley's criterion

The Findley criterion [13] is a shear stress based critical plane criterion which predicts failure on the plane that maximizes the damage parameter

$$f = \tau_a + \beta \sigma_{max} \quad (6.4.4)$$

Here τ_a is the shear stress amplitude, σ_{max} is the maximum normal stress occurring over a load cycle. β is an experimentally determined material factor describing the sensitivity to normal

stress. In its original formulation, infinite life was predicted if the damage parameter is below some experimentally determined threshold value $f \leq f_{crit}$.

Bruun and Härkegaard [6] rewrote the above expression in order to formulate an equivalent uniaxial stress amplitude $\sigma_{a,F}$ to be evaluated against the normal fatigue strength.

$$\sigma_{a,F} = \frac{\tau_a + \beta\sigma_{max}}{\frac{1}{2}(\beta + \sqrt{1 + \beta^2})} \quad (6.4.5)$$

The Findley criterion can thus be expressed as

$$\max_{\substack{0 \leq \theta \leq \pi \\ -\frac{\pi}{2} \leq \phi \leq \frac{\pi}{2}}} \sigma_{a,F}(\theta, \phi) \leq \sigma_R \quad (6.4.6)$$

6.4.3 Other criteria

For a full review of multiaxial criteria please refer to Papuga [59]. Here, we will look briefly at a few other criteria, just to get some perspective. All of them are expressed as equivalent uniaxial stress amplitudes, to be evaluated against the uniaxial fatigue strength σ_R

There are various approaches to the search; some criteria search for the plane of maximum damage, some for the plane of maximum shear and others use an integral value of the damage parameter across search planes.

The Sines criterion is based on the amplitude of the second stress invariant J_2 and the mean hydrostatic stress $\sigma_{H,m}$

$$\sigma_{a,S} = \alpha\sqrt{J_{2a}} + \beta\sigma_{H,m} \quad (6.4.7)$$

The Crossland criterion is identical, except that it employs the maximum hydrostatic stress instead of the mean.

The Dang Van criterion is very similar, but uses the shear stress amplitude

$$\sigma_{a,DV} = \alpha\tau_a + \beta\sigma_{H,max} \quad (6.4.8)$$

A relatively new criterion is by Carpinteri & Spagnoli

$$\sigma_{a,CS} = \sqrt{\alpha\tau_a^2 + \beta\sigma_a\sigma_{max}} \quad (6.4.9)$$

Lastly, the Papuga criterion deserves to be mentioned

$$\sigma_{a,P} = \sqrt{\alpha\tau_a^2 + \beta(\sigma_a + \gamma\sigma_m)} \quad (6.4.10)$$

Most authors will conclude that their criterion is the best, however, Papuga provides the most convincing proof in a comparison with other criteria [59]. The material constants α , β and γ can all be derived from the experimentally determined fatigue strength under, rotating bending $\sigma_{R,-1}$, pulsating tension $\sigma_{R,0}$ and fully reversed torsion $\tau_{R,-1}$.

It should be noted that some of the criteria includes the mean stress effect (more or less elegantly) while others do not.

Part II

Welded joints and steel structures

7 Fatigue of welded joints

Welded joints are very prone to fatigue failure. As opposed to machine elements, welded joints spend most of their life in the crack propagation phase, because of the existence of small crack-like features inherent with the welding process. The mechanisms governing fatigue life is thus different. Assessment is carried out using SN curves from codes rather than synthetic ones.

7.1 General

Comparing welded joints against machined components, they have significantly lower fatigue strength as illustrated in Figure 39a. In addition to this, the fatigue strength do not increase with increase tensile strength of the welded steel, Figure 39b. However, there are some indications that the fatigue strength of post weld treated joints benefit from this. Welded joints are generally a poor choice for fatigue loaded structures, but they are frequently used because of their low cost.

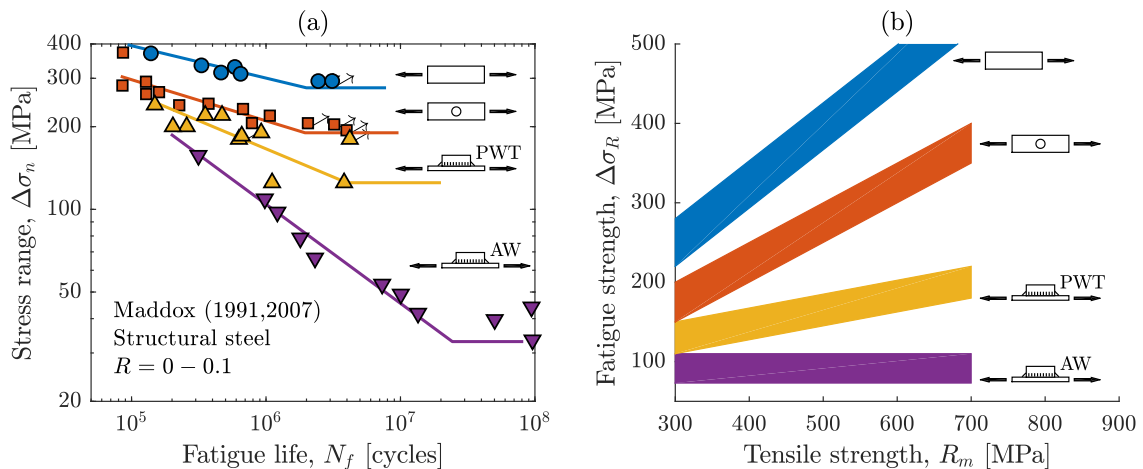


Figure 39: Comparison of fatigue strength of base material, machined component and welded joint, for various steels, adapted from Maddox [39] and Haagensen and Maddox [24].

The reasons for the low fatigue strength of welded joints are illustrated in Figure 40, which depicts the local stress in the critical location of the weld (typically the toe). As seen, regardless of the applied moderate loading, the local stress at the weld toe will be both scaled and elevated.

The stress is scaled up because of the stress concentration effects. This includes both the macroscopic geometry changes (e.g. section changes), but also on the microscopic level (e.g. weld defects, inclusions). The shifting up of the stress range is due to tensile residual stresses superimposed to the applied stress. These arise due to the contraction of the weld metal during cooling and solidification in the manufacturing process.

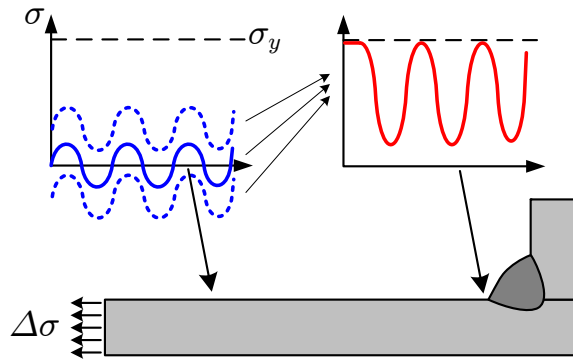


Figure 40: The local stress is much more severe than the applied [61].

Because of the residual stresses present in welded joints, the mean stress of the applied loading may be disregarded. The negative effect of the residual stresses are accounted for in the SN curves.

While the fatigue strength of welded steel joints is the same regardless of the steel strength, Fig. 39b, it is different for other materials, e.g. aluminum. In general, the fatigue strength of welded joints scales with the modulus of elasticity, such that e.g.

$$\frac{\Delta\sigma_{R,steel}}{\Delta\sigma_{R,alu}} \approx \frac{E_{steel}}{E_{alu}} \approx 3 \quad (7.1.1)$$

7.2 Toe vs. root failure

There are two critical locations in a weld where cracks may occur; the toe and the root, Figure 41. Toe cracks grow through the base plate whereas root cracks grow through the throat section of the weld.

Failure from the weld toe (outside) is generally preferred over root failures (inside) because it can be detected and monitored during the service life of the component. Root cracks on the other hand will only be visible, when they have grown through the weld throat.

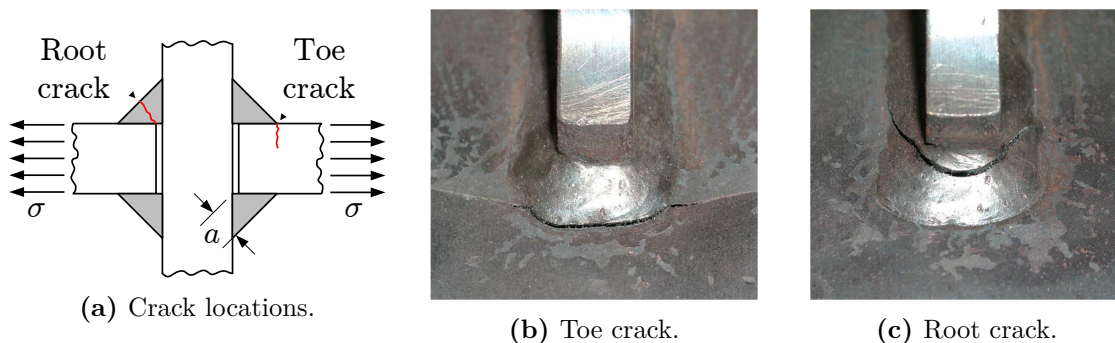


Figure 41: Possible weld failure modes, from [17].

There are several ways to increase the strength of the root in order to secure failure from the toe. The first option is to specify a fully penetrated weld in which case there will be no root face and hence no cracking from this. This option is expensive however, so another cheaper option would

be to increase the throat thickness (a in Figure 41a). A combination of e.g. partial penetration weld and large throat thickness may also be sufficient.

7.3 SN-curves for welded joints

SN-curves for welded joints are not synthesized, they are found from codes. Often they can be used as they are, but in some cases, they need modification as will be described in Chapter 8. Three of the most common sources are:

- Eurocode 3, Part 1-9: Fatigue [11]
- IIW recommendations by Hobbacher [27]
- DNV-GL recommended practice RP-C203 [8]

This text is primarily based on the IIW recommendations, which in the opinion of the author is the most comprehensive and scientifically supported system².

The SN curves obtained here are derived based on large collections of experimental results as exemplified in Figure 42. This approach is used, because the scatter in fatigue strength of welds are much larger than for machine components, e.g. identical welded components from two different manufacturers may have vastly different fatigue strength due to microscopic quality differences.

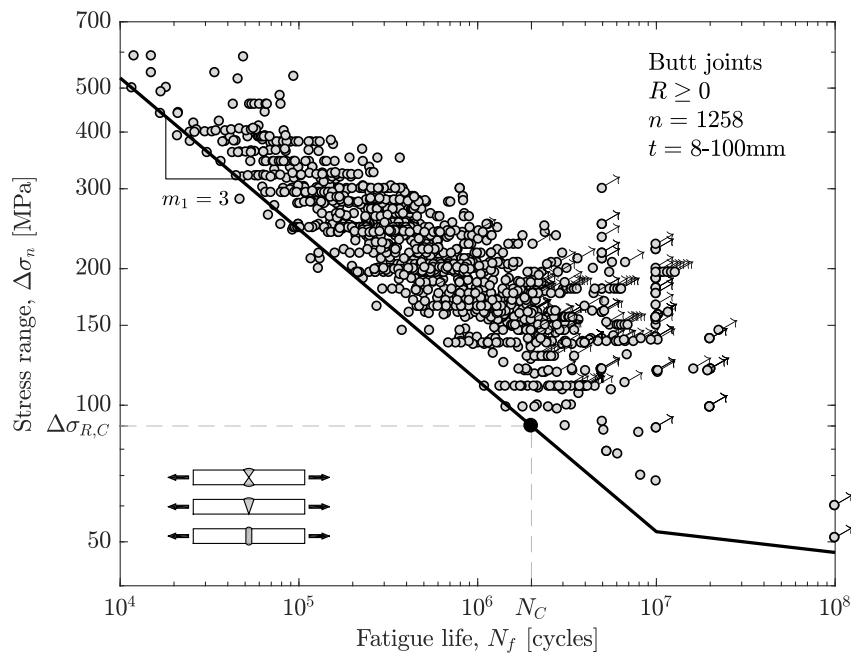


Figure 42: The FAT90 SN-curve for welded butt joints [65].

The SN curves of the codes are thus based on a large, representative volume of test results. Furthermore, they are derived for high stress ratios, preferably $R = 0.5$, in order to simulate high tensile residual stresses which may not be present to the same extent in the small scale test specimens as in large welded structures.

²The International Institute of Welding (IIW) is a global umbrella organisation, consisting of national welding institutions. They arrange conferences and workshops, where the leading specialists in the field meet twice a year for development and maintenance of a number of guidelines/recommendations.

The primary part of the curve is described by a fixed slope of $m_1 = 3$ and a curve is denoted by the *characteristic* stress range $\Delta\sigma_{R,C}$ or FAT class at $N_C = 2 \cdot 10^6$ cycles as shown in Figure 42. Note also, that the knee point is located further to the right, typically at $N_D = 5 \cdot 10^6 - 10^7$.

The secondary slope can be set to $m_2 = 22$ for constant amplitude loading and $m_2 = 5$ for variable amplitude loading [27]. The abolishment of the post-knee infinite life and the introduction of the slope of $m_2 = 22$ is described by Sonsino [74], Sonsino et al. [77].

Design SN curves given in codes are typically associated with a probability of survival of $P_S = 97.7\%$. These are constructed from offsetting the mean curve 2 standard deviations down.

7.4 Assessment approaches

A multitude of fatigue assessment approaches have been developed for welded joints. Figure 43 shows the conceptual difference between the 3 most common approaches; the nominal-, hotspot- and notch stress approaches.

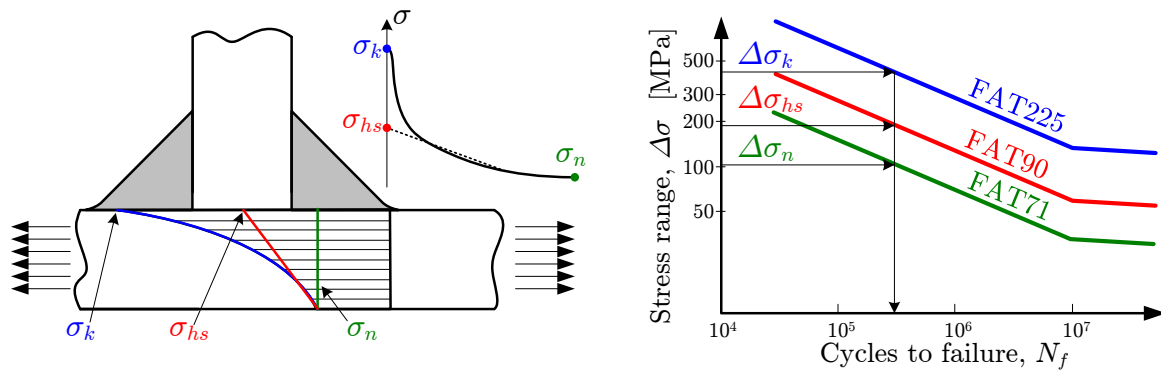


Figure 43: Comparison of the 3 most common assessment approaches for welded joints.

The local stress state at the weld toe is generally not well defined because the geometry is not well defined, i.e. there are small variations in the toe radius and flank angle along the weld.

Depending on the modeling approach chosen, the weld and joint may be idealized to various degrees as will be explained in the following. Before FEA became widely available it was preferred to perform the assessment of welded joints in terms of the *nominal stress range*, $\Delta\sigma_n$, i.e. stresses calculated with simple engineering formulas. Since this nominal stress range do not include the effect of different stress concentrations in different joints, a large array of SN curves are needed to assess different details.

Lately, however, so-called *local approaches* have become increasingly popular. Here a local stress in the weld toe (or root) is determined from an idealized geometry.

The stress range obtained in this manner includes (at least partly) the effect of stress concentration of the joint and hence only a single (or few) SN curves are needed. As illustrated in Figure 43, the local stress is higher than the nominal and hence, the local SN curves are equally higher. As shown in Figure 43 (right), all the approaches should ideally lead to the same estimation of fatigue life, however this is rarely the case.

7.4.1 The nominal stress approach

The nominal stress approach is probably the most common. It is often considered inferior to the local approaches, however this is not always the case. In fact, for joints where a matching detail is found in a code, it may very well be the most accurate and certainly the fastest approach.

Nominal stresses can generally be determined from Navier's equation in the section under consideration, e.g. the toe. Of course, this is only meaningful in the case where a cross-section can be appropriately defined, i.e. typically in plate/beam structures.

$$\sigma_n = \frac{F}{A} + \frac{M \cdot y}{I} \quad (7.4.1)$$

In general, the nominal stress must be calculated for both maximum and minimum loading in order to determine the range $\Delta\sigma_n$. Subsequently, a reference detail must be found from a catalog, e.g. Figure 44b, resembling the component at hand to the largest possible extent. From here, the associated FAT class may be found and hence the SN-curve, Figure 44a.

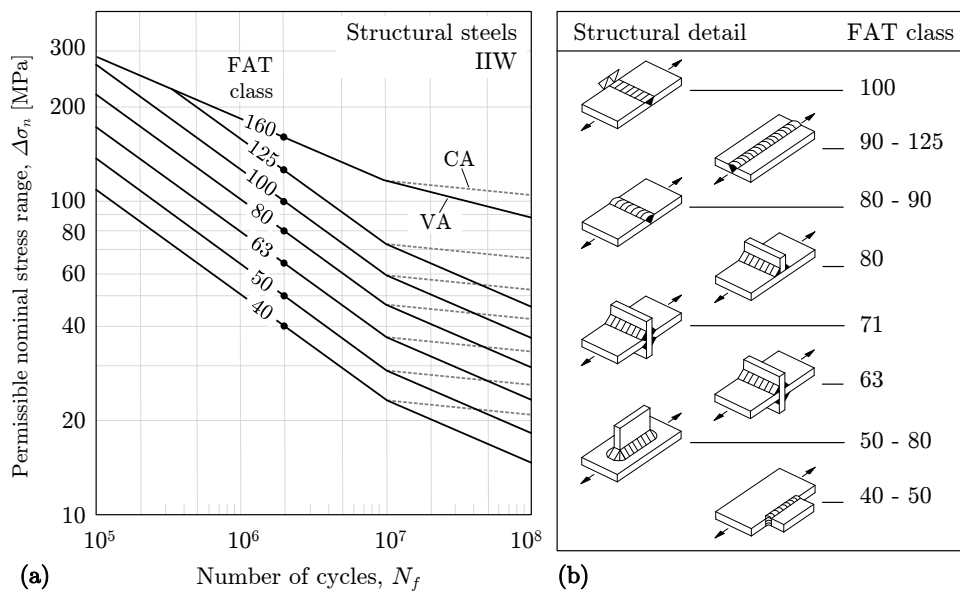


Figure 44: IIW catalog of SN curves and associated detail classification, from Radaj et al. [68].

Finding a suitable reference detail is sometimes difficult if the geometry of the component at hand is not simple. In any case, it is important to consider not just the geometry/shape of the detail, but also how the loading applies (indicated by arrows in the catalog).

7.4.2 Local approaches

In the case of complex geometry, local approaches become necessary. An overview of local approaches are given by Radaj et al. [68]. The two most common will be thoroughly treated in chapters 9 and 10.

It is important to realize, that the local stresses are linearly dependent on the nominal stress, such that

$$\sigma_{nom} \approx \frac{\sigma_{hs}}{K_{hs}} \approx \frac{\sigma_k}{K_t} \quad (7.4.2)$$

where K_{hs} and K_t are the stress concentration factors.

8 Factors affecting the fatigue strength of welded joints

Several conditions may alter the fatigue strength of welded joints both in the negative and positive direction. These are not the same as for machine components, because the damage mechanism is different, i.e. crack propagation rather than crack initiation.

8.1 General

As mentioned, the SN curves found in codes may often be applied directly, but in some cases corrections are needed. The uncorrected characteristic (reference) fatigue strength $\Delta\sigma_{R,C}^*$ is specified at $N_C = 2 \cdot 10^6$ cycles for the following conditions:

- Probability of survival $P_S = 97.7\%$
- High tensile residual stresses assumed, $R = 0.5$
- Good weld quality, ISO 5817 grade B
- Knee point is located at $N_D = 10^7$ cycles
- Limited misalignment, see Table 8
- Reference thickness $t \leq 25mm$
- Non corrosive environment

The SN curves must be corrected if conditions deviate from the those listed here. Each of these conditions will be treated in the following. Here, we denote the un-corrected fatigue strength associated with an SN curve or FAT class $\Delta\sigma_{R,C}^*$ and develop a correction scheme.

$$\Delta\sigma_{R,C} = k_{thick} \cdot k_{qual} \cdot k_{env} \cdot k_{rs} \cdot \frac{\Delta\sigma_{R,C}^*}{k_{mis}} \quad (8.1.1)$$

The design fatigue strength is then found by further scaling down using a partial material safety factor

$$\Delta\sigma_{R,C,d} = \frac{\Delta\sigma_{R,C}}{\gamma_{Mf}} \quad (8.1.2)$$

The reference fatigue strength is given in Table 7 for the most commonly applied SN curves within the IIW system. These are for welded joints in steel. The presented curves are for normal stress ranges. Different curves are provided for shear stress ranges in the references

Table 7: IIW SN curves for welded joints [16, 27, 48].

Nominal stress approach						
IIW	DNV ¹	m_1	$\Delta\sigma_{R,C}^*$ [MPa]	$\Delta\sigma_{R,D}^*$ [MPa]	$\log C_1$	Comments/examples
FAT160	B1	5	160	116.0	17.32	Base material
FAT140	B2	3	140	81.9	12.74	
FAT125	C	3	125	73.1	12.59	Thermal cut edges
FAT112	C1	3	112	65.5	12.45	
FAT100	C2	3	100	58.5	12.30	
FAT90	D	3	90	52.6	12.16	Butt joints
FAT80	E	3	80	46.8	12.01	
FAT71	F	3	71	41.5	11.85	
FAT63	F1	3	63	36.8	11.70	
FAT56	F3	3	56	32.7	11.55	
FAT50	G	3	50	29.2	11.40	
FAT45	W1	3	45	26.3	11.26	
FAT40	W2	3	40	23.4	11.11	
FAT36	W3	3	36	21.1	10.97	Failure from root
Hot spot approach						
IIW	DNV	m_1	$\Delta\sigma_{R,C}^*$ [MPa]	$\Delta\sigma_{R,D}^*$ [MPa]	$\log C_1$	Comments/examples
FAT100		3	100	58.5	12.30	
FAT90	T	3	90	52.6	12.16	Default
FAT61		3	61	35.7	11.66	Root assessment
Notch stress approach						
IIW	DNV	m_1	$\Delta\sigma_{R,C}^*$ [MPa]	$\Delta\sigma_{R,D}^*$ [MPa]	$\log C_1$	Comments/examples
FAT225		3	225	131.6	13.36	Use with principal stresses
FAT200		3	200	117.0	13.20	Use with von-Mises stresses

¹ DNV designation. Slight variations may occur, e.g. some curves have slope of $m_1 = 4$.

8.2 Misalignment

Misalignment, i.e. offset of the load-carrying plates in a joint (denoted e), cause additional bending to be superimposed on the applied loading. The local loading of the weld will thus be increased and the fatigue life reduced. Figure 45 shows the effect of increased misalignment on axially loaded butt joints.

Misalignment is usually considered through correction factors k_{mis} of the following format. They are used either to scale up the stress range (DNV) or scale down the fatigue strength (IIW). Here, we scale down the fatigue strength. Please refer to e.g. the IIW recommendations for more detailed corrections factors for specific joint types or to Lotsberg [38] for guidance in case of butt joints with different thicknesses.

$$k_{mis} = 1 + 3\frac{e}{t} \quad (8.2.1)$$

Table 8 gives an overview as to how much misalignment effect is already covered by the IIW

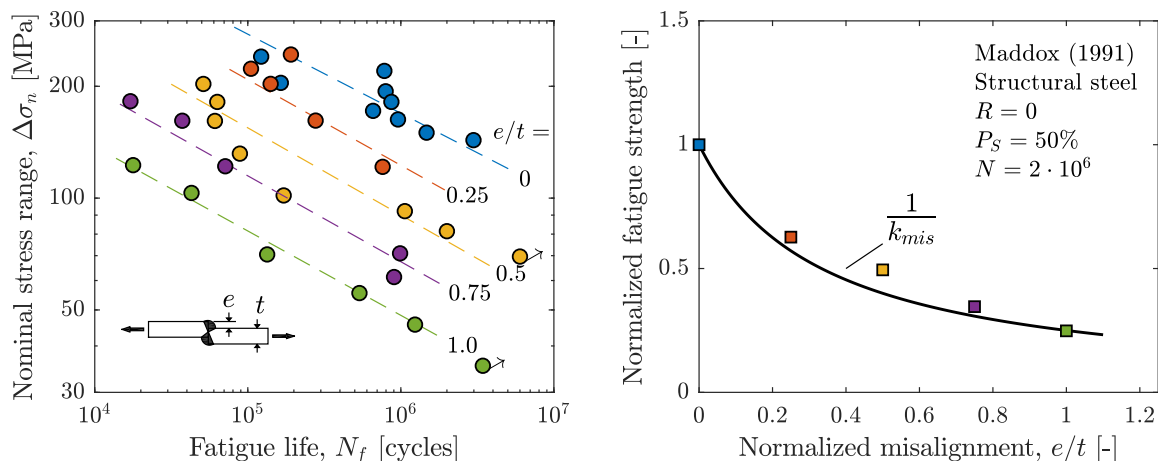


Figure 45: Effect of misalignment, adapted from Maddox [39].

FAT classes and how much should be included when using the local approaches. The guidance given in Table 8 for the local approaches refers to the situation, where the FE model is based on the idealized geometry, i.e. with no misalignment or other imperfections - in that case, the k_{mis} should be applied. Another option is to include the misalignment in the FE model. In this case, it is possible to evaluate more specifically the effect of various levels of misalignment and determine the critical/acceptable level for the component at hand.

Table 8: Misalignment already included in FAT class and default values to be used[27].

Detail	Nominal stress		Hotspot- and notch stress	
	k_{mis} included	k_{mis} included	k_{mis} included	k_{mis} to be used
Butt joints made in shop	1.15	1.05	1.05	1.10 ¹
Other butt joints	1.30	1.05	1.05	1.25 ¹
Cruciform joints	1.45	1.05	1.05	1.40 ¹
Fillet welds on one plate surface	1.25	1.05	1.05	1.20 ²
Fillet welds on both plate surfaces	1.25	1.05	1.05	1.10 ³

¹ Default value, but not more than $(1 + 2.5 \cdot e_{max}/t)$.

² Default value, but not more than $(1 + 0.2 \cdot t_{ref}/t)$.

³ Default value, but not more than $(1 + 0.1 \cdot t_{ref}/t)$.

8.3 Thickness

Experiments show that the fatigue strength reduces for thicker welded joints, Figure 46. The causes of this thickness effect are the same as those described for machine components in section 2.4.

For welded joints, the geometrical (stress gradient) size effect is presumably the most dominant. As seen in Figure 46, the thickness effect is more pronounced in bending compared to tensile loading, indicating a dependency of the stress gradient.

The thickness effect is generally included in design rules by scaling the fatigue strength with the following factor

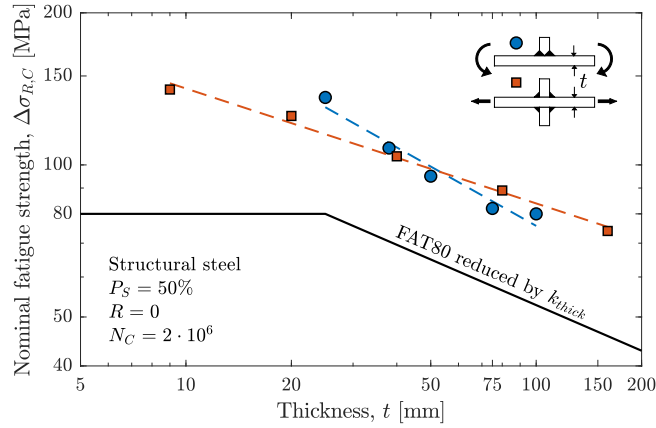


Figure 46: Comparison of the IIW correction against experimental data from [4, 53].

$$k_{thick} = \left(\frac{t_{ref}}{t} \right)^{\alpha_t} \quad (8.3.1)$$

According to the IIW recommendations [27], the reference thickness should be taken as $t_{ref} = 25\text{mm}$ and the exponent α_t is found from Table 9 depending on the detail under consideration.

Table 9: Values of the thickness correction exponent [27].

Detail	Condition	α_t
Transverse fillet welds	as-welded	0.3
	toe ground	0.2
Transverse butt welds	as-welded	0.2
	flush ground	0.1
Base material, longitudinal welds	any	0.1

The thickness effect is only considered for joint thicknesses over $t > 25\text{mm}$, i.e. for thinner joints, use $k_{thick} = 1$. This is because the SN curves in codes are based on fatigue test data in the range of $10 - 25\text{mm}$. Figure 46 shows also a positive effect for very thin joints, e.g. 9mm , however this is not to be included in the assessment.

Ohta et al. [56] investigated the thickness effect in butt joints and found significant effect when testing at $R = 0$, however, when repeating the test at a higher mean stress (cycling down from yield, $\sigma_{max} = \sigma_y$) the effect vanished. They argued that the difference was due to residual stresses, i.e. that the residual stresses were more prone to relaxation in thin joints than thick. Another investigation by Pedersen et al. [65] also showed very limited thickness effect for butt joints in tension, proposing $\alpha_t = 0.05$ for this particular case.

8.4 Environmental effects

Corrosion reduces the fatigue strength of welded joints. It is difficult to specify how much, because it depends on several factors, e.g. exposure time, load spectrum, temperature, etc. Figure 47 shows the results of an investigation of the effect of corrosion. As seen, the specimens in corrosive environments endured significantly shorter fatigue lives. Note the very low testing frequency applied.

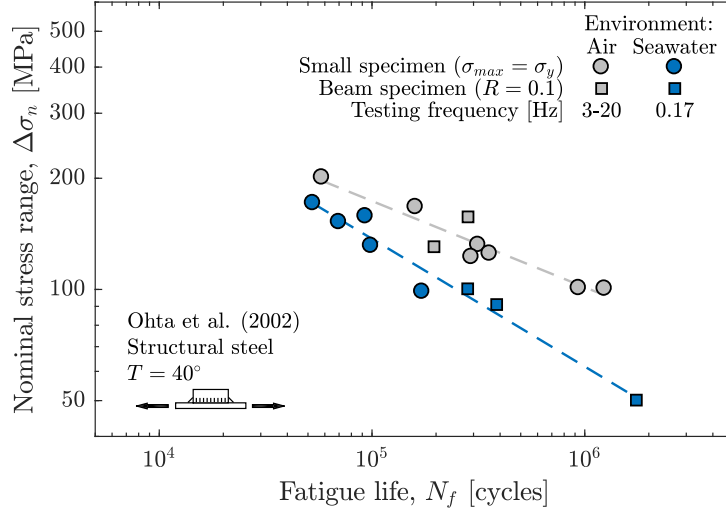


Figure 47: Effect of corrosion, data from Ohta et al. [57].

A typical recommendation is to reduce the fatigue strength by

$$k_{env} \leq 0.7 \quad (8.4.1)$$

and assuming no fatigue limit, i.e. no knee point, such that

$$m_2 = m_1 = 3 \quad (8.4.2)$$

A good overview of the topic is given in Naess [46]. Design guidance are provided by DNV GL [8]. Cathodic protection and/or painting may alleviate some of the reduction in fatigue strength.

8.5 Post weld treatment (PWT)

Post weld treatment has been applied in repair of existing welded structures, but is getting more and more interesting for application to new structures. Especially for high strength steel structures, post weld treatment can be used to reduce the gap between the fatigue strength and static strength. This section is based primarily on Pedersen [61]. Another good overview of post weld treatment is given by Haagensen and Maddox [24].

The two main factors governing the fatigue strength of welded joints are the local geometry of the weld toe and the residual stress state here. One or both of these can be improved in order to improve the fatigue performance, as shown in Figure 48.

Improving the geometry of the weld toe leads to a reduction of the stress concentration here. The weld will therefore experience a reduced stress range, as shown in Figure 48b. Geometry improvement considers both reduction of the macroscopic stress concentration due to the section change of the joint, but also reduction or removal of stress concentrations on the microscopic level due to weld defects.

By improving the residual stress state, the local stress ratio is reduced, so that all or part of the local stress range becomes compressive, Figure 48c. Local compressive loading significantly reduces the crack growth rate.

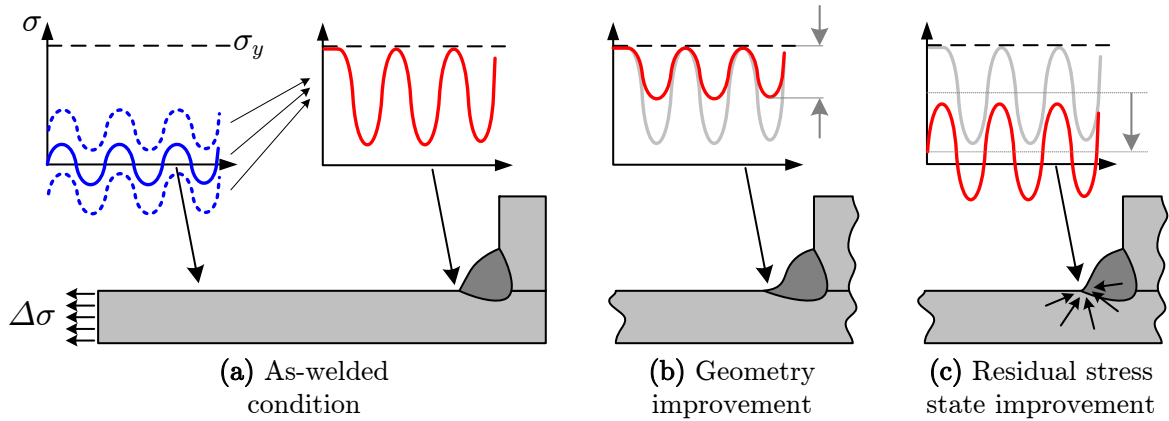


Figure 48: The two main types of improvement of welded joints [61].

Generally, geometry improvement can be considered more stable/robust than residual stress state improvement, since the latter improvement can be destroyed by overloading, which causes the beneficial compressive residual stress state to relax. But on the other hand, residual stress state improvement tends to be more effective under the right conditions, i.e. high cycle/low stress range and low stress ratio.

8.5.1 PWT techniques

A selection of the most widely applied post weld treatment techniques is shown in Figure 49, divided according to their working principle. A large number of techniques exist, both generic, such as grinding, and proprietary, e.g. ultrasonic impact treatment (UIT). Most peening techniques provide some degree of geometry improvement, but their primary improvement is related to residual stress state improvement.

RESIDUAL STRESS STATE IMPROVEMENT	GEOMETRY IMPROVEMENT	
<ul style="list-style-type: none"> • Shot peening/blasting • LTT electrodes • Thermal stress relieving 	<ul style="list-style-type: none"> • Hammer peening • Needle peening • High frequency peening (UIT, UP, HiFIT, etc.) 	<ul style="list-style-type: none"> • Disc grinding • Burr grinding • TIG dressing

Figure 49: Post weld treatment techniques [61].

Figure 50 shows the resulting weld toe profiles due to three of the most popular PWT techniques; burr grinding, TIG dressing and ultrasonic impact treatment. Each of these treatments will be discussed in the following.

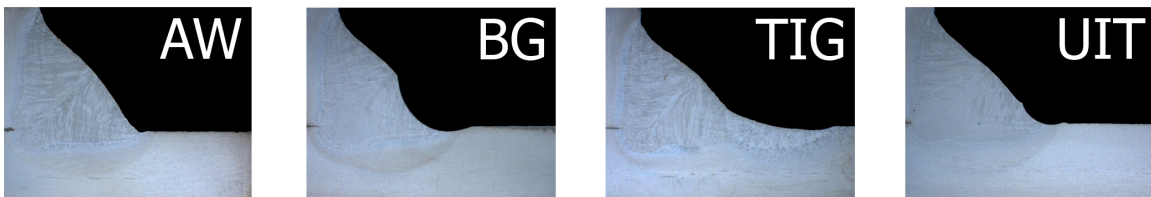


Figure 50: Micrographs of toe geometries obtained by post-weld treatment [61].

The purpose of burr grinding and TIG dressing is to remove minor weld defects in the weld toe by machining or remelting, while at the same time reducing the stress concentration factor of the weld toe. The use of a burr grinder instead of a disc grinder leaves the grinding marks parallel to the direction of loading, which prevents them from acting as crack initiation sites.

Several types of high frequency peening (HFP) treatments exist, however their properties and resulting improvement in fatigue strength appear to be similar. They all operate in a manner similar to ordinary hammer peening equipment, only at a considerably higher frequency, which reduces vibration and noise. The tip of the tool oscillates at about 200Hz with a displacement of only about $40\mu\text{m}$. Usually, the tip of the tool is fitted with several hardened pins, e.g. 3-4 on a line, but many different configurations exist.

The HFP treatments improve the fatigue strength of the welded joint in several ways by plastic deformation of the weld toe. Firstly, the tensile residual stress state present in the weld seam is relieved and beneficial compressive residual stresses are introduced. Secondly, the sharp notch in the weld toe is blunted and the treatment leaves behind a smooth trace with a radius of $2 - 3\text{mm}$, see Figure 50. Finally, the surface material is mechanically hardened, which locally increases the fatigue strength of the material in the notch.

The effect of post weld treatment varies between details and test conditions, but usually an improvement in the range of $30 - 100\%$ on the fatigue strength can be gained, see e.g. Figure 51. This effect may be included in the assessment scaling the fatigue strength with a k_{PWT} and possibly a modifying the slope as given in Table 10. It should be noted though, that in practice, the use of post weld treatment is better handled through the weld quality system as will be described in the following section. The k_{PWT} is therefore not used here and thus absent in eq. (8.1.1)

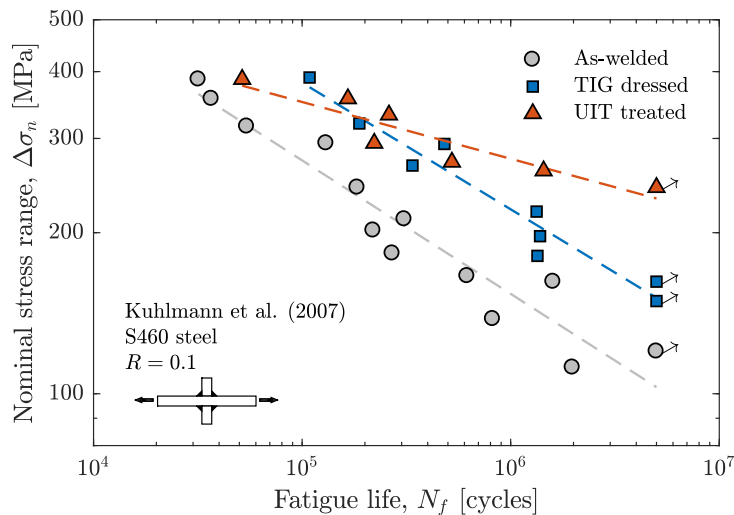


Figure 51: Effect of post-weld treatment, data from [34].

Post weld treatment is sometimes considered an expensive solution, but in many cases, only a very small part of a component is stressed to such extent, that post weld treatment is necessary. Thus, applying post weld treatment locally - where needed - can actually be the cheaper solution, as opposed to increasing the plate thickness in order to reduce stresses.

It should be noted, that when improving the fatigue strength of the weld toe, the critical location may shift to the next most critical, e.g. the weld root or plate edge/surface.

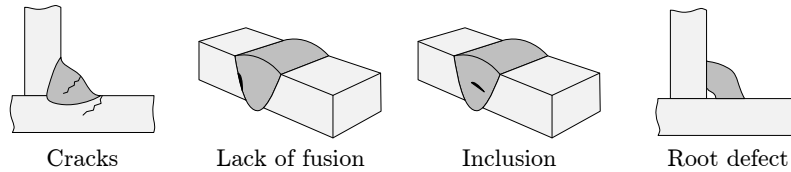
Table 10: Correction for some post weld treatments.

Treatment	k_{PWT}	m_1
Burr grinding	1.3	3
TIG dressing	1.3	3
HFP treatment	1.5	5

8.6 Weld quality

Weld quality is typically specified by weld classes D, C and B according to ISO5817 [29]. The weld classes are defined by various tolerances to weld imperfections, as shown in Figure 52. Some defects such as cracks are not allowed, whereas imperfections such as undercuts may be tolerated to some extent. Eurocode 3 (through EN1090-2) has an elaborate system for selecting weld qualities based on consequences, production and material quality. According to the IIW, on the other hand, **welds subjected to fatigue should always be quality B** [27]. The argumentation is that the specimens which the SN curves are based on are all made to good quality (when welders know their welds will be tested, they can do a very good job).

(a) Not allowed:



(b) Main requirements:

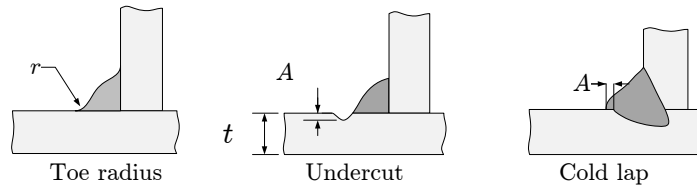


Figure 52: Examples of weld defects/imperfections.

For a long time, however, there has been a consensus among researchers that the current ISO5817 weld quality system is inconsistent and in some cases irrelevant regarding fatigue. The problem being that the acceptance limits of the different defects/imperfections is not set according to the inherent fatigue performance, but instead according to a subjective measure of good workmanship.

A completely revised weld quality system was therefore developed at Volvo Construction Equipment in Sweden. The basic idea of the system is that when increasing the quality by one level, e.g. from VC to VB, the fatigue life should be doubled. The acceptance limits were then derived according to this premises.

The main feature of the system is the specification of the weld toe radius, which is not given ISO5817. Figure 53 shows examples of the span of weld toe radii that can be obtained in production from a completely sharp to a very smooth transition. The stress concentration and hence the fatigue strength correlates very well with the toe radius. The Volvo system is therefore build around this feature.

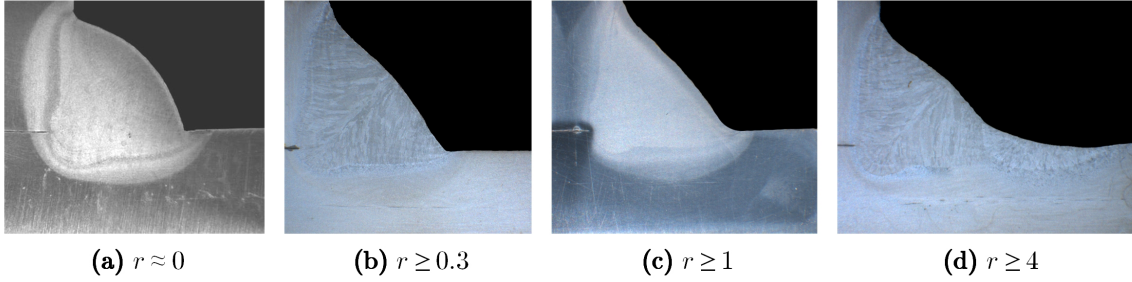


Figure 53: Examples of welds with increasing toe radius.

Table 11 lists some of the acceptance limits and also provides correction factors for scaling the fatigue strength. Note that the class VD is the one that best fits the classical class B and thus is the one associated with the normal SN curves.

Table 11: Volvo STD181-0004 [85] acceptance limits and correction factors.

Weld class Description	VS Static	VE Cheap	VD Normal	VC Good	VB PWT
Min. toe radius, r	-	-	0.3mm	1mm	4mm
Max. undercut (BW), A	$0.2t$	$0.10t$	$0.05t$	$0.04t$	NA
Max. undercut, (FW), A	$0.2t$	$0.15t$	$0.10t$	$0.08t$	NA
Max. misalignment, e	5mm	$0.1t$	$0.1t$	$0.05t$	NA
Max. cold lap, A	-	1mm	0.3mm	1mm	NA
Example Fig. 53	-	(a)	(b)	(c)	(d)
k_{qual}	-	0.75	1.00	1.25	1.50

The highest quality VB can only be obtained by post weld treatment, e.g. grinding or TIG dressing. The VC quality is produced by using the gravity trick described by Jonsson et al. [30]. The normal quality VC is not achieved per default in production - only by careful execution with skilled welders. The VS class is for statically loaded welds only.

8.7 Residual stress

Usually, high tensile stresses are expected in welded joints in actual components. The negative effect of this is included in the SN curves, such that no further correction is necessary.

When performing fatigue tests on small scale specimens one will typically observe a significant mean stress dependency as illustrated in Figure 54a. This behavior is in contrast to that observed when testing full scale components, Figure 54b.

The difference have been shown to stem from difference in residual stresses. The components have high levels whereas the small scale specimens cannot sustain as high levels. This is due to the lack of surrounding material providing restraint.

The question may thus be posed; which stress ratio is appropriate for generating the SN curve? It depends on the specimen - if it is small, presumably it does not hold realistic high levels of residual stress. Here, the IIW recommends using $R = 0.5$. For larger (e.g. full scale) it does not matter.

The IIW distinguishes between 3 cases for which one may correct the SN curve due to residual stresses.

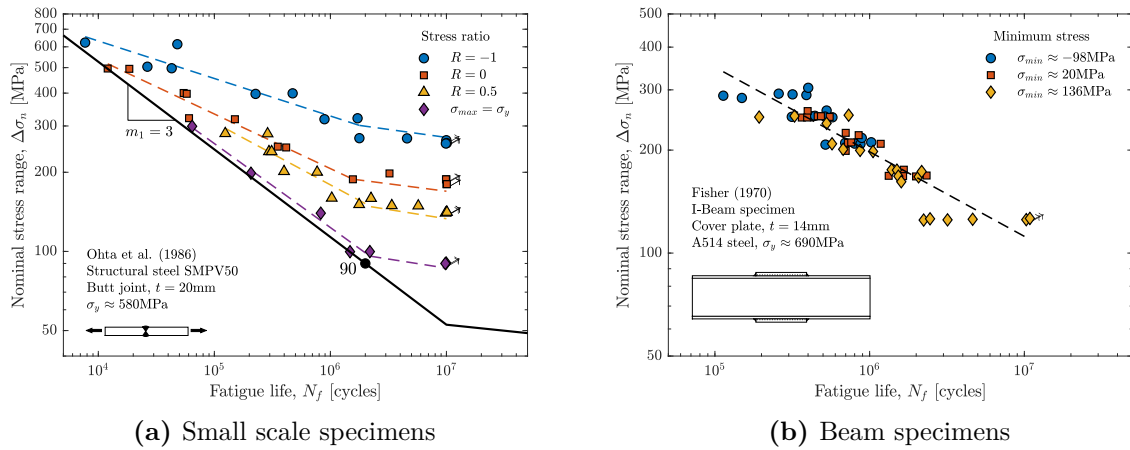


Figure 54: Mean stress dependency in small scale specimens and actual components, data from [14, 55].

1. High RS; Normal case typical for welded structures/components.

$$k_{rS} = 1.0 \quad (8.7.1)$$

2. Medium RS; small scale simple structural elements containing short welds. No constraints in assembly.

$$k_{rS} = \begin{cases} 1.3 & \text{for } R \leq -1 \\ -0.4R + 0.9 & \text{for } -1 < R < 0.5 \\ 1.0 & \text{for } R \geq 0.5 \end{cases} \quad (8.7.2)$$

3. Low RS; unwelded or stress relieved components with no constraints in assembly.

$$k_{rS} = \begin{cases} 1.6 & \text{for } R \leq -1 \\ -0.4R + 1.2 & \text{for } -1 < R < 0.5 \\ 1.0 & \text{for } R \geq 0.5 \end{cases} \quad (8.7.3)$$

Remember to also consider so-called long range residual stresses, i.e. not from the weld it self, but from assembly of parts with imperfect fit.

9 Hot-spot approach

The hotspot approach, or structural stress approach, is presented. This approach is probably the most commonly applied in industry, because it is developed for use with FE analysis. Detailed guidance for meshing and stress analysis are provided along with background documentation regarding the associated SN curves.

9.1 Introduction

The working principle of the hotspot approach is shown in Figure 55. Several variants of the approach exist, however, in the following we shall consider the most commonly applied approach. It all begins with an FE model which may or may not include the weld. The model is sliced in order to place nodes at specific locations. The FE model is meshed with a relatively coarse mesh with element side length of approximately half the plate thickness t .

Due to the sharp notch in the model, the stresses will not converge here, and the assessment is thus based on stresses a small distance away. Generally two stress read-out points are used, located at $0.4t$ and $1.0t$ away from the weld toe. Principal stresses are obtained here and extrapolated linearly to the weld toe. The resolved stress range may then be evaluated against the FAT90 SN curve (or in some cases FAT100).

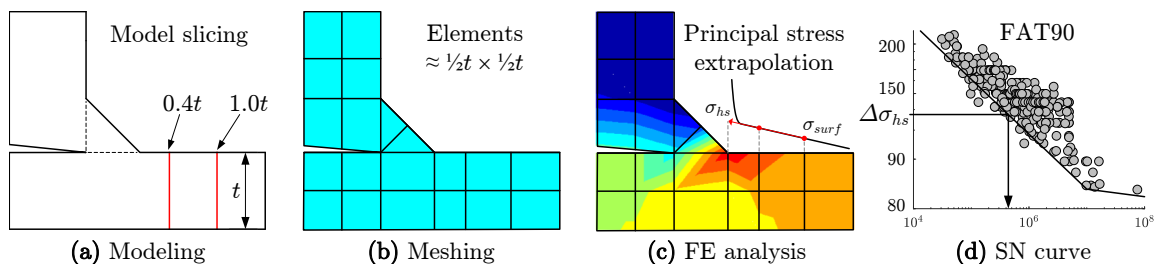


Figure 55: Principles of the hotspot approach.

The hotspot approach was developed for assessment of weld toes only, but several extensions have been proposed in order to assess also weld roots, as will be discussed later. The hotspot approach distinguishes itself by the ability to measure the stresses (strains) at extrapolation points using strain gauges.

9.2 Definition of the hotspot stress

The local stress state in a weld toe is nonlinear as illustrated in Figure 56, due to the stress concentration effect of the weld. It may be separated in three parts however; membrane stress, bending stress and a non-linear stress peak.

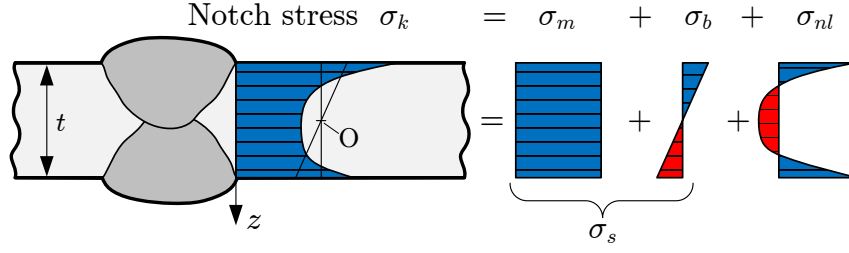


Figure 56: Separation of the notch stress, after Niemi [48].

It is important to realize that neither of these stress components necessarily equals the nominal stress. In some cases, they may coincidentally match, but it is not given. If we denote the normal stress through the thickness of the plate as $\sigma(z)$, then the three stress components can be found as follows [27]

$$\sigma_m = \frac{1}{t} \int_0^t \sigma(z) dz \quad (9.2.1)$$

$$\sigma_b = \frac{6}{t^2} \int_0^t (\sigma(z) - \sigma_m) \left(\frac{t}{2} - z \right) dz \quad (9.2.2)$$

$$\sigma_{nl}(z) = \sigma(z) - \sigma_m - \left(1 - \frac{2z}{t} \right) \sigma_b \quad (9.2.3)$$

Any good FE software will also provide easy calculation of these stress components. The structural stress σ_s is defined as the membrane and bending parts only, i.e.

$$\sigma_s = \sigma_m + \sigma_b \quad (9.2.4)$$

The fundamental idea of the hotspot approach is to exclude the non-linear part of the local stress, because it depends on unknown quantities such as the weld toe radius and flank angle, etc. which are typically unknown. The notch effect is thus excluded from the stress and handled in the SN curve instead.

The hotspot stress σ_{hs} is then defined as the peak value of the structural stress at the weld toe

$$\sigma_{hs} = \sigma_{s,toe} \quad (9.2.5)$$

The hotspot stress includes the macrogeometric stress concentrations due to the overall shape of the structure, (e.g. due to holes or cut-outs), but excludes the small local stress concentration of the weld toe.

The hotspot stress may be related to the nominal stress by a special stress concentration factor

$$\sigma_{hs} = K_{hs} \sigma_n \quad (9.2.6)$$

The hotspot stress concentration factor is typically in the range of 1-2.

9.3 Determination of the hotspot stress

The hotspot stress is determined from FE analysis. The IIW provides an elaborate guide on meshing for various elements and geometries [48]. Here, we shall consider only the typical situation.

Several approaches exist as shown in Figure 57; extrapolation of the surface stress or linearization of the stress through the thickness.

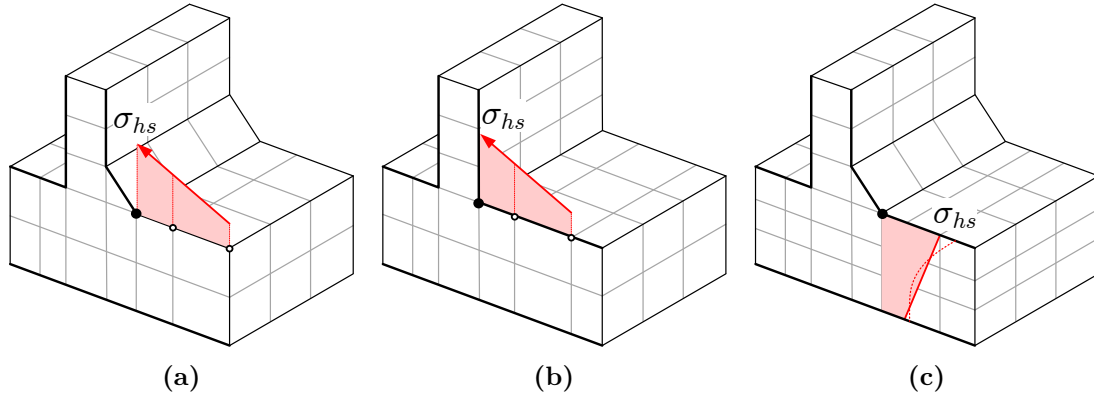


Figure 57: Determination of hotspot stress by extrapolation of surface stress (a,b) or linearization of stress through thickness (c). The weld is not necessarily modeled. After Niemi [48]

The surface stress at two read-out points located at $0.4t$ and $1.0t$ may be extrapolated to the weld toe using

$$\sigma_{hs} = 1.67\sigma_{0.4t} - 0.67\sigma_{1.0t} \quad (9.3.1)$$

The extrapolation procedure should always be verified by plotting the stress as shown in Figure 58. As seen, the extrapolation catches the linear trend in the surface stress quite well and the nonlinear part is excluded nicely.

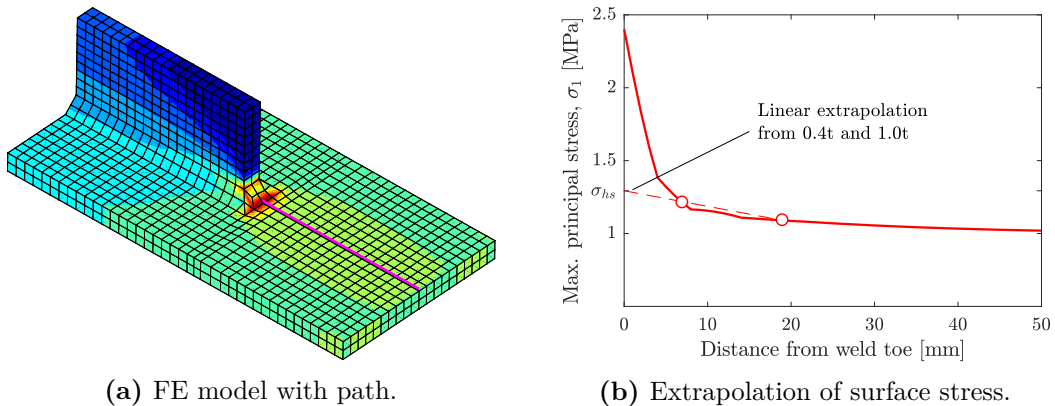


Figure 58: Evaluation of stress extrapolation.

The IIW distinguishes between two types of hotspots as shown in Figure 59. The determination of the hotspot varies according to the type. So far we have been discussing type *a*, for which eq. (9.2.1) and (9.3.1) are valid.

Consider instead hotspots on a plated edge in Figure 59. These are called type *b* hotspots. Here, the stress read-out points are not defined relative to the thickness of the plate, but rather placed

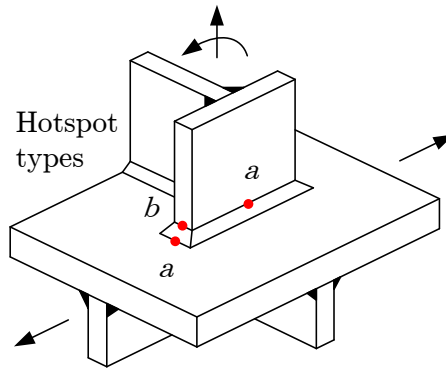


Figure 59: Hotspot types; a (on surface) and b (on edge), from [27].

at fixed distances e.g. at 4, 8 and 12mm away from the weld toe. In this case, the hot spot stress would be determined using quadratic extrapolation

$$\sigma_{hs} = 3\sigma_{4mm} - 3\sigma_{8mm} + \sigma_{12mm} \quad (9.3.2)$$

9.4 SN curve

According to Maddox [40], the logical choice for an SN curve to use with the hotspot stress is that for transverse butt joints, FAT90. This is because the hotspot stress includes all stress concentration effects, except that of the local weld toe. The butt joint SN curve on the other hand includes exactly this effect. A collection of test data is shown in Figure 60 illustrating the appropriate fit for many different specimens and components.

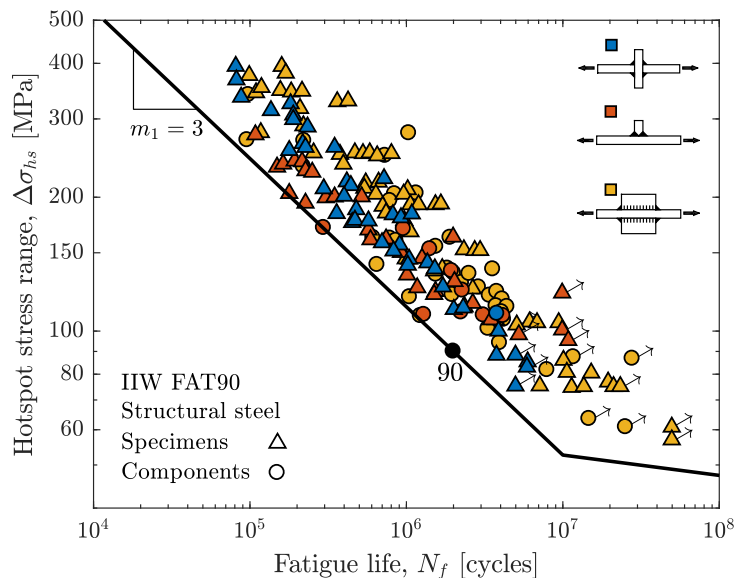


Figure 60: Fatigue data used by Maddox [40] for supporting the FAT90 SN curve.

9.5 Weld root assessment

The original hotspot approach as discussed so far only applies to weld toes. Several extensions have been proposed for assessing weld roots also using the hotspot approach. Fricke [17] gives a comprehensive overview, but in the following we shall consider the proposal by Sørensen et al. [79].

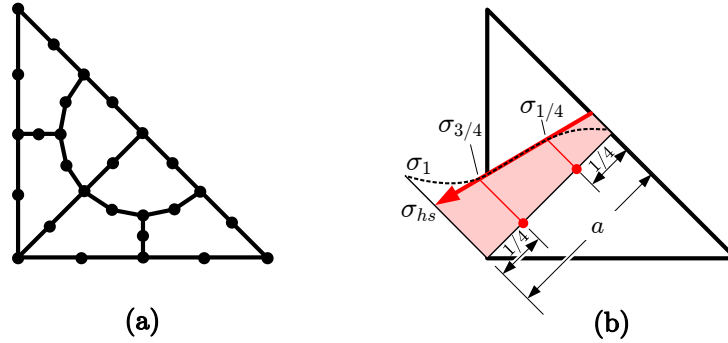


Figure 61: Meshing and extrapolation to obtain the root hot-spot stress, after [17, 79].

The basic idea is to extrapolate the reasonably linear distribution of principal stress in the throat section in order to obtain a mesh independent structural stress value in the weld root, 61b. To achieve this, the weld is modeled with second order solid elements, with at least two elements in the throat section as shown in Figure 61a. Finer meshing is also allowed. Two read out points are located 1/4 inside the weld throat from both sides. The largest principal stress is extracted here and used to extrapolate to the root according to

$$\sigma_{hs} = 1.5\sigma_{1/4} - 0.5\sigma_{3/4} \quad (9.5.1)$$

Sørensen et al. [79] derived an SN curve associated with the above definition of hotspot stress, i.e. FAT61, see Figure 62. It is clear, that the curve is based on relatively few test results and that more verification studies should be done, but this simple approach appears to be working well.

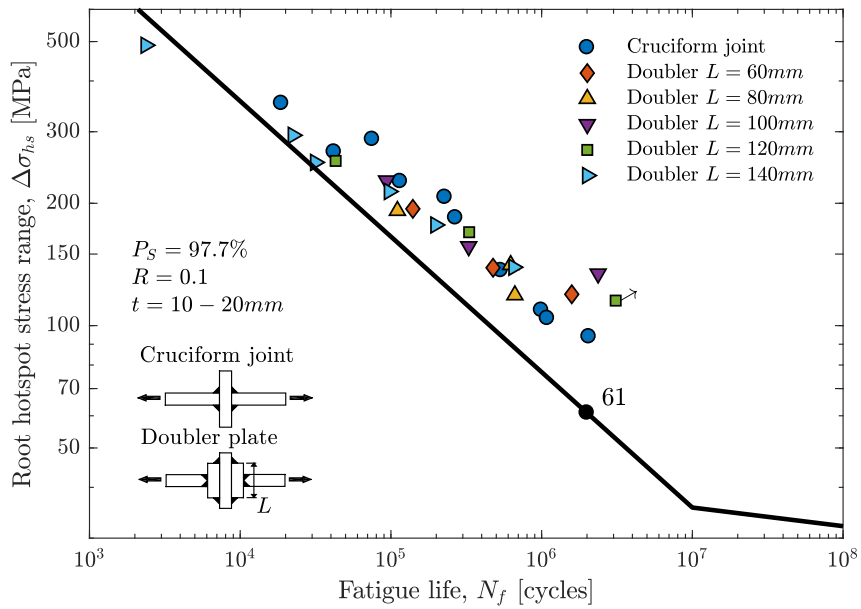


Figure 62: SN curve for root assessment using the hotspot approach, data from [79].

10 Notch approach

A detailed presentation of the effective notch stress approach is given. This approach distinguishes itself in that it considers the actual weld geometry. With it, it is possible to study the effects of changes in the finer details of weld geometry, for example the flank angle. Firstly, the working principle is explained, then the background theory is presented along with the associated SN curves. Lastly, some drawbacks and currently unresolved issues will be discussed.

10.1 Introduction

The overall principle of the notch approach is shown in Figure 63. An FE model is created, including an idealized geometry of the weld with fillet radii in the weld toe and root equal to $r_{ref} = 1mm$. The FE model is solved for the principal stresses using a fine mesh in the fillet, in order to secure convergence of the stress result. Second order elements with side length of max. $0.25mm$ should be used. The stress range is then resolved and evaluated against a single SN curve given by FAT225 [16] for welded joints in steel.

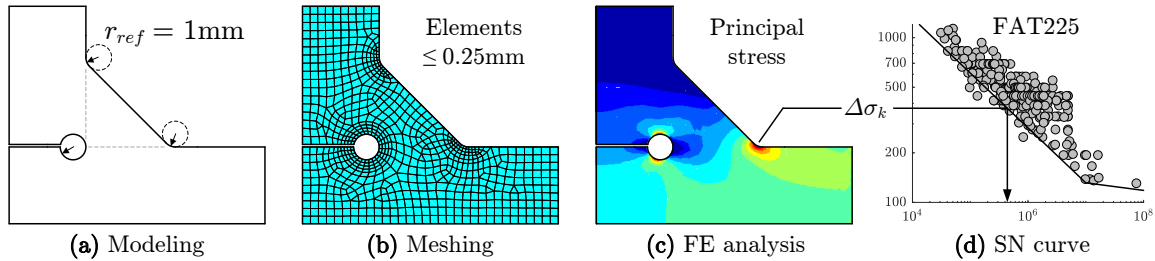


Figure 63: Principles of the notch stress approach, after [64].

The notch stress is denoted σ_k and its relation to the nominal stress may be recalled

$$\sigma_k = K_t \sigma_n \quad (10.1.1)$$

The notch stress is thus proportional to the nominal stress. Due to the above definition, we may write a similar relationship regarding the fatigue strength.

$$\Delta\sigma_{R,k} = K_t \Delta\sigma_{R,n} \quad (10.1.2)$$

It is thus possible to translate results back and forth between the nominal- and notch stress systems. E.g., from notch stress analysis, it is possible to derive the nominal stress fatigue strength by

$$\Delta\sigma_{R,n} = \frac{\Delta\sigma_{R,k}}{K_t} \quad (10.1.3)$$

One of the advantages of this approach is that both the weld toe and root can be assessed using the same modeling approach. Likewise, it is the only approach which can be used to evaluate the local geometry of the weld. Indeed, if measurements of actual weld toe to is available (not often though), the reference radius may set to

$$r_{ref} = r_{real} + 1mm \quad (10.1.4)$$

which in the worst case scenario of a completely sharp toe reduces to $r_{ref} = 1mm$.

Furthermore, the thickness correction is automatically included in the notch stress approach and should thus not be considered separately. Misalignment on the other hand must be considered, e.g. using the default k_{mis} factors in Table 8, alternatively by including the misalignment in the FE model. The latter approach can also be used to investigate the effect of misalignment and to determine a critical/acceptable level to specify in production.

10.2 Background

The approach was originally conceived by Radaj in the late 1970's [68], but did not become widely used until Fricke [16] published an IIW guideline detailing how to use it in 2009. It probably also helped, that sufficient computational power had then become available.

Radaj proposed to use the microstructural support hypothesis by Neuber for welded joints although it was developed for machined components. As mentioned, Neuber found that the local stress in a notch did not correlate well with the fatigue life - instead an average value of stress over a small depth ρ^* should be used. He also found a clever way to avoid the averaging process, i.e. by fictitiously enlarging the notch radius as shown in Figure 64 such that the local stress in the enlarged notch corresponded to the averaged local stress in the original notch.

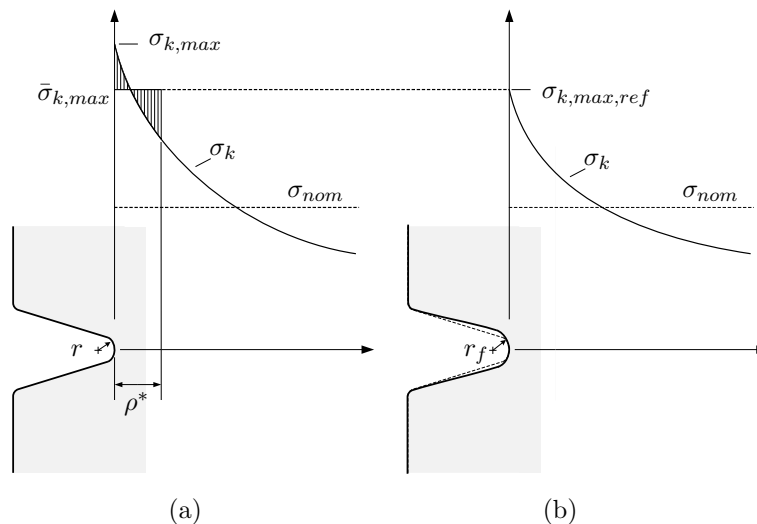


Figure 64: Fictitious notch rounding concept: The original notch radius in (a) is fictitiously enlarged in (b) such that the local stress obtained here equals the averaged stress in (a). After Sonsino et al. [76].

Recall that the increase in stress due a notch K_t was typically larger than the reduction in fatigue strength K_f . Neuber handled this by fictitiously enlarging the notch radius by a cleverly chosen amount, i.e. using r_f instead of r such that

$$K_f = K_{t,r_f} \quad (10.2.1)$$

The size of the fictitious notch radius was found from

$$r_f = r + s\rho^* \quad (10.2.2)$$

where $s = 2.5$ is a loading parameter and $\rho^* = 0.4$ is the material dependent depth over which Neuber averaged the stress [47].

Later, the above theoretical explanation were superseded by a more practical version by the IIW. Instead of the fictitiously enlarged radius calculated as above, one should just apply a fixed *reference radius* of $r_{ref} = 1mm$. This choice corresponds approximately with the mean value of measurements.

10.3 SN curves

The FAT225 SN curve was derived by the IIW based on a large database of fatigue test results for welded joints established by Olivier et al. [58]. They gathered data for the joint types shown in Figure 65 and subjected them to statistical analysis. For each joint, the mean nominal fatigue strength were found and by scaling this with the fatigue notch factor K_f , obtained using the notch stress approach, they found the mean local fatigue strength. As seen in Figure 65, this value is almost identical across joint types.



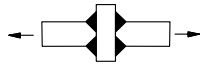
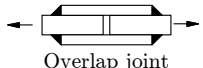

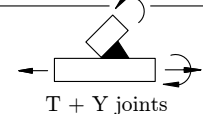
Welded joint type (structural steels)	Fatigue notch factor K_f Fracture initiation	Nominal fatigue strength ($R=0$) $\sigma_{R,n}$ [MPa], $P_S=$			Local fatigue strength $\Delta\sigma_{R,k}=2K_f\sigma_{R,n}$ [MPa]
		10%	50%	90%	
 Butt joint	30° : 1.89 45° : 2.27 Weld toe	61	78	99	
 Transverse stiffener	2.45 Weld toe	52	69	91	
 Cruciform joint	2.50 Weld toe	54	67	83	
 Overlap joint	3.20 Weld toe	47	55	65	
 Cruciform joint	4.03 Weld root	32	43	57	
 T + Y joints	Results for crane constructions	As-welded Stress relieved			

Figure 65: Local fatigue strength associated with the $r_{ref} = 1mm$ modeling technique [58]

Kranz and Sonsino [32] explains the derivation of the design SN curve. The average local fatigue strength in Figure 65 for $R = 0$ and $P_S = 50\%$ is

$$\Delta\sigma_{R,C,k,50\%}^* = 347MPa \quad (10.3.1)$$

Scaling down with $f_R = 1.1$ to account for high tensile residual stress ($R = 0.5$) and $j_\sigma = 1.37$ to consider the usual survival probability of $P_S = 97.7\%$ we get

$$\Delta\sigma_{R,C,k,97.7\%}^* = 231MPa \quad (10.3.2)$$

Since the SN curves in the IIW system are equally spaced at 12.5% intervals, the above value was rounded down to fit these intervals, yielding a final value of

$$\Delta\sigma_{R,C,k}^* = 225MPa \quad (10.3.3)$$

This is the characteristic fatigue strength for a survival probability of $P_S = 97.7\%$ at $N_C = 2 \cdot 10^6$ cycles, for welded joints of normal quality containing high tensile residual stresses, without any misalignment.

The proposed FAT225 was evaluated by Pedersen et al. [63] who found it to be a good fit with many recent experimental data as seen in Figure 66, however slightly less conservative when compared against the nominal stress approach. The evaluation also uncovered some shortcomings of the approach which will be discussed in the next section.

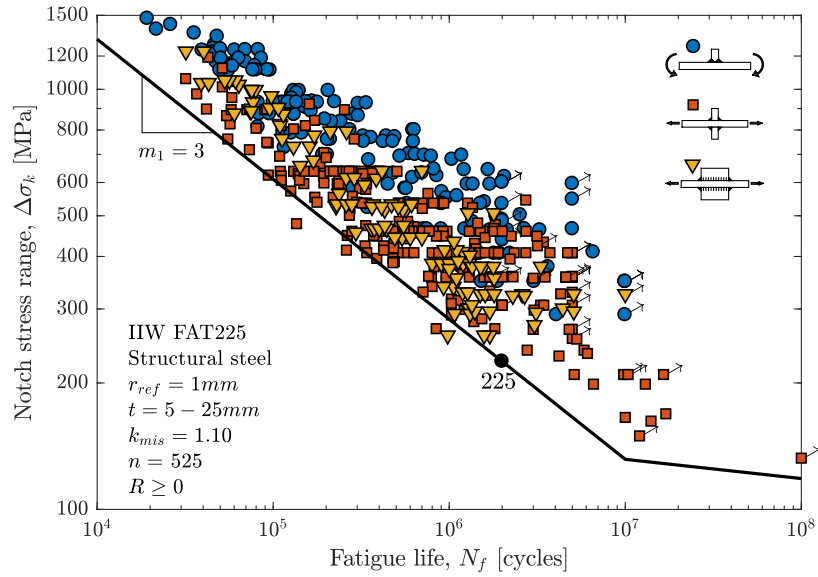


Figure 66: Evaluation of the FAT225 SN curve, data from [63].

10.4 Mild notch joint issues

Pedersen et al. [63] found the notch stress approach to be non-conservative in some cases for butt joints. Figure 67 shows a comparison of a large amount of fatigue data for butt joints in terms of both nominal- and notch stresses. As seen, the test results of especially thin joints seem to fall below the SN curve indicating non-conservative assessment in the notch stress system, but not in the nominal stress system.

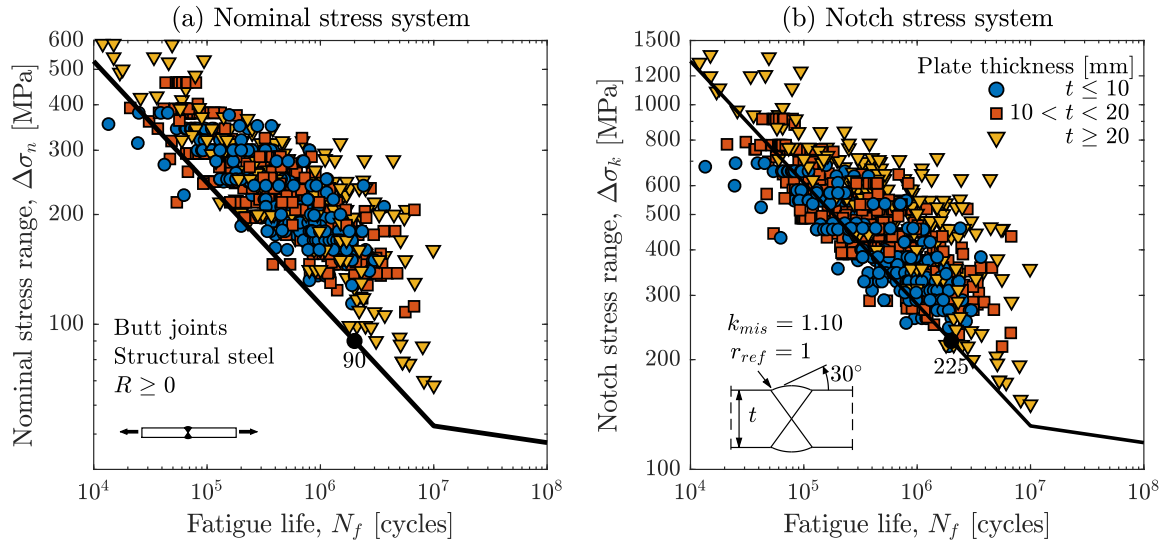


Figure 67: Assessment of butt joints using the notch stress approach, data from [63].

This illustrates a known issue of the notch stress approach when used with so-called *mild notch joints*, i.e. joints with a low stress concentration factor. Here, the notch stress approach simply does not work very well.

For the case of butt joints, this does not pose much of a problem, because the nominal stresses are easily calculated for those and hence the nominal stress approach would be the obvious choice for assessment.

The problem is not limited to butt joints alone, however. Figure 68 shows another example of a mild notch joint investigated experimentally and using the notch approach. The critical weld toe was modeled using $r_{ref} = 1\text{mm}$ and the measured flank angle of 15° . As seen, most of the data points lie below the FAT225 SN curve.

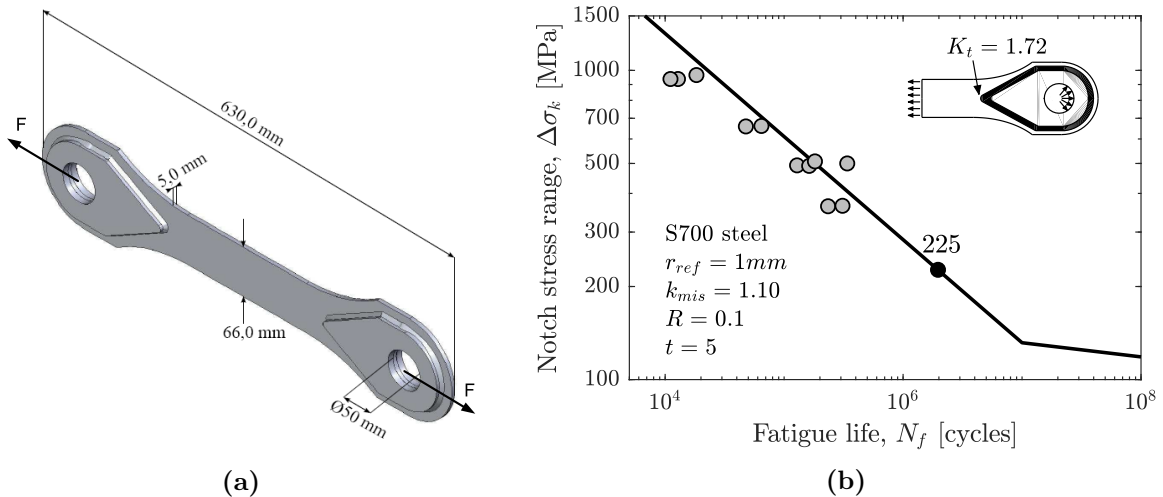


Figure 68: Mild notch crane detail investigated with the notch approach, data from [69].

In order to avoid the problems of mild notch joints, one should check the notch factor

$$K_w = \frac{\sigma_k}{\sigma_{hs}} \quad (10.4.1)$$

i.e. the stress concentration factor of the notch stress relative to the hotspot stress. For this check, the hotspot stress can be taken as the converged stress in the notch-model 2mm away from the reference radius.

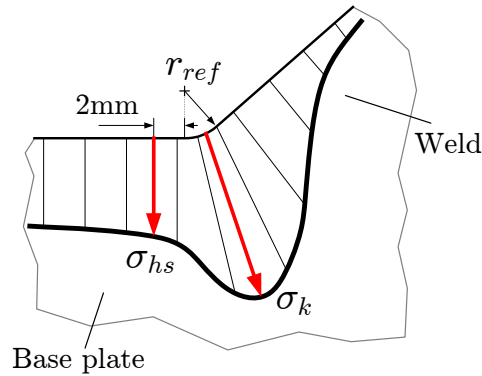


Figure 69: Stress distribution at weld toe, from [16].

The IIW [16] proposes a preliminary requirement that $K_w \geq 1.6$. This is insufficient in the opinion of the author, who would recommend at least $K_w \geq 2.0$, and further that the flank angle always be idealized to $\geq 45^\circ$ also for butt joints.

10.5 Comparative studies

The notch approach is an excellent choice for comparative studies of weld geometry. Figure 70 show an example of a parametric study of the influence of the penetration depth of the fillet welds in a cruciform joint. Such investigations are good for determining the requirements for welds in production.

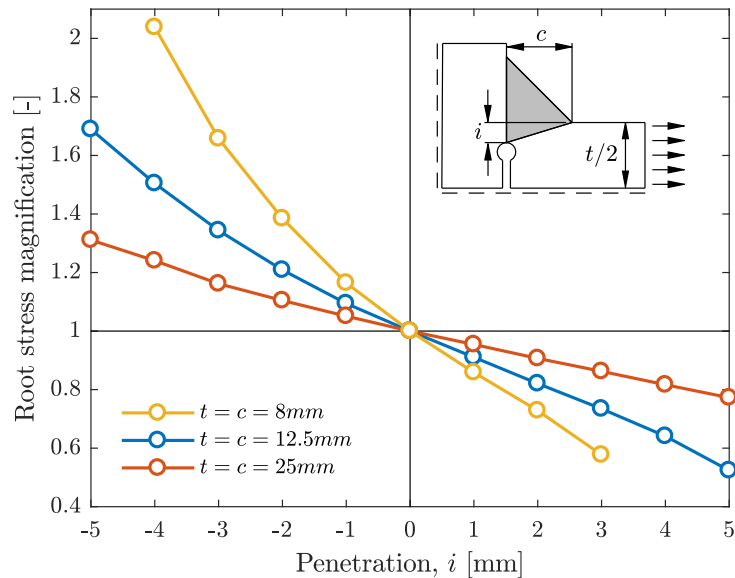


Figure 70: Investigation of the effect of penetration depth in cruciform joint.

10.6 Limitations and variants

The approach described here is the standard, which only applies to welded joints in steel plate thicker than $t \geq 5mm$. In case of thinner joints and e.g. spot welds, the IIW recommends using a reference radius of $r_{ref} = 0.05mm$ and FAT630.

Other materials than steel may also be assessed. The IIW provides SN curves for aluminum and magnesium. Otherwise, one may estimate the fatigue strength of a particular material from eq. (7.1.1).

11 Fracture mechanics approach

This chapter illustrates how to perform a fatigue assessment of a welded joint using fracture mechanics. Fracture mechanics is particularly useful in some special cases, e.g. if a crack has been detected in a component and the remaining life needs to be determined. It is also well suited for determining acceptable crack sizes for different levels of production quality.

11.1 Introduction to fracture mechanics

A very brief review of fracture mechanics will be given, focusing only on the main few concepts needed for simple assessments of welded joints. For a proper introduction to fracture mechanics see e.g. Anderson [1]. Here, we restrict the discussion linear elastic fracture mechanics (LEFM) - i.e. assuming linear elastic material behavior only. For this to hold, the plastic zone in front of the crack must be small compared to the crack length. Furthermore, we consider only mode-I crack growth (typical in fatigue).

11.1.1 The stress intensity factor

So far, our fatigue assessment has been based on the stress range or amplitude, either nominal or local. For cracked components, the local stress is not applicable since it approaches infinity at the crack tip. Instead we will use the *stress intensity factor*. Consider the transverse stress field in front of the crack in Fig. 71 - regardless of the loading and geometry σ_y will have roughly the shape shown in the close vicinity of the crack, i.e. approaching infinity.

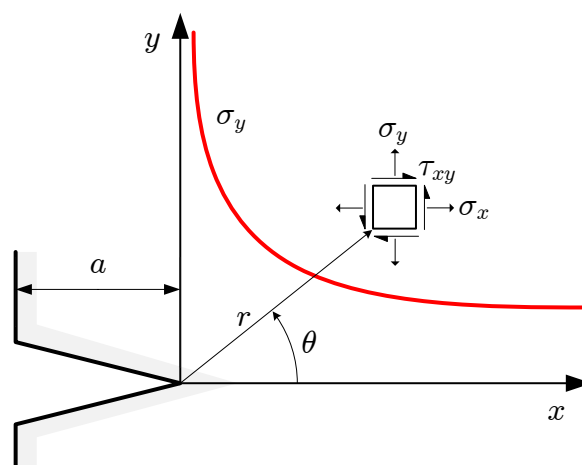


Figure 71: Stress field in front of crack.

Very close to the crack tip, the following approximation holds

$$\sigma_y = \frac{K}{\sqrt{2\pi r}} \cos \frac{\theta}{2} \left[1 + \sin \frac{\theta}{2} \sin 3\frac{\theta}{2} \right] \quad (11.1.1)$$

where K is the stress intensity factor. Thus K is a measure of *how fast* the stresses at the crack tip approaches infinity.

The stress intensity factor may be calculated in many ways, e.g. analytically from the far field (nominal) stress σ as

$$K = f\sigma\sqrt{\pi a} \quad (11.1.2)$$

where f is a geometry factor and a is the crack length. Analytical expressions of f are tabulated in textbooks [1] for common geometries and particularly for welded joints in e.g. the IIW recommendations [27]. For complex geometries, FE analysis may be used to establish the stress intensity factor. Many approaches have been developed for this [35].

It is important to note, that the stress intensity factor changes with the crack length a and also with the geometry as the crack grows, i.e. $f = f(a)$. It is thus necessary to establish the stress intensity factor in the entire range of expected crack depth.

The stress intensity factor fluctuates with the applied stress/load, thus the range can determined from the range of stress

$$\Delta K = f\Delta\sigma\sqrt{\pi a} \quad (11.1.3)$$

or by calculating the stress intensity factor at maximum and minimum loads and subtracting

$$\Delta K = K_{max} - K_{min} \quad (11.1.4)$$

Finally, a warning of unit-problems should be given. As evident from eq. (11.1.2), the units of the stress intensity factor will be [*stress* · *length*]. Unfortunately a variety of units are in use, e.g. [$MN/m^{3/2}$] or [$MPa\sqrt{mm}$]. What you get depends on the units used for calculation of K . Here we prefer the later, which arise from calculating stresses in [MPa] and crack length in [mm].

11.1.2 Fatigue crack growth

Referring to Fig. 72, Paris et al. [60] found by experiments, that the crack propagation rate da/dN correlates well with the range of the stress intensity factor in a certain range, such that

$$\frac{da}{dN} = A \cdot \Delta K^n \quad (11.1.5)$$

where A (the intercept at $\Delta K = 1$) and the slope n are fitting parameters, usually called material parameters but they depend on many more factors such as mean stress, specimen size, environment, etc.. In the literature, C and m are also often used. Eq. (11.1.5) is known as Paris' equation or Paris' law. It expresses what is the increment in crack length da per increment in cycles dN at some ΔK .

Interestingly, the slope of the da/dN curve turns out to be the same as that of the SN curve, i.e. $m = n$. More on this later.

Obviously, the linear behavior described by eq. (11.1.5) only apply to the central Region II part of the ΔK range. Many extensions have been proposed to cover also the two nonlinear parts of the plot (Regions I and III).

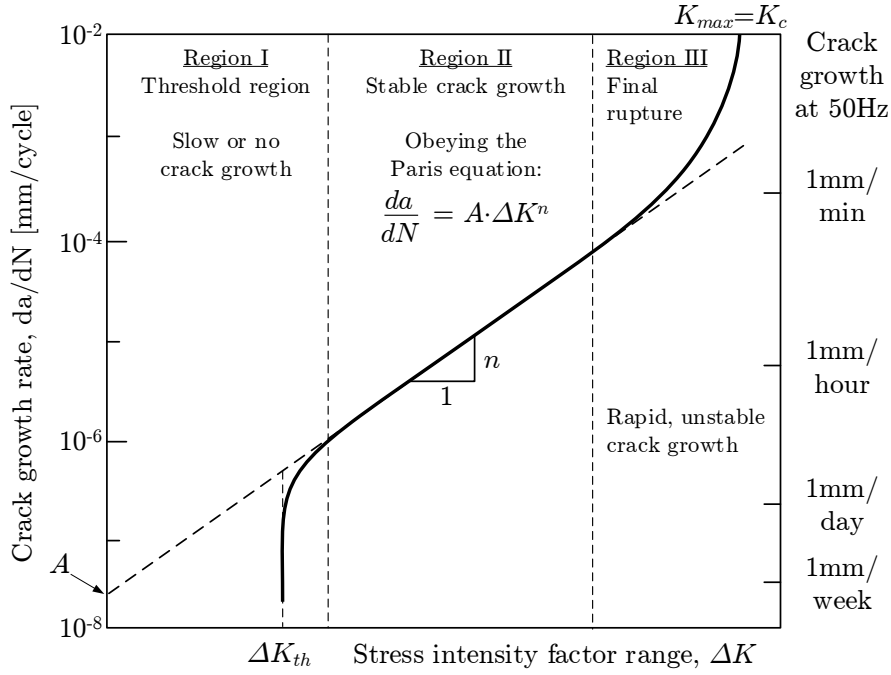


Figure 72: Schematic illustration of crack growth rate as a function of stress intensity factor range.

11.1.3 Life estimation

Having an expression of the stress intensity factor throughout the expected range of crack growth eq. (11.1.2) and an expression for the rate of crack propagation eq. (11.1.5), we may estimate the life to fracture under these conditions.

Rearranging the Paris equation

$$dN = \frac{da}{A \cdot \Delta K^n} \quad (11.1.6)$$

we may simply integrate to get the total life (no. cycles) for a crack to propagate from initial a_i to final a_f length

$$N = \int dN = \int_{a_i}^{a_f} \frac{da}{A \cdot \Delta K^n} \quad (11.1.7)$$

Assuming constant $f(a) = f$, the integration may be carried out analytically

$$N = \int_{a_i}^{a_f} \frac{da}{A(f\Delta\sigma\sqrt{\pi a})^n} \quad (11.1.8)$$

$$= \frac{1}{A(f\Delta\sigma\sqrt{\pi})^n} \int_{a_i}^{a_f} a^{-n/2} da$$

$$= \frac{2}{(n-2)A(f\Delta\sigma\sqrt{\pi})^n} \left[\frac{1}{a_i^{(n-2)/2}} - \frac{1}{a_f^{(n-2)/2}} \right] \quad (11.1.9)$$

Including $f = f(a)$ is much more demanding, and not necessarily possible analytically, but numerically the integration is very easy. The most influential parameter is the initial crack

length a_i , whereas the final crack length is almost insignificant. Typically a_f is set to half or the full plate thickness, the difference in resulting life is in the order of $< 1\%$.

11.1.4 Equivalence between SN and LEFM approaches

It will be shown that, for certain conditions, e.g. under constant amplitude loading, the fracture mechanical approach to life estimation is equivalent to the previously discussed SN approaches.

We begin by inserting eq. (11.1.3) in eq. (11.1.5)

$$\frac{da}{dN} = A \cdot \Delta K^n = A \cdot \left(f(a) \Delta \sigma \sqrt{\pi a} \right)^n = A \left(f(a) \sqrt{\pi a} \right)^n \Delta \sigma^n \quad (11.1.10)$$

then rearranging to isolate dependence of a on the left and dependence of N on the right

$$\frac{da}{\left(f(a) \sqrt{\pi a} \right)^n} = A \cdot \Delta \sigma^n \cdot dN \quad (11.1.11)$$

integrating crack increments from initial a_i to final a_f size and employing $N = \int dN$

$$\int_{a_i}^{a_f} \left(f(a) \sqrt{\pi a} \right)^{-n} da = A \cdot \Delta \sigma^n \cdot N \quad (11.1.12)$$

we note, that the integral on the left is only depending on the geometry and the slope, such that for a given parameters of $a_i, a_f, f(a)$ and n , the integral will yield a constant

$$I = \int_{a_i}^{a_f} \left(f(a) \sqrt{\pi a} \right)^{-n} da = \text{constant} \quad (11.1.13)$$

Inserting in eq. (11.1.12), we get the familiar equation for the SN curve

$$I = A \cdot \Delta \sigma^n \cdot N \quad (11.1.14)$$

or

$$C = \Delta \sigma^m \cdot N \quad (11.1.15)$$

where $C = I/A$ and $n = m$.

This means, that we can predict SN curves using fracture mechanics, e.g. in order to investigate the influence of various initial crack depth (weld quality) or differences in geometry, through f .

11.2 Application to welded joints

The specific application of fracture mechanics to welded joints is described thoroughly by Maddox [39], Gurney [23] and many others. Here, we merely scrape the surface to give an introductory overview.

11.2.1 Stress intensity factor for welded joints

Figure 73 shows an example of a welded butt joint with 3 potential cracks which may be analyzed using fracture mechanics; 1) undercut, 2) overlap and 3) root gap. Unfortunately, the most important parameter - the actual crack lengths/depths a_i - is typically unknown, very difficult

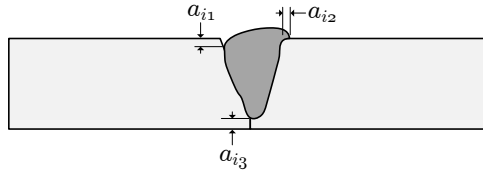


Figure 73: Potential initial cracks in a butt joint.

to measure and varies a lot in production. Thus, instead of assuming initial crack depths, the analysis is often carried out as a sensitivity study on different crack depths.

In order to include the finer details of the local geometry, it is recommended to use FE analysis for determining the stress intensity factor. Figure 74 shows an example of the stress intensity factor calculated for the undercut crack with a comparison between an FE solution and a simple analytical approach, i.e. a standard edge crack. It is clear that the correspondence is pretty good, but as will be shown, the resulting fatigue life will deviate significantly.

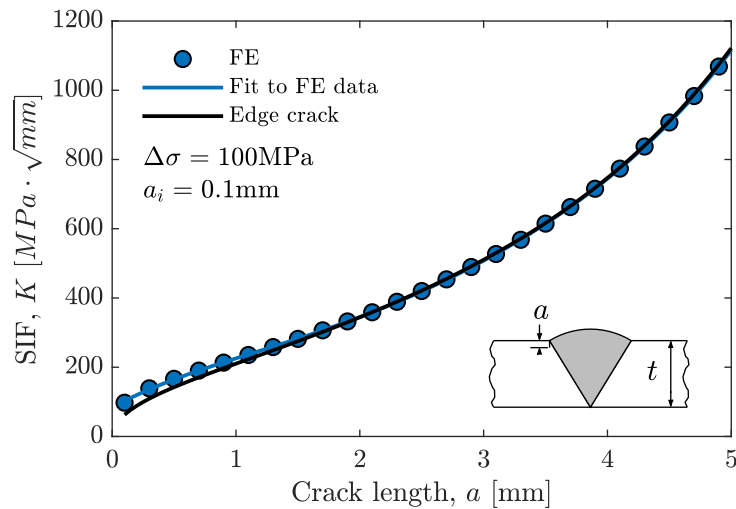


Figure 74: Stress intensity factor in butt joint.

For design purposes, the IIW recommends using $a_i = 0.1mm$, however in the opinion of this author one should be very careful with this. At least it is highly recommended to study the sensitivity and also follow up with measurements of produced welds (destructive). Moreover, one should remember to include misalignment and any other correction necessary in the otherwise idealized analysis.

11.2.2 Crack propagation in welded joints

There are many publications on the crack growth rate in welded joints with varying trustworthiness. Too often, results are reported from small scale CT specimens, which will not include the high level of tensile residual stresses typically found in welded joints. Fig. 75 shows a collection of measurements of crack growth rate in actual welded joints compared against the IIW recommended da/dN curve, Table 12. These are conservative design values (i.e. higher crack propagation rate than experiments) with safety comparable to that of design SN curves.

Comparing the experimental data in Fig. 75, it is interesting how the crack propagation rate is independent on the steel strength and also the stress ratio. This is accredited to the tensile residual stresses, which negates any closure effects, by keeping the crack open during the entire

Table 12: IIW recommended Paris constants for welds [27].

Material	n	A	ΔK_{th}
Steel	3.0	$5.21 \cdot 10^{-13}$	63
Aluminum	3.0	$1.41 \cdot 10^{-11}$	21

Units: $K : [MPa \cdot \sqrt{mm}]$ and $da/dN : [mm/cycle]$.
 Threshold value for high residual stresses: $R = 0.5$.

load cycle [54]. Using small scale CT specimens on the other hand may lead to very non-conservative results, because these cannot sustain as high level of residual stresses as actual welds.

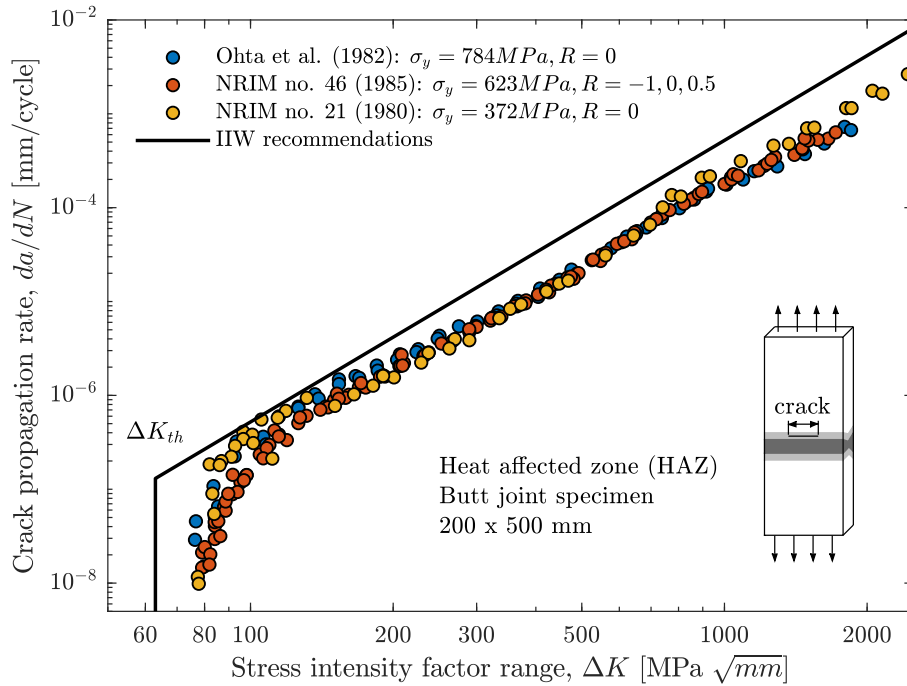


Figure 75: Measurements of crack growth rate in welded joints. Data from [51, 52, 54].

Continuing the example of the butt weld in Figure 74 we now integrate the fatigue life using eq. (11.1.7) numerically. The result is usually shown as an $a - N$ curve, Figure 76. It is now clear, that the relatively small deviation in stress intensity factor leads to a substantial deviation in the calculated fatigue lives.

It may be observed how the majority of the life is spent at a relatively short crack length, $a < 1mm$, hence the initial value of the stress intensity factor is by far the most important. It is also evident from Figure 76 that towards the end of the life, the curve approaches vertical i.e. very rapid crack growth per cycle. Thus, setting the final crack length a_f to either half the plate thickness or the full thickness does not alter the resulting life much.

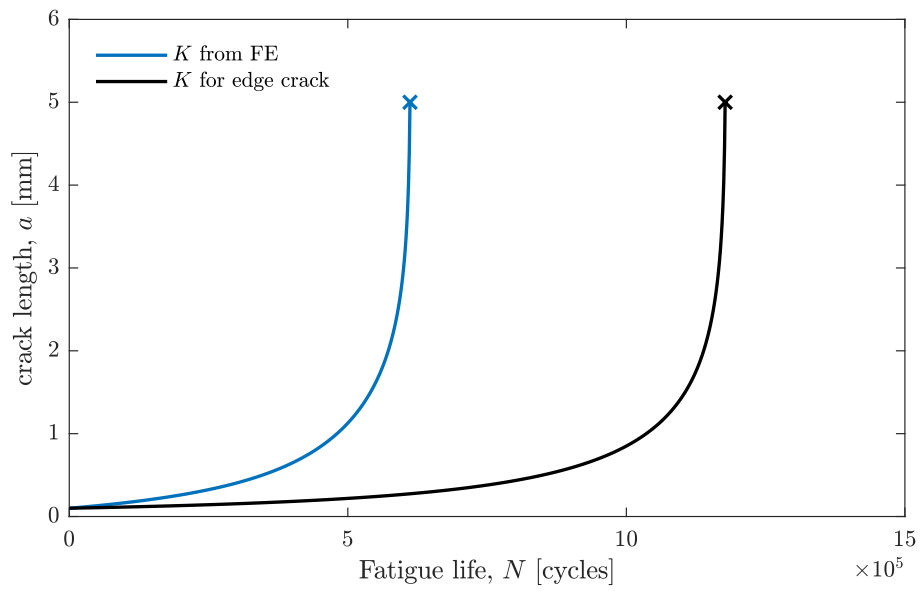


Figure 76: Fatigue life obtained from integration of Paris equation.

Bibliography

- [1] Anderson, T. L. *Fracture Mechanics: Fundamentals and Applications*, volume 58. CRC, 4th edition, 2012.
- [2] ASTM. *E 1049-85: Standard practices for cycle counting in fatigue analysis*. American Society for Testing and Materials, 1997.
- [3] Bleicher, C., Wagener, R., Kaufmann, H., and Melz, T. Fatigue strength of nodular cast iron with regard to heavy-wall applications. *Materials Testing*, 57(9):723–731, 2015.
- [4] Booth, G. The Effect of Thickness on the Fatigue Strength of Plate Welded Joints. In *Proc. 3rd Int. Conf. on Steel in Marine Struct SIMS87*, pages 259–268, Delft, The Netherlands, 1987.
- [5] Brogaard, B. F. *Investigation of notch support effects in ductile cast iron*. Master thesis, Aarhus University, 2017.
- [6] Bruun, A. and Härkegaard, G. A comparative study of design code criteria for prediction of the fatigue limit under in-phase and out-of-phase tension-torsion cycles. *International Journal of Fatigue*, 73:1–16, 2015.
- [7] Budynas, R. G. and Nisbett, J. K. *Shigley's Mechanical Engineering Design*. McGraw Hill, 9th edition, 2011.
- [8] DNV GL. RP-C203: Fatigue Design of Offshore Steel Structures. *Recommended Practise*, 2016.
- [9] Dürr, A. *Zur Ermüdungsfestigkeit von Schweißkonstruktionen aus höherfesten Baustählen bei Anwendung von UIT-Nachbehandlung*. PhD thesis, University of Stuttgart, 2007.
- [10] Eichlseder, W. Fatigue analysis by local stress concept based on finite element results. *Computers and Structures*, 80:2109–2113, 2002.
- [11] Eurocode 3. *Eurocode 3, Design of Steel Structures, Part 1-9: Fatigue*. CEN, 2005.
- [12] Fatemi, A. and Yang, L. Cumulative fatigue damage and life prediction theories: a survey of the state of the art for homogeneous materials. *International Journal of Fatigue*, 20(1): 9–34, 1998.
- [13] Findley, W. N. A theory for the effect of mean stress on fatigue of metals under combined torsion and axial load or bending. *Journal of Engineering for Industry*, pages 301–306, 1959.
- [14] Fisher, J. Fatigue strength of welded A514 steel beams. *Proc. Conference on Fatigue of Welded Structures*, 1(358), 1971.

- [15] FKM Guideline. *Analytical strength assessment of components*. VDMA Verlag, 6th edition, 2012.
- [16] Fricke, W. Guideline for the Fatigue Assessment by Notch Stress Analysis for Welded Structures. *IIW Doc. XIII-2240r1-08*, 2009.
- [17] Fricke, W. IIW Guideline for the Assessment of Weld Root Fatigue Table of Contents. *IIW Doc. XIII-2380r3-11*, 2012.
- [18] Fröschl, J., Decker, M., and Eichseder, W. Neuer Ansatz zur Bewertung von Stützwirkung und statistischem Größeneinfluss im Auslegungsprozess. *Materials Testing*, 53(7-8):1–4, 2011.
- [19] Gaenser, H. P. Some notes on gradient, volumetric and weakest link concepts in fatigue. *Computational Materials Science*, 44(2):230–239, 2008.
- [20] GL. *Guideline for the Certification of Offshore Wind Turbines*. Germanischer Lloyd, 2012.
- [21] Gough, H. and Pollard, H. The Strength of Metals under Combined Alternating Stresses. In *Proceedings of the Institution of Mechanical Engineers*, vol. 31, pages 3–18, 1935.
- [22] Gudehus, H. and Zenner, H. H. *Leitfaden für eine Betriebsfestigkeitsberechnung*. Stahleisen, 4th edition, 2004.
- [23] Gurney, T. R. *Fatigue of Welded Structures*. Cambridge University Press, London, 2nd ed. edition, 1979.
- [24] Haagensen, P. J. and Maddox, S. J. Recommendations on Post Weld Fatigue Life Improvement of Steel and Aluminium Structures. *IIW Doc. XIII-2200-07*, 2010.
- [25] Haibach, E. The Allowable Stresses Under Variable Amplitude Loading. In *Proc. Fatigue of Welded Structures, Vol. 2.*, pages 328–339. TWI, Cambridge, 1971.
- [26] Härkegaard, G. and Halleraker, G. Assessment of methods for prediction of notch and size effects at the fatigue limit based on test data by Böhm and Magin. *International Journal of Fatigue*, 32(10):1701–1709, 2010.
- [27] Hobbacher, A. *IIW Recommendations for Fatigue Design of Welded Joints and Components*. Springer, IIW-2259-15, 2nd edition, 2016.
- [28] Hück, M., Thrainer, L., and Schütz, W. *Berechnung von Wöhlerlinien für Bauteile aus Stahl, Stahlguss und Grauguss*. ABF 11, 1983.
- [29] ISO-5817. Welding - Fusion-welded joints in steel, nickel, titanium and their alloys (beam welding excluded) - Quality levels for imperfections, 2014.
- [30] Jonsson, B., Barsoum, Z., and Bazou, A. G. Influence from weld position on fillet weld quality. *IIW Doc. XIII-2273-09*, 2009.
- [31] Kaufmann, H. *Zur schwingfesten Bemessung dickwandiger Bauteile aus GGG-40 unter Berücksichtigung giesstechnisch bedingter Gefügeungängen*. PhD thesis, Fraunhofer LBF, 1998.
- [32] Kranz, B. and Sonsino, C. M. Verification of the notch stress concept for the reference radii of $r=1.00$ and 0.05mm . *IIW Doc. XIII-2274-09*, 2009.

- [33] Kuguel, R. A relation between theoretical stress concentration factor and fatigue notch factor deduced from the concept of highly stressed volume. In *ASTM Proceeding, 61*, pages 732–748, 1961.
- [34] Kuhlmann, U., Bergmann, J., Dürr, A., and Thumser, R. *Effizienter Stahlbau aus höherfesten Stählen unter Ermüdungsbeanspruchung*. Universität Stuttgart, 2006.
- [35] Kuna, M. Finite elements in fracture mechanics: Theory - Numerics - Applications. *Solid Mechanics and its Applications*, 201:1–472, 2013.
- [36] Lemaitre, J. and Chaboche, J.-L. *Mechanics of solid materials*. Cambridge University Press, 1994.
- [37] Lin, C.-K. and Lee, W.-J. Effects of highly stressed volume on fatigue strength of austempered ductile irons. *International Journal of Fatigue*, 20(4):301–307, 1998.
- [38] Lotsberg, I. Stress concentrations due to misalignment at butt welds in plated structures and at girth welds in tubulars. *International Journal of Fatigue*, 31(8-9):1337–1345, 2009.
- [39] Maddox, S. J. *Fatigue Strength of Welded Structures*. Abington, 2nd edition, 1991.
- [40] Maddox, S. J. Recommended Hot-Spot Stress Design S-N Curves for Fatigue Assessment of FPSOs. In *Proc. 11th Int. Offshore and Polar Engineering Conference*, pages 97–104, Stavanger, Norway, 2001.
- [41] Maddox, S. J. and Razmjoo, G. Interim fatigue design recommendations for fillet welded joints under complex loading. *Fatigue Fract Engng Mater Struct*, pages 329–337, 2001.
- [42] Marquis, G. and Rabb, B. High Cycle Variable Amplitude Fatigue of a Nodular Cast Iron. *Journal of ASTM international*, 1(8):1–17, 2004.
- [43] Marquis, G. and Solin, J. *Long-life fatigue design of GRP 500 nodular cast iron components*. VTT Technical Research Center of Finland, Research Notes 2043, Espoo, 2000.
- [44] McDonald, K. *Fracture and fatigue of welded joints and structures*. Woodhead, 2011.
- [45] Meyer, N. *Effects of mean stress and stress concentration on fatigue behavior of ductile iron*. M.sc. thesis, Toledo, 2014.
- [46] Naess, A. *Fatigue Handbook*. Tapir, Trondheim, Norway, 1985.
- [47] Neuber, H. *Kerbspannungslehre*. Springer, 2 edition, 1958.
- [48] Niemi, E. Structural Hot-spot Stress Approach to Fatigue Analysis of Welded Components, Designer’s Guide. *IIW Doc. XIII-1819-00*, 2000.
- [49] Norberg, S. and Olsson, M. A fast , versatile fatigue post-processor and criteria evaluation. *International Journal of Fatigue*, 27:1335–1341, 2005.
- [50] Norton, R. L. *Machine Design, An Integrated Approach*. Prentice Hall, 2nd edition, 2000.
- [51] NRIM. Fatigue data sheet no. 21: fatigue crack propagation properties for butt welded joints of SM50B rolled steel for welded structure, 1980.
- [52] NRIM. Fatigue data sheet no. 46: fatigue crack propagation properties for butt welded joints of SPV50 steel plate for pressure vessels, 1985.

- [53] NRRM. Fatigue data sheet no. 114: fatigue properties of non-load-carrying cruciform joint welded joints of SM490B rolled steel for welded structure, 2011.
- [54] Ohta, A., Sasaki, E., Nihei, M., Kosuge, M., Kanao, M., and Inagaki, M. Fatigue crack propagation rates and threshold stress intensity factors for welded joints of HT80 steel at several stress ratios. *International Journal of Fatigue*, 4(4):233–237, 1982.
- [55] Ohta, A., Maeda, Y., Mawari, T., Nishijima, S., and Nakamura, H. Fatigue strength evaluation of welded joints containing high tensile residual stresses. *International Journal of Fatigue*, 8(3):147–150, 1986.
- [56] Ohta, A., Mawari, T., and Suzuki, N. Evaluation of effect of plate thickness on fatigue strength of butt welded joints by a test maintaining maximum stress at yield strength. *Engineering Fracture Mechanics*, 37(5):987–993, 1990.
- [57] Ohta, A., Maeda, Y., and Suzuki, N. Fatigue Strength of Corner Welded Joints with Web Stiffener in Synthetic Seawater by Smax = Sy Test. *IIW Doc. XIII-1923-02*, 2002.
- [58] Olivier, Köttgen, and Seeger. *Schweissverbindung II, FKM Forschungshefte 180*. VDMA Verlag4, 1994.
- [59] Papuga, J. A survey on evaluating the fatigue limit under multiaxial loading. *Int. Journal of Fatigue*, 33(2):153–165, 2011.
- [60] Paris, P., Gomez, M., and Anderson, W. A Rational Analytic Theory of Fatigue. *The trend in Engineering*, 13:9–14, 1961.
- [61] Pedersen, M. M. *Improving the Fatigue and Control Performance of Loader Cranes*. PhD thesis, Aalborg University, 2011.
- [62] Pedersen, M. M. Multiaxial fatigue assessment of welded joints using the notch stress approach. *International Journal of Fatigue*, 83:269–279, 2016.
- [63] Pedersen, M. M., Mouritsen, O., Hansen, M. R., Andersen, J. G., and Wenderby, J. Re-analysis of fatigue data for welded joints using the notch stress approach. *Int. Journal of Fatigue*, 32:1620–1626, 2010.
- [64] Pedersen, M. M., Mouritsen, O. Ø., Hansen, M. R., and Andersen, J. G. Experience with the notch stress approach for fatigue assessment of welded joints. In *Swedish Conference on Light Weight Optimised Welded Structures, LOST*, Borlänge, Sweden, 2010.
- [65] Pedersen, M. M., Andersen, J. G., and Ólafsson, Ó. M. Investigation of the thickness effect for butt welded joints. *IIW Doc. XIII-WG1-154-12*, 2012.
- [66] Petrucci, G. A critical assessment of methods for the determination of the shear stress amplitude in multiaxial fatigue criteria belonging to critical plane class. *International Journal of Fatigue*, 74:119–131, 2015.
- [67] Radaj, D. and Vormwald, M. *Ermüdungsfestigkeit*. Springer, 3rd edition, 2007.
- [68] Radaj, D., Sonsino, C. M., and Fricke, W. *Fatigue assessment of welded joints by local approaches*. Woodhead, 2nd edition, 2007.
- [69] Rasmussen, L. V. *Levetidsbestemmelse og analyse af typisk svejst krandedetalje i højstyrkestål*. Master thesis, Aalborg University, 2008.

- [70] Schijve, J. *Fatigue of Structures and Materials*. Springer, 2nd edition, 2004.
- [71] Shirani, M. *Probabilistic and defect tolerant fatigue assessment of wind turbine castings*. PhD thesis, NTNU Trondheim, Norway, 2011.
- [72] Sonsino, C. and Fischer, G. Local assessment concepts for the structural durability of complex loaded components. *Materialwissenschaft und Werkstofftechnik*, 36(11):632–641, 2005.
- [73] Sonsino, C. M. Multiaxial fatigue of welded joints under in-phase and out-of-phase local strains and stresses. *International Journal of Fatigue*, 1995.
- [74] Sonsino, C. M. Course of SN-curves especially in the high-cycle fatigue regime with regard to component design and safety. *International Journal of Fatigue*, 29(12):2246–2258, 2007.
- [75] Sonsino, C. M. and Moosbrugger, E. Fatigue design of highly loaded short-glass-fibre reinforced polyamide parts in engine compartments. *International Journal of Fatigue*, 30(7):1279–1288, 2008.
- [76] Sonsino, C. M., Radaaj, D., Brandt, U., and Lehrke, H. P. Fatigue assessment of welded joints in AlMg 4.5Mn aluminum alloy (AA 5083) by local approaches. *International Journal of Fatigue*, 21(9):985–999, 1999.
- [77] Sonsino, C. M., Maddox, S. J., and Haagenen, P. A Short Study on the Form of the SN-Curves for Weld Details in the High-Cycle-Fatigue Regime. *IIW Doc. XIII-2045-05*, 2005.
- [78] Sonsino, C. Zur Bewertung des Schwingfestigkeitsverhaltens von Bauteilen mit Hilfe Örtlicher Beanspruchungen. *Konstruktion*, 45(1):25–33, 1993.
- [79] Sørensen, J. D., Tychsen, J., Andersen, J. U., and Brandstrup, R. D. Fatigue Analysis of Load-Carrying Fillet Welds. *ASME Journal of Offshore Mechanics and Arctic Engineering*, 128:65–74, 2006.
- [80] Stephens, R., Fatemi, A., Stephens, R., and Fuchs, H. *Metal Fatigue In Engineering*. Wiley, 2nd edition, 2001.
- [81] Suresh, S. *Fatigue of Materials*. Cambridge University Press, 2nd edition, 1998.
- [82] Svärd, H. A branch and bound algorithm for evaluation of the Findley fatigue criterion. *International Journal of Fatigue*, 73:27–38, 2015.
- [83] Ugural, A. and Fenster, S. K. *Advanced Mechanics of Materials and Applied Elasticity*. Prentice Hall, 2012.
- [84] Van Hooreweder, B., Moens, D., Boonen, R., and Sas, P. Fatigue strength analysis of notched aluminium specimens using the highly stressed volume method. *Fatigue and Fracture of Engineering Materials and Structures*, 35(2):154–159, 2012.
- [85] Volvo. STD 181-0004 Weld classes and requirements, 2016.
- [86] Weber, B., Kenmeugne, B., Clement, J., and Robert, J. Improvements of multiaxial fatigue criteria computation for a strong reduction of calculation duration. *Computational Materials Science*, 15(4):381–399, 1999.
- [87] Wittel, H., Muhs, D., Jannasch, H., and Voissiek, J. *Roloff/Matek Maschinenelemente*. Springer, 21st edition, 2013.

M. M. Pedersen, Introduction to Metal Fatigue, 2018